ARISTOTLE UNIVERSITY OF THESSALONIKI
SCHOOL OF GEOLOGY
DEPARTMENT OF GEOPHYSICS

ANNA SIDIROPOULOU
Geologist

CONTRIBUTION TO THE BETTER UNDERSTANDING OF PHYSICAL PROCESSES ASSOCIATED WITH MICROSEISMICITY

MASTER THESIS

POSTGRADUATE STUDIES PROGRAMME 'APPLIED & ENVIRONMENTAL GEOLOGY',
DIRECTION: 'APPLIED GEOPHYSICS & SEISMOLOGY'

THESSALONIKI
2021

ANNA SIDIROPOULOU
ΑΝΝΑ ΣΙΔΗΡΟΠΟΥΛΟΥ
Πτυχιούχος Γεωλόγος

CONTRIBUTION TO THE BETTER UNDERSTANDING OF PHYSICAL PROCESSES ASSOCIATED WITH MICROSEISMICITY

ΣΥΜΒΟΛΗ ΣΤΗΝ ΚΑΤΑΝΟΗΣΗ ΤΩΝ ΦΥΣΙΚΩΝ ΔΙΑΔΙΚΑΣΙΩΝ ΤΗΣ ΜΙΚΡΟΣΕΙΣΜΙΚΟΤΗΤΑΣ

Υποβλήθηκε στο Τμήμα Γεωλογίας στα πλαίσια του Προγράμματος Μεταπτυχιακών Σπουδών 'Εφαρμοσμένη και Περιβαλλοντική Γεωλογία', Κατεύθυνση 'Εφαρμοσμένη Γεωφυσική και Σεισμολογία'

Ημερομηνία Προφορικής Εξέτασης: 22/12/2021
Oral Examination Date: 22/12/2021

Three-member Examining Board

Papadimitriou Eleftheria Professor AUTH, Supervisor
Karakostas Vassileios Professor AUTH, Member
Łukasz Rudziński Professor PAN, Member

Τριμελής Εξεταστική Επιτροπή

Παπαδημητρίου Ελευθερία Καθηγήτρια, Επιβλέπουσα
Καρακώστας Βασίλειος Καθηγητής, Μέλος Τριμελούς Εξεταστικής Επιτροπής
Łukasz Rudziński Καθηγητής, Μέλος Τριμελούς Εξεταστικής Επιτροπής

CONTRIBUTION TO THE BETTER UNDERSTANDING OF PHYSICAL PROCESSES ASSOCIATED WITH MICROSEISMICITY– *Master Thesis*

ΣΥΜΒΟΛΗ ΣΤΗΝ ΚΑΤΑΝΟΗΣΗ ΤΩΝ ΦΥΣΙΚΩΝ ΔΙΑΔΙΚΑΣΙΩΝ ΤΗΣ ΜΙΚΡΟΣΕΙΣΜΙΚΟΤΗΤΑΣ– *Μεταπτυχιακή Διπλωματική Εργασία*

Preface

The present study was accomplished within the framework of the Postgraduate Program in Applied and Environmental Geology (specialization field: Applied Geophysics and Seismology) of the School of Geology of the Aristotle University of Thessaloniki. The aim of this study is to investigate the seismotectonic properties of Amfikleia area in central Greece where a seismic sequence took place in 2013. To achieve this target, the seismic activity is assessed by its spatiotemporal and magnitude distribution along with the state of stress. For this latter purpose its fault plane solutions are determined. Then, the responsible for the sequence fault structure is delineated, Coulomb stress changes are calculated and associated with the evolution of seismicity.

The seismic excitation includes three strong events: the first (Mw=5.4) occurred on August 7, after 3 days on August 10 the second one (Mw=5.0) struck and on September 16 the third one (Mw=5.3) occurred.

The **first chapter** is the introduction where the general seismotectonic setting of Greece is described, emphasis is placed to the study area. Reviews of previous studies related to the seismicity of the broader study area are presented.

In the **second chapter** the Amfikleia sequence is described in detail. This procedure is based on the examination of the space, time, time-space and magnitude distribution of the earthquakes. The sequence is distinguished into spatiotemporal clusters and an effort is made to define the activated fault segments.

In the **third chapter** the theoretical background for the calculation of the fault plane solutions is described. Focal mechanisms along with maps and cross sections of the study area are combined in order to identify the fault geometry.

In the **fourth chapter** the Coulomb stress calculations are presented. The results are associated with the seismicity evolution.

Finally, in the **last chapter** conclusions of the research and perspectives for future investigations are presented.

I would like to thank all those who taught me, shared their experience with me and contributed to the completion of this work. First of all, I would like to express my sincere gratitude to my supervisor, Professor Eleftheria Papadimitriou who gave me the opportunity to compose this research. I deeply appreciate her constant support, her patience and her mentorship. Without her guidance, this work would never have been made possible.

I would like to express my appreciation to my supervisor, Professor Vassilios Karakostas, of the Geophysics Department of Aristotle University of Thessaloniki for the substantial scientific advice he offered me and his interest in my progress. I’m also very grateful to my supervisor, Professor Łukasz Rudziński, from the Institute of Geophysics, Polish Academy of Sciences.

I warmly thank the M.Sc. and Ph.D. students that encouraged me throughout my thesis. Particularly, I thank Tasos Kostoglou who helped me many times during the elaboration of the present study.

Last but not least, I want to express my gratitude to my family and friends for the constant motivation and moral support they offered me during my studies. They have been a great encouragement for me. Thank you all.

TABLE OF CONTENTS

Preface……………………………………………………………………………….I

Abstract (In English)…………………………………………………………VI

Abstract (In Greek)………………………………………………………..VII

CHAPTER 1: INTRODUCTION……………………………………………...1

1.1 Seismotectonic setting………………………………………………………..1

1.1.1 Broader Greek area……………………………………………………………1

1.1.2 Broader study area……………………………………………………………4

1.2 Past Seismicity…………………………………………………………………10

CHAPTER 2: EVALUATION OF THE SEISMIC SEQUENCE…………..11

2.1 Introduction…………………………………………………………………….11

2.1.2 Origin of the earthquake sequences……………………………………….14

2.1.2.1 Asperity and barrier models………………………………………..15

2.2 Retrospective of earthquake sequences research in Greece ……………......16

2.3 Spatial distribution of the seismic sequence………………………………...20

2.4 Space- time distribution of the seismic sequence…………………………...21

2.5 Magnitude distribution of the seismic sequence…………………………....25

2.5.1 b-value……………………………………………………………………...25

2.5.2 Determination of completeness magnitude (M_c)……………………………...27

2.5.2.1 Methodology…………………………………………………………..28

2.5.2.2 Goodness-of-Fit Test (GFT)…………………………………………..30

2.5.3 Results……………………………………………………………………...31

2.5.4 Temporal and spatial variations of b-value…………………………………..33

2.6 Mean magnitude distribution……………………………………………..37

2.7 Temporal distribution…………………………………………………….39

CHAPTER 3: FOCAL MECHANISMS…………………………………......45

3.1 Introduction…………………………………………………………....45

3.2 Computing focal mechanisms…………………………………………45

3.3 Results………………………………………………………………47

3.3.1 T-axis orientation……………………………………………………..55

CHAPTER 4: COULOMB STRESS CALCULATIONS

4.1 Introduction…………………………………………………………....57

4.2 ΔCFS calculations……………………………………………………..61

4.3 Results……………………………………………………………........65

CHAPTER 5: CONCLUSIONS……………………………………………....69

References…………………………………………………………………71

Abstract

On 2013 August 7, an M=5.4 earthquake struck the area near the town of Amfikleia in central Greece and an earthquake sequence was initiated. The mainshock caused severe damage to buildings of the nearby villages. The study area is part of the back arc region of the Hellenic arc and is located between three morphotectonic regions, the Kalidromon mountain, the Lokris basin and the Voiotikos Kifissos basin. The area is seismically active and is characterized by normal faulting and extension.

The seismic activity was recorded during a time interval of almost one year from the mainshock and 1080 aftershocks were detected. The seismic sequence is characterized by clustering which is probably attributed to the activation of adjacent fault segments. The spatiotemporal evolution showed an eastward activation pattern of fault segments. Forty-one days after the mainshock the seismicity migrated towards the east and the largest aftershock occurred (M=5.3). The aftershock activity is concentrated into four clusters. The first and the third clusters comprise the mainshock (M=5.4) and the largest aftershock of the sequence (M=5.3), whilst the other two clusters include lower-magnitude aftershocks. Temporal variations in the b-value showed that the occurrence of $M \geq 4.0$ aftershocks corresponds to the lowest values of the b parameter.

Fault plane solutions for 62 earthquakes with magnitudes M>2.5 were determined using P-wave first motion polarities. The solutions exhibited normal faulting and were used along with the aftershock hypocenters in cross sections. The cross sections were perpendicular to the strike of each cluster and revealed the geometry of each fault segment as well as the depth of the seismogenic layer. The average T-axis orientation is in agreement with the regional sub-horizontal extension.

Coulomb stress changes associated with the coseismic slips of the three strongest events ($M \geq 5$) of the Amfikleia sequence were calculated. The calculations provide evidence of stress interaction among the fault segments.

Abstract (in Greek)

Στις 7 Αυγούστου 2013 ένας σεισμός μεγέθους M=5.4 έπληξε την περιοχή κοντά στην πόλη της Αμφίκλειας, στην Κεντρική Ελλάδα, ξεκινώντας μια σεισμική ακολουθία. Ο κύριος σεισμός προκάλεσε σοβαρές ζημιές στα κτήρια των γειτονικών χωριών. Η περιοχή μελέτης αποτελεί τμήμα της οπισθότοξης περιοχής του Ελληνικού τόξου και τοποθετείται μεταξύ τριών μορφοτεκτονικών περιοχών που είναι το βουνό του Καλλιδρόμου, η λεκάνη της Λοκρίδας καθώς και η λεκάνη του Βοιωτικού Κηφησού. Ακόμη, η περιοχή μελέτης είναι σεισμικά ενεργή και χαρακτηρίζεται από κανονικά ρήγματα καθώς και από καθεστώς εφελκυσμού.

Η χρονική διάρκεια καταγραφής της σεισμικής δραστηριότητας ήταν περίπου ένα έτος από την εκδήλωση του κύριου σεισμού. Σε αυτό το χρονικό διάστημα 1080 μετασεισμοί ανιχνεύθηκαν. Η σεισμική ακολουθία χαρακτηρίζεται από συσταδοποίηση η οποία πιθανώς αποδίδεται στην ενεργοποίηση γειτονικών τεμαχών του ρήγματος. Η χωροχρονική εξέλιξη έδειξε ένα μοτίβο ενεργοποίησης των τεμαχών του ρήγματος προς τα ανατολικά. Σαράντα ημέρες μετά τον κύριο σεισμό, η σεισμικότητα μετανάστευσε προς τα ανατολικά και εκδηλώθηκε ο μεγαλύτερος μετασεισμός (M = 5.3). Η μετασεισμική δραστηριότητα συσκεντρώνεται σε τέσσερις συστάδες. Η πρώτη και η τρίτη συστάδα περιλαμβάνουν την εκδήλωση του κύριου σεισμού καθώς και του μεγαλύτερου μετασεισμού αντίστοιχα, ενώ οι υπόλοιπες δυο συστάδες περιέχουν μετασεισμούς με μικρότερα μεγέθη. Οι χρονικές διακυμάνσεις στην τιμή της παραμέτρου b έδειξαν πως οι μετασεισμοί με $M \geq 4.0$ αντιστοιχούν στις χαμηλότερες τιμές της παραμέτρου αυτής.

Με τη χρήση της μεθόδου των πρώτων αποκλίσεων των επιμήκων κυμάτων υπολογίσθηκαν οι μηχανισμοί γένεσης 62 σεισμών με μέγεθος M>2.5. Οι λύσεις των μηχανισμών γένεσης δείχνουν κανονικές διαρρήξεις και χρησιμοποιήθηκαν μαζί με τις εστίες των μετασεισμών σε κατακόρυφες τομές. Οι κατακόρυφες τομές κατασκευάστηκαν κάθετα στην παράταξη της κάθε συστάδας προσδιορίζοντας τη γεωμετρία της κάθε συστάδας καθώς και το βάθος του σεισμογόνου στρώματος. Η μέση διεύθυνση του T-άξονα τάσης έρχεται σε συμφωνία με τον σχεδόν οριζόντιας διεύθυνσης εφελκυσμό σε τοπικό επίπεδο.

Υπολογίσθηκαν οι μεταβολές των τάσεων Coulomb λόγω των σεισμικών ολισθήσεων των τριών κύριων σεισμών (M ≥ 5) της ακολουθίας της Αμφίκλειας. Οι υπολογισμοί παρέχουν αποδείξεις σχετικά με την αλληλεπίδραση των τάσεων Coulomb μεταξύ των τεμαχών του ρήγματος

CHAPTER 1: INTRODUCTION

1.1 Seismotectonic setting

1.1.1 Broader Greek area

The area of Greece constitutes part of the Eurasian zone that is part of the continental rift system that is defined by its high seismic activity. The high seismic activity of this area implies a tectonically active area. The regional seismotectonics is characterized by complexity mainly due to the convergence between two major lithospheric plates (Eurasian and African). However, the motion between these two plates it is not adequate to describe the complex seismotectonic regime of Greece. Therefore, the motions of three smaller tectonic plates such as Aegean, Anatolian and Apulian (microplates) have been accepted. The convergence leads the oceanic crust of the eastern Mediterranean, which constitutes the front of the continental African plate to subduct below the Eurasian plate along the Hellenic arc. The calculated convergence rate is ~5–10 mm/yr. (Papazachos and Comninakis, 1971, Minster and Jordan, 1978, DeMets et al., 1990). The subduction takes place from the western Peloponnese through Crete to western Turkey. Hellenic arc or Aegean arc has a total length of about 1200km (Ganas and Parsons, 2009, Kalligeris et al., 2012).

The broader Aegean region is positioned along the convergence boundary between Eurasian and African lithospheric plates. McKenzie (1970, 1972) was the first to define a small plate (microplate) that moves rapidly and contains the Aegean, part of Greek mainland, Crete and part of western Turkey. He named it the “Aegean plate”. According to fault plane solutions at its southern boundary it has been shown that the motion between African and Aegean plate has undertaken a N-S extension. Seismological evidence suggests that the Aegean microplate moves southwest relative to Eurasia (McKenzie, 1970, 1972, 1978, Jackson, 1994, Oral et al., 1995, Papazachos et al., 1998a, Papazachos, 1999a) at a rate of 3.5 cm/yr (Papazachos et al., 2001). More than 60% of seismicity in Europe is manifested here, with magnitudes up to Mw=8.3 (Papazachos, 1990).

This seismicity is resulted by the active deformation caused by three main geodynamic processes (**Fig.1.1**).

1) The Eastern Mediterranean ocean lithosphere, which constitutes the front part of the African plate, subducts bellow the Aegean continental microplate due to the African's plate northward motion (Papazachos and Comninakis, 1971, Le Pichon and Angelier, 1979).
2) The Arabian plate moves northward relative to Eurasia, likewise the African plate. The Arabian plate moves faster than the African plate thus it pushes the Eurasian boundary in Anatolian peninsula. As a result of this continuous movement, the Anatolian microplate is squeezed out westwards. Therefore, the Anatolian microplate moves westward relative to Eurasia, along the North Anatolian fault (NAF) and continues along the North Aegean Trough (NAT) region. This region is the boundary between Eurasian plate and Aegean microplate (McKenzie, 1970, 1972, Jackson and McKenzie, 1988, Papazachos and Kiratzi, 1996, Papazachos et al., 1998, Kiratzi and Louvari, 2003).
3) The Apulian/Adriatic microplate rotates counterclockwise about a pole located in northwestern Italy and collides with Eurasia along the Adriatic, Albania and northwest Greek coast (Anderson and Jackson, 1987).

Based on similar seismotectonic features, Papazachos et al. (1998) divided the broader area of Greece into five general seismicity zones (**Fig.1.1**). The first zone occupies the western coastal area of Albania and the northwest Greek coast. It is a thrust type zone with low angle faults striking parallel to the coastline (**Fig.1.1**). This thrust faulting type is ascribed to the continental collision of the Adriatic microplate with the Eurasian plate along the eastern Adriatic and northwest Greek coast (Anderson and Jackson, 1987).

The second zone covers the convex side of the Hellenic arc. It is also a thrust type zone with low angle faults that strike to NW-SE parallel to the coast (**Fig.1.1**). This low angle thrust faulting type is related to the subduction of the Eastern Mediterranean ocean lithosphere bellow the Aegean continental microplate (Papadimitriou, 1993).

The third zone covers an extensive area including the Aegean Sea, the northern Greece along with the central Greece, the western Turkey, the southern Bulgaria and the former southern Yugoslavia. This zone is characterized by a N-S extensional field along E-W striking normal faults (**Fig.1.1**). The N-S extensional regime could be attributed to the gravitational collapse of the expanding area. This gravitational collapse results from the rollback of the descending African lithospheric slab in the direction of the remnants of the oceanic crust bellow the Ionian Sea (McKenzie, 1970, 1972, 1978, LePichon and Angelier, 1981, Dewey, 1988, Doutsos and Kokkalas, 2001, Jolivet et al., 2013).

The fourth zone begins from Albania extending across the Hellenides Mountain Range. In eastern Epirus is interrupted and then it continues to southern Peloponnese until Rhodes. It is dominated by an E-W extensional regime along N-S striking normal faults (**Fig.1.1**). Considering that this zone is intercepted in eastern Epirus, it can be distinguished into a northern part and a southern part. The cause of the E-W extension in the northern part differs from that in the southern part and has not yet fully interpreted.

The fifth belt begins from the North Anatolian Fault (NAF) and continues up to the North Aegean Sea. In central Greek is interrupted and then is detected again in western Peloponnese and Ionian islands. This zone seems to be terminated in the Cephalonia Transform Fault (CTF). It is a dextral strike-slip fault zone which indicates the boundaries between the Eurasian plate and the Aegean microplate (**Fig.1.1**). These faulting type characteristics are ascribed to the fast (~3.5 cm/yr) southwestward movement of the Aegean microplate (Le Pichon et al., 1995).

The Cephalonia Transform Fault (CTF) is a major tectonic structure that dominates the central Ionian Sea (**Fig.1.1**). It is a right lateral strike slip fault with a thrust component that defines the boundary between the collision of the Adriatic and Aegean microplates to the north and the oceanic subduction to the south (Eastern Mediterranean- Aegean) (Scordilis et al., 1985, Papazachos et al., 1994, Louvari et al., 1999).

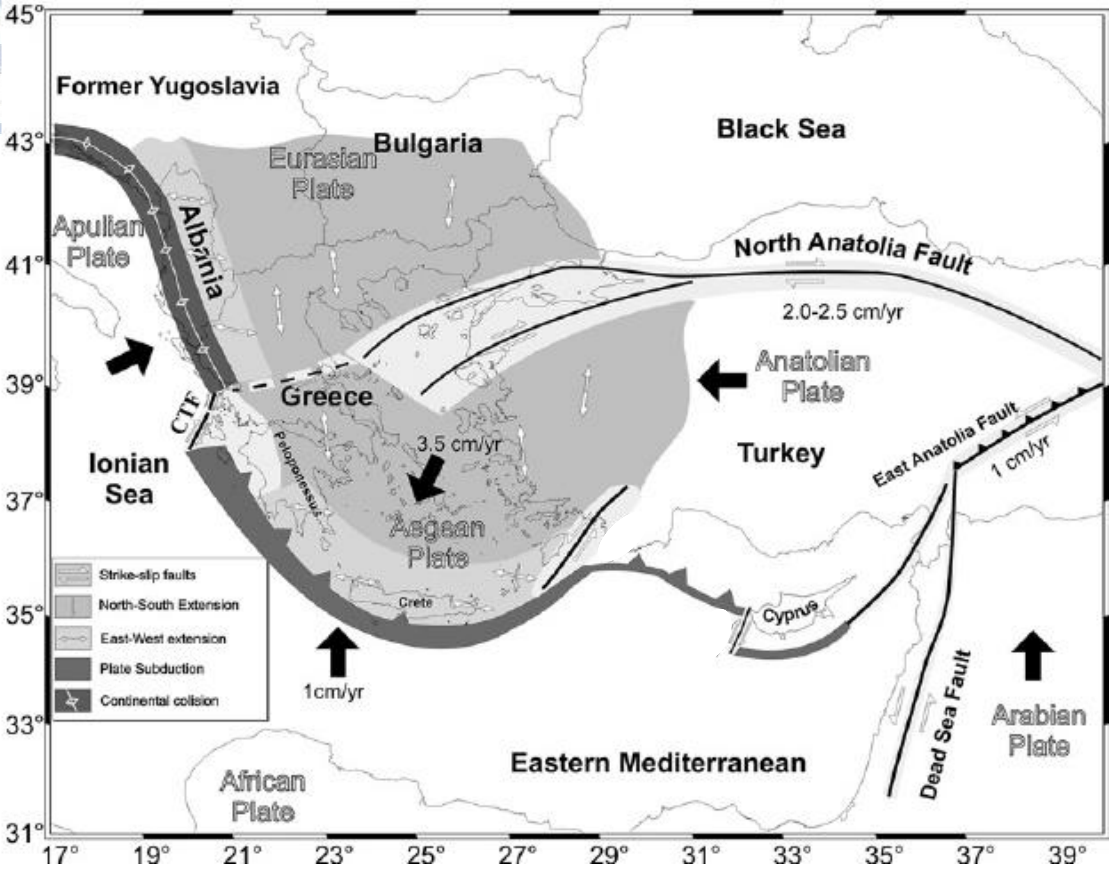

Figure 1.1 Tectonic features of the broader Hellenic area, modified by Papazachos et al., 1998. The motions of the microplates relative to the Eurasian plate are denoted black arrows. The double white arrows represent the extensional stress regime. CTF: Cephalonia Transform Fault.

1.1.2 Broader study area

The study area is located in the Greek mainland which is in the back arc area of the Hellenic arc. It exhibits high seismic activity that has been affected by mean WNW-ESE extension since early Miocene (Le Pichon and Angelier, 1979, Mercier et al., 1989). It is dominated by a localized extension within a regional transtensional field that is associated with the westward propagation of the North Aegean Trough (NAT) and the ongoing back-arc extension (Armijo et al., 1996, Goldsworthy et al., 2002, Burchfiel, 2004). GPS surveys have shown that central mainland Greece undergoes a combination of horizontal shear and extension (McClusky et al., 2000, Burchfiel, 2004).

The study area is located between two active deformation marine areas, the Gulf of Evoia in the north and the Gulf of Corinth in the south (**Fig.1.3**). The region between them hosts several major WNW-ESE normal faults or fault zones such as the Atalanti, the Arkitsa – Agios Konstantinos – Kamena Vourla and the Kallidromon (Kranis, 2007). These fault zones bound a number of successive horsts and grabens such as the Kallidromon mountain, the Voiotikos Kifissos basin and the Lokris basin (**Fig.1.2**).

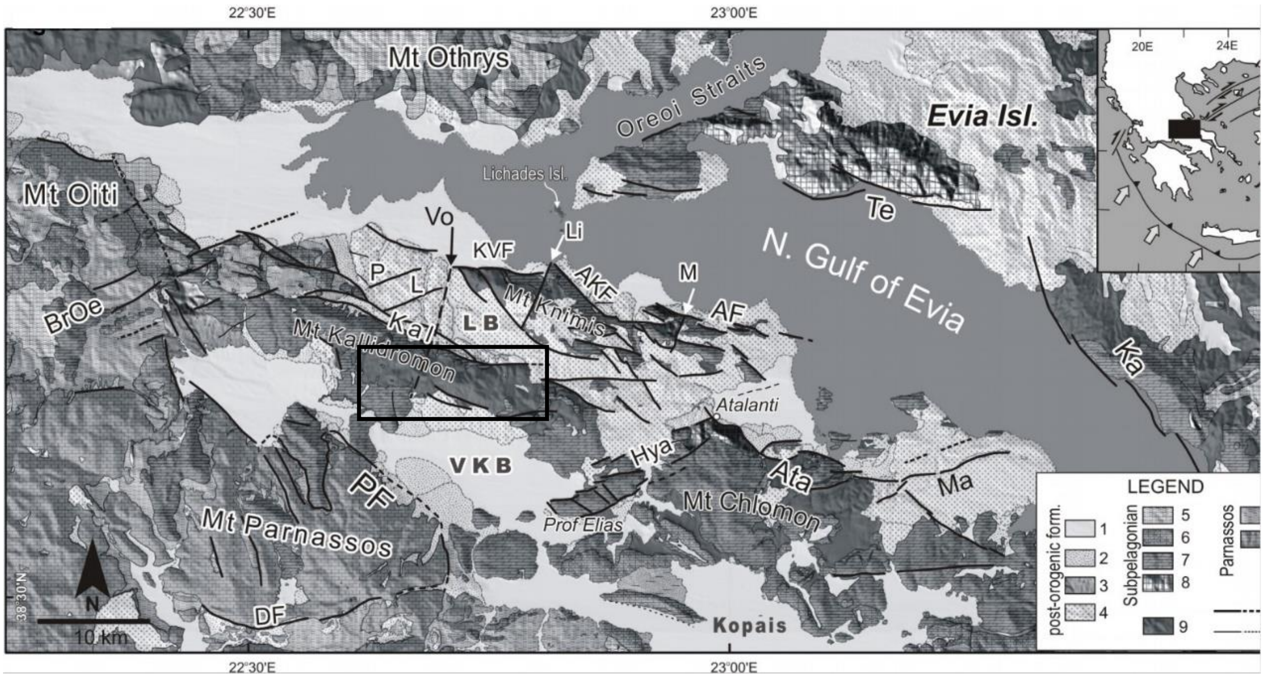

Figure 1.2 Activated faults and geological map of the study area. Some of the fault zones and faults have been referenced in text. PF: Parnassos fault, Kal: Kallidromon fault zone, Ata: Atalanti fault zone, AKF: Agios Konstantinos fault zone, KVF: Kamena Vourla fault zone, AF: Arkitsa fault zone, LB: Lokris basin, VKF: Voiotikos Kifissos basin (Tzanis et al., 2010).

Kallidromon fault zone runs sub-parallel to Evoikos coast and it belongs to the Sperchios Fault System (Kilias et al., 2008). Its total length is approximately 33 km and it has a thickness of 300-500m (Migiros et al., 2010). It separates the Alpine from the post-Alpine formations. It comprises two segments, the western and the eastern ones that trend WNW-ESE and E-W, respectively. It is characterized as oblique-normal with a right-lateral sense of movement, unlike the coastal Arkitsa – Agios Konstantinos – Kamena Vourla fault zone which is normal left-oblique (Kranis, 1999).

The 2013 Amfikleia aftershock sequence has a WSW - ENE direction with a length of 18 km (Ganas et al., 2014). Its SW side occupies the area between Voiotikos Kifissos basin and Kallidromon mountain while its NE side covers the SE part of the Lokris basin (**Fig.1.4**).

Kallidromon mountain is a WNW-ESE striking tectonic horst that is bounded by the Sperchios and the Lokris basins to the north and the Voiotikos Kifissos basin to the south. It is characterized by WNW-ESE normal faults that are parallel to each other (Philip, 1974, Mercier et al., 1979, Roberts and Jackson, 1991, Ganas, 1997, Kranis, 1999, Palyvos, 2001). These sub-parallel faults follow a progressive hanging wall directed north migration towards the Kamena Vourla (Goldsworthy and Jackson, 2001, Migiros et al., 2010). Mt Kallidromon is mainly characterized by three fault groups (Migiros et al., 2010):

1) Normal and oblique normal faults that dip 60^o -70^o towards NE and SW. They trend N310^o-N130^o and their rake is above 60^o. Their activity lasted form Upper Miocene to Lower Pliocene. They have formed the postalpine basins of Modi and Reginio at the southern and the northern edge of the Mt. Kallidromon respectively.
2) Normal and oblique normal faults that dip 60^o -80^o towards NW and SE. They trend N030^o-N210^o and their rake is between 50^o- 60^o. They were strike slip faults that they were reactivated as normal during the post alpine era.
3) Normal faults that dip 60^o -80^o towards N and S. Their strike is almost E-W (N080^o-N260^o) and their rake is between 50^o- 60^o. They have been active since Upper Pliocene thus they are the youngest. They bound the postalpine basins of Modi and Reginio and they crosscut the faults of group 1 and 2.

Lokris or Reginio basin (Leeder and Jackson, 1993) is an elongated WNW-ESE tectonic structure that is parallel to the Kallidromon fault zone. Its total length is 30 km and it covers an area of 190 km^2. Its southern-southwestern margin is bounded by the Kallidromon fault zone whilst Mt. Chlomon and Mt.Knimis bound its southeastern and northern margins, respectively (Kranis, 2007) (**Fig.1.2, 1.3**). This basin is also related to the Sperchios basin by the Kamena Vourla fault. It's a tectonic active area that hosts small order horsts (Mariolakos et al., 2001). Sedimentation occurred in the Upper Miocene and continues till nowadays.

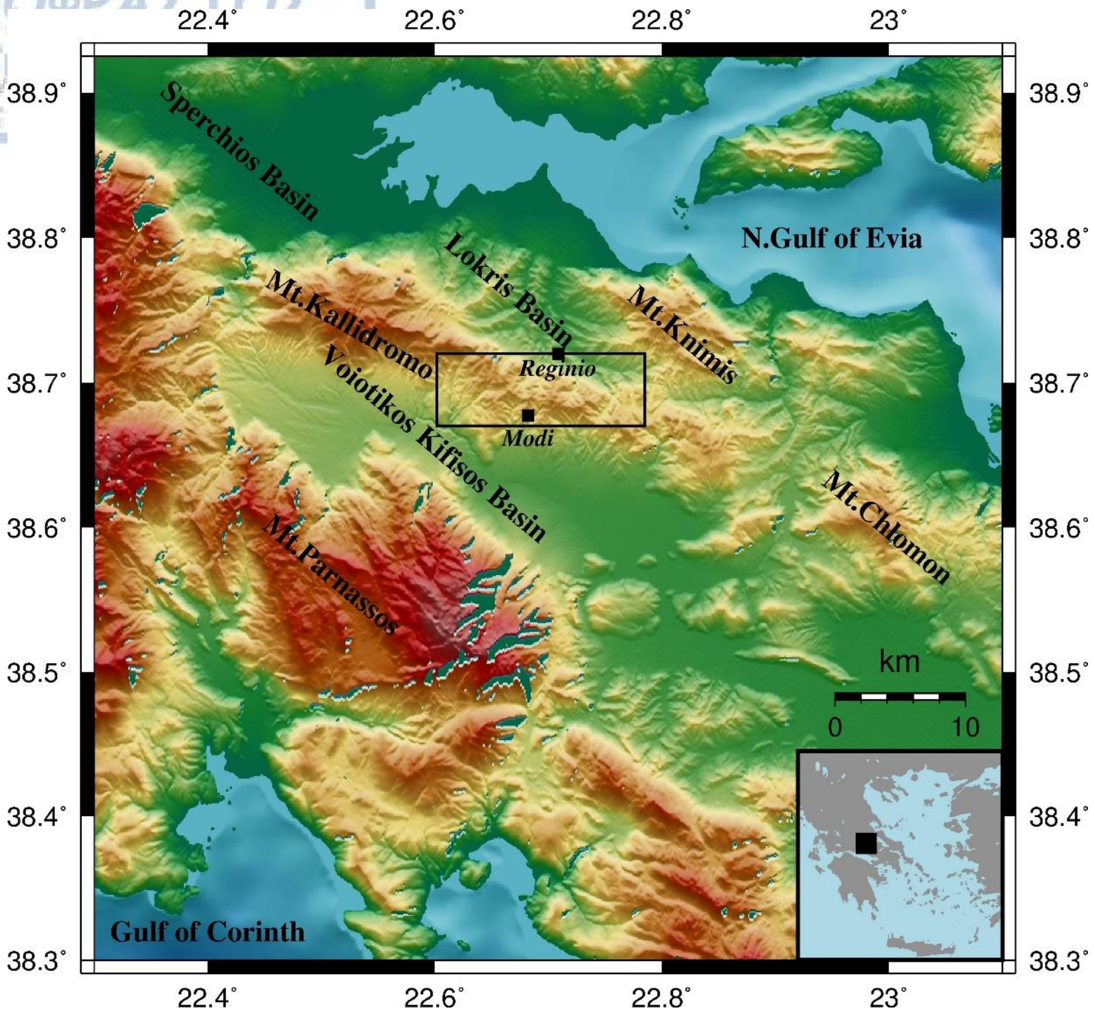

Figure 1.3 Map of the broader study area showing the main morphological features. The rectangle indicates the area of the Amfikleia sequence.

Voiotikos Kifissos basin is a composite WNW-ESE half graben that is located between the southern and northern margins of the Mt. Kallidromon and the Mts Parnassos – Giona, respectively. The basin is divided into two sub-basins that are associated with the upper (Gravia sub-basin) and median flow sections (Tithorea sub-basin) of the Voiotikos Kifissos River. Each sub-basin covers an area of ~200 km^2 and they are separated by a narrow passage close to the town of Amfikleia (Valnakiotis, 2009) (**Fig.1.4**).

Voiotikos Kifissos basin is bounded by the Voiotikos Kifissos fault zone (or Parnassos detachment) which comprises seven segmented normal faults such as Tithorea, Amfikleia, Lilaia, Mariolata, Gravia, Kastellia and Apostolia (**Fig.1.4**). Morphotectonic structures suggest that the faults of Tithorea, Amfikleia, Lilaia, Mariolata and Gravia are still active whilst the faults of Kastellia and Apostolia aren't (Ganas and White 1996, Valkaniotis, 2009). The upper flow section (Gravia sub-basin) of Voiotikos

Kifissos basin is bounded by the Lilaia, Mariolata, Gravia, Kastellia and Apostolia faults whilst the median flow section (Tithorea sub-basin) is bounded by the Tithorea and Amfikleia faults. These detachment faults are probably related to the southwestward propagation of the North Anantolian Fault (NAF) into the North Aegean Fault zone (Mariolakos and Papanikolaou, 1987, Jackson, 1994). Fault trace that was exposed in a quarry near the Amfikleia town revealed information about the detachment kinematics. It's a north-dipping normal fault that trends NW-SE and slides towards NE (Kranis and Papanikolaou, 2001, Papanikolaou and Royden, 2007). The formation of Voiotikos Kifissos and Lokris basins are related to the northeastward sliding on the detachment. Indications of an underlying detachment at the Lokris basin are: 1) The increase in the dip of synthetic NNE-dipping faults as the distance from the Parnassos front to the Gulf of Evia grows. 2) The intense segmentation of WNW-ESE faults, most of the segments' length is about 8 km (Kranis and Papanikolaou, 2001, Swanson, 2008).

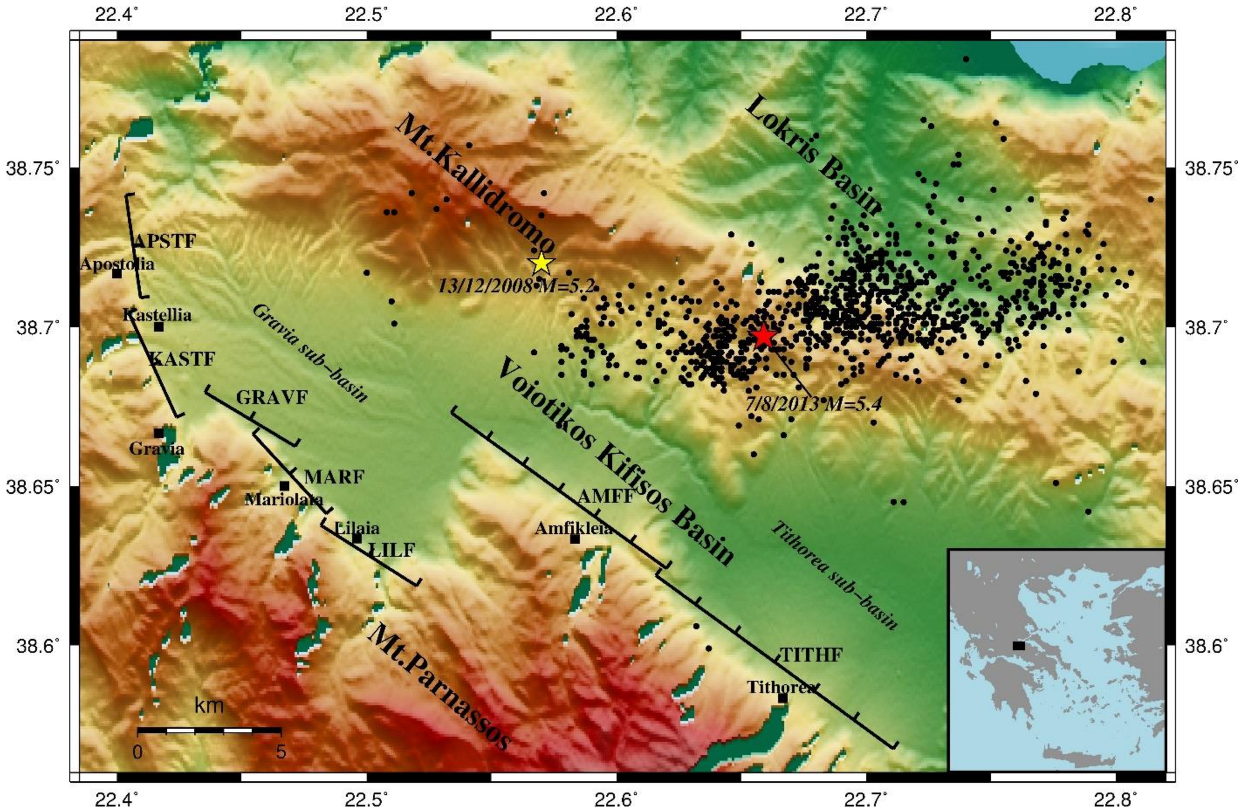

Figure 1.4 Seismicity and activated faults of Voiotikos Kifissos basin (modified from Kranis, 1999). The epicenters of the Amfikleia 2013 seismic sequence are shown with the black dots. The mainshock epicenter is shown with the red star. The 2008 M5.2 event is depicted by a yellow star. Black lines represent normal faults. APSTF: Apostolia, KASTF: Kastellia, GRAVF: Gravia, MARF: Mariolata, LILF: Lilaia, AMFF: Amfikleia and TITHF: Tithorea.

The Amfikleia sequence started from the median flow section within the Voiotikos Kifissos basin and migrate progressively towards the SE part of the Lokris basin. The linear pattern of the sequence reveals the activity of an ENE–WSW striking fault. The mainshock epicenter is located north of Amfikleia and Tithorea faults and, therefore, it could be attributed to one of them. According to the aforementioned analysis for the broader study area there is no evidence to support activity on a ENE–WSW striking normal fault at the surface. However, Miggiros et al., (2010) suggested that Modi and Reginio basins are bounded by active normal faults striking almost E-W and dip to the south. In this frame, the sequence might be associated with an antithetic to the Amfikleia and Tithorea faults. The absence of surface rupture may indicate the reactivation of a pre-existing normal fault that strikes ENE–WSW.

The mainshock caused severe structural damages (wall cracks and plaster falls) at the nearby Kallidromon villages (**Fig.1.5**). The most damage was reported at the oldest buildings and some churches whilst hospitals and schools remained functional. Reginio village suffered the greatest damage where more than 35% of the houses were classified as uninhabitable. There were also limited landslides and rock falls that didn’t cause severe traffic interruptions (Ganas et al., 2014, Delaportas, 2016).

Figure 1.5 Structural damages caused by the Amfikleia earthquake on August 7, 2013 (Delaportas, 2016).

1.2 Past Seismicity

The study area is characterized by moderate earthquakes during the instrumental era. The most recent moderate event was the M=5.2 on the 13th of December 2008 which occurred in Voiotikos Kifissos basin close to the Amfikleia (**Fig.1.4**). It is mapped 8.3 km west of the 2013 main event and its aftershock distribution shows an ENE-WSW striking fault. The epicenter of this event is located north of Lilaia, Mariolata and Gravia faults, thus it could probably linked to an antithetic to one of these (Valnakiotis, 2009, Karamanos et al., 2010, Roumelioti and Kiratzi, 2010).

Notable historical events (M> 6) that were reported in the vicinity of the study area, include: the 426 BC at Skarfia, the 226 BC at Tithorea, the 279 BC at Delphoi, the 1740 AD at Thermopylae and the 1894 AD double event at Atalanti (Guidoboni et al., 1994, Ambraseys and Jackson 1997, Papazachos and Papazachou, 2003). The latter double event (M=6.4 and M=6.6) is associated with the Atalanti Fault in the Lokris area. This fault is a large (~60 km) active normal fault that strikes WNW-ESE and dips to the northeast (Ambraseys and Jackson, 1990, Ganas et al., 1998, Pavlides et al., 2004, Savaidis et al., 2012). The earthquakes demolished thousands of properties and severe loss of life was reported (Ganas et al., 2006).

CHAPTER 2: EVALUATION OF THE SEISMIC SEQUENCE

Examination of spatial, temporal and magnitude distribution of earthquakes in a sequence is vital for estimating the occurrence of the strongest earthquake, understanding the underlined physics of the seismic source and comprehending local seismic processes. One of the oldest ways to evaluate a seismic sequence is the illustration of hypocenters distribution on maps and cross sections. This way of display is valuable because spatial distribution is non-random thus, it reveals information about the fault dimensions and kinematics and allows the identification of subsurface fault planes (Eneva and Hamburger, 1989). Analysis of temporal and magnitude distributions statistically confirms the empirical scaling laws that describe the aftershock process (Ranalli, 1969). Such analysis provides essential information about the type of sequence, the migration of seismic activity and the periodicity of strong events.

2.1 Introduction

Earthquakes are natural phenomena that are related with slip on faults. Generally, earthquakes are not individual events and their occurrence is characterized by clustering in time and space. Earthquake clustering is the most remarkable attribute of the observed seismicity (Zaliapin et al., 2008). Numerous methods have been developed based on space- time clustering to forecast future seismicity (Sornette and Sornette, 1990, Utsu et al., 1995, Morales-Esteban et al., 2010, Hashemi and Karimi, 2016). Specifically, earthquake forecasting requires an adequate understanding of a short-term clustering where numerous, nearby events occur in a narrow space- time window. Earthquakes that occur very close in space and time can be correlated to magnitude as well (Lippiello et al., 2009) thus, providing reliable information about the properties of earthquake occurrence. This short- term clustering is called seismic sequence and has been categorized into three types: the mainshock sequence which is the most common, the foreshock sequence and the swarms. A first attempt to classify the sequences was made by Mogi (1963) who presented three frequency curves from three different sequences that displayed the number of their events as a function of time (days)

(**Fig.2.1**). Each curve shows a different pattern according to the temporal distribution of the events comprised in each data set. The classification of a sequence can only be done retrospectively by examining the whole collection of the recorded data. The definitions of three types of sequences are described below.

Mainshock sequence

A mainshock sequence is identified by at least one dominant event that is followed by many smaller earthquakes or aftershocks. The dominant event is characterized by the largest magnitude and is called mainshock.

Generally, the larger the magnitude of the mainshock, the larger and much more the aftershocks will be and the higher the occurrence rate will be. The above relation has been expressed by three empirical scaling laws of *Gutenberg- Richter (1954), Omori (1894) and Båth (1965).* According to the frequency- magnitude power law of Gutenberg- Richter (1954), the amount of aftershocks depend on the magnitude of the mainshock. Omori (1894) proposed that the rate of aftershocks temporarily decay. Båth (1965) suggested that the largest aftershock after the mainshock has an average magnitude of about 1.2 smaller than the mainshock magnitude.

Foreshock sequence

A seismic sequence is considered as foreshock sequence when it starts before the mainshock occurrence with smaller magnitude events that are called foreshocks. Foreshocks usually occur in close proximity to the mainshock hypocenter (Das and Scholz, 1981). The foreshock activity is characterized by earthquake migrations associated with aseismic slip toward the mainshock nucleation point (Kato et al., 2016, Tamaribuchi et al., 2018, Yabe and Ide, 2018). Mainshock's occurrence is followed by aftershocks as they described in the mainshock sequence.

Swarms

A swarm activity does not include any dominant event among the others thus a mainshock is unidentifiable. All the stronger earthquakes have similar magnitudes and they usually occur for a relatively short period, they can continue from days up to months. Swarms do not obey the Omori law or Båth's law.

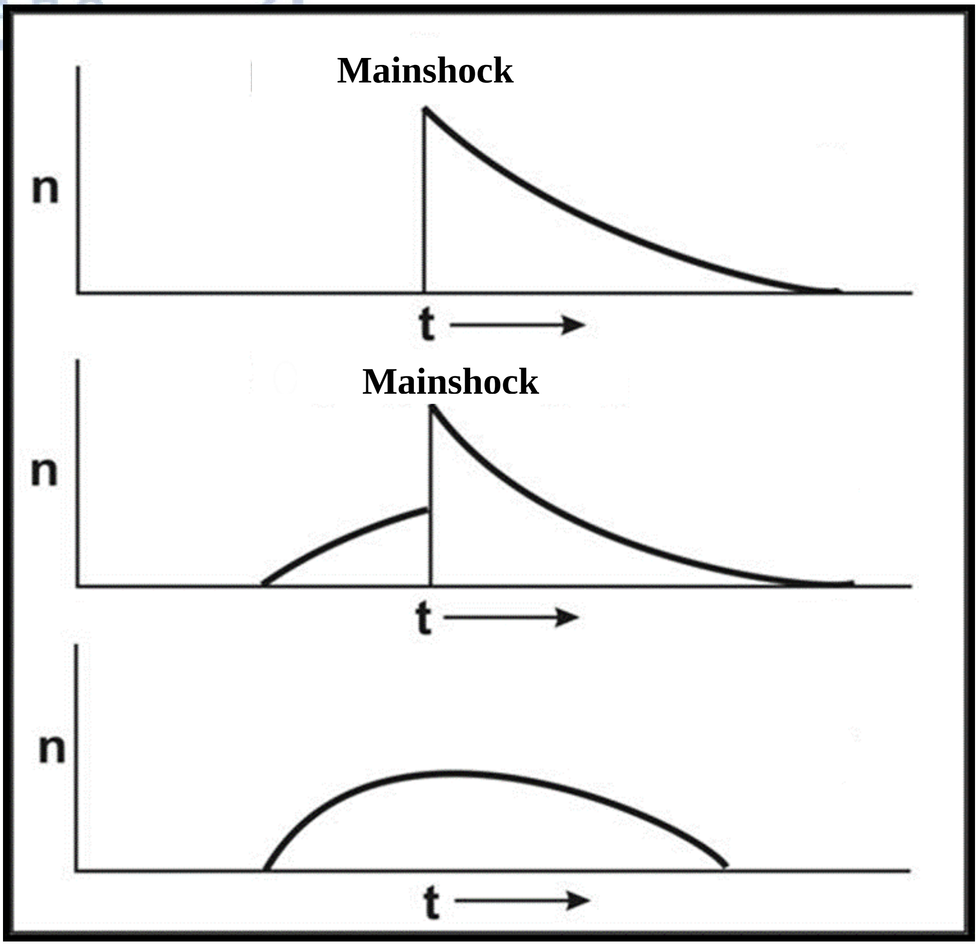

Figure 2.1 Schematic diagram showing the three types of earthquake sequences (Mogi, 1963).

The aforementioned empirical scaling laws have been widely used in order to describe seismicity in space, time and magnitude. One of the fundamental empirically derived relationships is the Gutenberg- Richter law which describes the frequency- magnitude distribution (FMD):

$$\log N(m) = a_N + b_N m \qquad \text{Eq. (2.1).}$$

Where N(m) is the number of earthquakes with magnitudes equal or larger than magnitude m and a_n and b_n are the corresponding parameters. The b- value describes the ratio of large to small earthquakes. Large b-values indicate areas with a higher proportion of smaller magnitude earthquakes, while small b- values characterize areas with an increased occurrence of strong events. The a- value describes the total number of earthquakes and m is the magnitude of interest.

Omori (1894) investigated the occurrence of aftershocks and suggested an equation that describes the temporal decay of aftershock rate. This equation was refined later by Utsu (1961) and is known as the modified Omori law or the Omori- Utsu law:

$$n(t) = K(t + c)^{-p} \qquad \text{Eq. (2.2).}$$

Where n(t) is the frequency of aftershocks per unit time, K, c and p are constants, t is the elapsed time since the mainshock and it is usually measured in days. K is associated with the aftershock productivity that describes the number of the aftershocks that could be triggered by a mainshock as a function of its magnitude. P and c values characterize individual mainshock sequences (Utsu, 1961, 1969). The p value is the power law exponent and determines the speed of decay in the aftershock rate, its value range is typically from 0.8 to 1.2 (Utsu et al., 1995). The c value is related to the difficulties in recording small, early aftershocks after the mainshock (Kagan, 2004, Peng et al., 2007).

Another well-known scaling law is Båth's law which declares that the average magnitude difference between a mainshock and its largest aftershock is approximately constant and it usually equals 1.2, without depending on the mainshock magnitude (Båth, 1965). Båth's law significance stems from the fact that it is possible to calculate the maximum expected magnitude of an aftershock in a certain seismic sequence.

2.1.2 Origin of the earthquake sequences

Earth's lithosphere which includes the crust and the brittle uppermost part of the mantle is divided into tectonic plates. Beneath the brittle lithospheric layer lies the semi fluid asthenosphere that includes the ductile region of the upper mantle. The viscous flow of the asthenosphere is transmitted to the lithosphere by the deep mantle convection currents and cause the interaction (movement) of the tectonic plates. When the tectonic plates interact in response to persistent forces applied to their boundaries an amount of stress is concentrated. This amount of stress is built-up to a level that will cause slip to occur on tectonic plate boundaries and pre-existing faults, resulting to an earthquake. After the earthquake, the fault locks until the stress reaches a sufficient level which will cause displacement, resulting in the next earthquake. During the stress accumulation, elastic energy is stored in the rocks around the fault and when displacement occurs this energy is dissipated in the form of frictional heat and seismic waves. This process is known as elastic rebound (Reid, 1910).

The occurrence of earthquakes can alter the stress state in the vicinity of their ruptured areas. Such instabilities in the stress state can trigger further seismicity. Stress loading on the rupturing fault originates from two separate contributions (Marsan et al., 2013):

1) tectonic loading which is related to the motions of the tectonic plates and the associated stress regime. Additionally, aseismic forcing such as fluid flow, magmatic intrusions, or slow slip events can change the stress state and trigger further seismicity,
2) elastic loading which is associated with stress changes from previous earthquakes.

These two contributions are generally related to mainshocks and their accompanied aftershocks, respectively. Thus, *seismic sequences* are generated by stress perturbations during rupture propagation and they emerge from tectonic loading or an aseismic phenomenon such as fluid pressure transient (Marsan et al., 2013, Reverso et al., 2015). Events that are triggered by stress changes from the mainshock or other preceding earthquakes are classified into the *mainshock type* (Mogi, 1963). *Swarm* sequences are usually caused by fluid or magmatic intrusions and they can be observed in volcanic or geothermal areas (Vidale and Shearer, 2006, Pacchiani and Lyon-Caen, 2010, Daniel et al., 2011, Llenos & McGuire, 2011).

Seismic sequences that develop in the vicinity of the geothermal fields or volcanic areas are sometimes characterized by hypocenter migration. This is considered to be caused by fluid movement and pore pressure relaxation (Antonioli et al., 2005, Lombardi et al., 2010). When the fluid intrudes the rock pores it induces higher pore pressure and reduces the stress concentration to the fault. These changes in stress state promote the seismic failure (Yoshida and Hasegawa, 2018, Yazdi, 2019).

2.1.2.1 Asperity and barrier models

Various models have been developed in order to describe the way that foreshocks and aftershocks are generated. The most frequently used are the asperity model and the barrier model which can adequately interpret the occurrence of foreshocks and aftershocks, respectively (**Fig.2.2**). Both asperities and barriers are patches of the fault plane that resist breaking (Aki, 1984). According to the asperity model (Kanamori and Stewart 1978), stress drop is high before the mainshock due to the breaking of these asperities. After the mainshock, stress drop is decreased due to slippage that occurs along the entire free fault surface where there isn't stress accumulation. Thus, mainshock in this model is considered as a stress-smoothing process.

According to the barrier model (Aki, 1979), stress drop is low before the mainshock because rupture propagates over the fault plane leaving barriers unbroken. After the occurrence of mainshock, stress drop is increasing due to the release of stress concertation around barriers through static fatigue. Therefore, the barrier model represents the mainshock as a stress-roughening process.

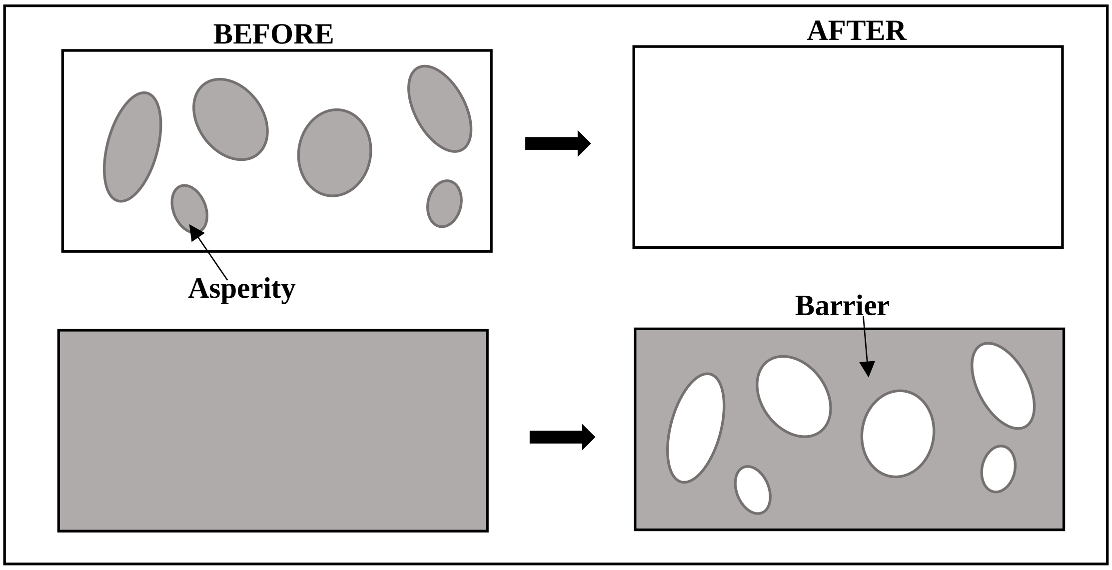

Figure 2.2 Asperity (top) and barrier (bottom) models, before and after the occurrence of the mainshock. Modified from Aki, 1984.

2.2 Retrospective of earthquake sequences research in Greece

The first research about earthquake sequences in Greece was made by Galanopoulos (1955) who studied the 1953 seismic sequence in Cephalonia. He described the elastic relaxation of the aftershock area and he reported the macroseismic effects.

Papazachos et al. (1967) investigated the deformation characteristics, the magnitude and temporal distribution of 40 seismic sequences occurred in Greece between 1926 and 1964. It was shown that the magnitude of the largest aftershock is related to the magnitude of the mainshock and the largest aftershock could occur within 14 days after the mainshock. It was observed that the b-value of the cumulative frequency function of the magnitude is decreasing with depth. It was also observed that the b-value for foreshocks is smaller than the b-value for aftershocks.

Comninakis et al. (1968) examined the magnitude, the temporal and the spatial distribution of the foreshock and mainshock sequences occurred in the artificial lake of Kremasta. They evidenced that the earthquake activity is related to the water loading of the artificial lake. They also demonstrated that the b-value of reservoir-associated seismic sequences is larger for foreshocks than for aftershocks. These results have been ascertained by Gupta et al. (1972) and Papazachos (1974).

Papazachos (1971) used a data set of 216 mainshock sequences occurred in the Greek region between 1911 and 1969. He proposed a relation between the number of the aftershocks (N) and the magnitude of the mainshock (Mo):

$$\log(N) = -3.7 + 0.74Mo \qquad \text{Eq. (2.3).}$$

It was also found that the average value of the difference between the magnitude of the mainshock and the magnitude of the largest aftershock equals 1.1. This difference doesn’t depend on the magnitude of the mainshock.

Papazachos (1975a,b) investigated the temporal and magnitude distribution of foreshock sequences and ascertained that b-values are smaller before the mainshock than after it. He also determined that the average value of the difference between the magnitude of the mainshock and the magnitude of the largest foreshock equals 1.9 and this difference is independent of the magnitude of the mainshock.

The Thessaloniki 1978 seismic sequence of the M=6.5 mainshock has been investigated by numerous researchers (Carver and Henrisey, 1978, Fintel, 1978, Kulhanec and Meyer, 1979, Carver and Bollinger, 1981, Soufleris and Stewart, 1981, Papazachos et al., 1983, Paradisopoulou et al., 2006, Roumelioti et al., 2007). This sequence occurred in the Mygdonian graben, almost 25 km northeast of the city of Thessaloniki which is the second major Greek city. The sequence caused extensive damage to villages around the epicenter and to the city of Thessaloniki, the death toll was 45. Papazachos et al. (1983) indicated that the spatiotemporal and magnitude distribution of the smaller earthquakes in the sequence could have helped to predict the mainshock.

Karakaisis (1984) investigated the spatial distribution of several foreshock and mainshock sequences that took place in the broader Aegean area for the period 1970-1983. He proposed a relation between the magnitude of the mainshock and the length of the aftershock area. He assessed the b-values of the foreshock and mainshock sequences and found that the average b-value for the foreshock sequences is 0.71 and the average b-value for the aftershock sequences is 1.08.

Scordilis et al. (1985) examined the seismic sequence of the 1983 (M=7) mainshock in Cephalonia island. He concluded that the spatial distribution of the foci, the fault pane solutions of the mainshock and the largest aftershock and the geomorphological information evidence the existence of a right- lateral transform fault at the northwestern boundary of the Hellenic arc. The existence of this fault has been ascertained by Anderson and Jackson (1987), Papazachos et al., (1991, 1998) and Papadimitriou (1993).

The Kozani-Grevena earthquake sequence of the 1995 (M=6.6) mainshock has been researched by many scientists (Hatzfeld et al., 1995, 1997, 1998, Papazachos et al., 1998, Mountrakis et al. 1998, Karakaisis et al., 1998). The data set obtained from a portable network in the area revealed useful information about the 3D velocity structure of the region and the geometry of the activated fault. The seismic activity was possibly related to the water loading of the Polyfytos artificial lake (Papazachos et al., 1998, Karakaisis et al., 1998).

Papadimitriou et al. (2001) examined whether a strong earthquake can bring the next strong mainshock of a seismic sequence closer to failure. The study area was the broader Aegean Sea. They discovered that after a strong earthquake the next strong mainshock occurred in areas of high values of positive Coulomb stress changes (ΔCFF). The ΔCFF were calculated soon after the strong earthquake.

The 2003 Lefkada sequence of the (M=6.2) mainshock has been investigated by Karakostas et al. (2004). The seismic activity was related to the Cephalonia Transform Fault (CTF). Particularly, the aftershocks distributed along the Lefkada and the northern part of the Cephalonia faults which are segments of the CTF. Calculations of Coulomb stress changes (ΔCFF) caused by the (M=6.2) mainshock evidenced future seismicity.

Karakostas et al. (2015) and Sokos et al. (2015) evaluated the 2014 Cephalonia seismic sequence of the earthquake doublet (Mw6.1 and Mw6.0). They defined the kinematic and structural properties of the activated fault, the seismotectonic properties of the study area and the fault plane solutions.

Kostoglou et al. (2020) investigated the 2019 seismic swarm that took place in the offshore region north of the Lefkada Island. The seismic activity was located at the junction between the Kephalonia Transform Fault Zone (KTFZ) and the collision between Adriatic and Aegean microplates. The geometry and kinematics of the associated faults were delineated revealing the seismotectonic properties of the area. The temporal variation of the b-value was examined in order to separate the foreshock from the aftershock phase.

2.3 Spatial distribution of the seismic sequence

Figure 2.3 illustrates the spatial distribution of the epicenters in the area of Amfikleia where different magnitude ranges are denoted with different symbols and colors, the mainshock epicenter is depicted by the pink star. The aftershocks are color coded by a 20 day time interval for 360 days in total since the mainshock. The total number of aftershocks is 1080 and they occurred in an almost a year interval since the mainshock. From the map view is revealed an ENE- WSW striking zone that covers an area with a total length of 18 km.

Based on the color code of the aftershocks it appears that the seismic activity propagates towards the east. The aftershocks occurred during the first 80 days cover the majority of the rupture zone. Most of the aftershocks occurred during the first 20 days. These aftershocks occupy the entire western part of the rupture zone, reaching up to the central part. After the first 80 days the rate of aftershocks is decreasing and aftershocks are located at the eastern part of the rupture zone.

In figure 2.3, it is possible to observe that the seismic excitation forms two main clusters (dashed rectangles) corresponding to the mainshock and the largest aftershock. The clusters may be attributed to the activation of adjacent fault segments.

The westernmost cluster encompasses earthquakes that took place during the first 20 days. The key features in this cluster include the mainshock, the majority of $M \geq 4.0$ events and a moderate earthquake with magnitude M=5.0 that is close to the western end.

The easternmost cluster encompasses the aftershocks that occurred throughout the seismic sequence comprising the second largest aftershock (M=5.3) and several aftershocks with $M \geq 4.0$. Cross sections of the seismic activity will be discussed in the next chapter along with the fault plane solutions.

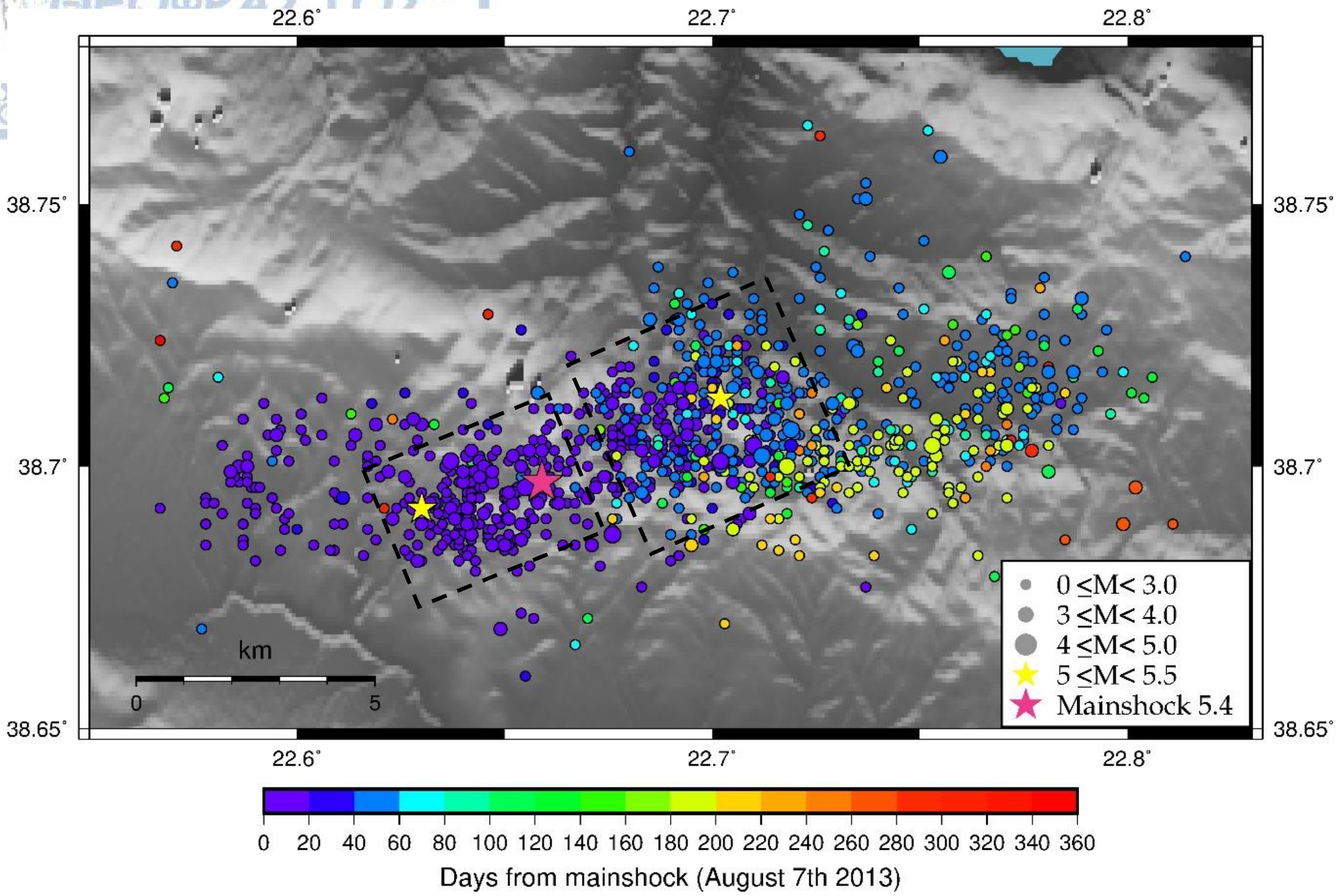

Figure 2.3 Spatial distribution of the seismicity**,** magnitudes are plotted with different colors and symbols. Aftershocks are color coded as a function of time (days) from mainshock.

2.4 Space- time distribution of the seismic sequence

Spatiotemporal distribution illustrates the distance of each epicenter from the dominant strike of the aftershock zone against time. Time is measured in days since the mainshock. Spatiotemporal distribution generally defines seismicity patterns including seismic migration and areas of seismic activity and seismic quiescence. Areas of seismic quiescence which are also pronounced lulls are probably attributed to the decrease in stress due to slip weakening prior to a large earthquake and they are usually last from hours to days (Scholz, 1988, Main and Meredith, 1991). Seismically active areas imply stress changes associated with the coseismic slip of previous strong events and trigger off fault aftershocks (Papadimitriou and Sykes, 2001, Rhoades et al., 2010, Karakostas et al., 2014, 2015, Papadimitriou et al., 2017). A spatiotemporal distribution analysis can also help to delineate which segments of the fault have been activated during the seismic excitation. As can be seen in figure 2.4 the epicenters migration can evidence the activation of different fault segments.

Figure 2.4 (a., b.) shows the space time plot where different colored symbols denote earthquakes belonging to different clusters. Magnitude ranges are also depicted by the use of different symbols. It is observed that the seismic activity is propagated towards the east. For the first ten days the seismicity (blue symbols) was developed in a cluster (**Cluster A**) which occupied 10.4 km in length. Seismic sequence started with an M=4.2 earthquake on 7 August (0 day on the time axis), followed by the mainshock M=5.4 after four minutes. The activity after the mainshock propagated to the east and then within two days to the west where an M=5 event (orange star) struck and most of the $M \geq 3$ aftershocks occurred. After a few days the number of events gradually decreased and the activity migrated 1.3 km to the east (yellow symbols) where two $M \geq 4$ events struck. The length of this cluster (**Cluster B**) is about 3.6 km. After a few days the activity began to cease. Forty days after the beginning of the sequence, the second largest aftershock struck (M=5.3). The seismic activity propagated 6 km to the east, the total length of this cluster (**Cluster C**) is 10 km. After a few days, the aftershock activity appears to decay as a function of time. A fourth cluster is noticed initiating from the 182nd day (**Cluster D**) defining the final shape of the aftershock zone. This cluster includes two $M \geq 4$ events and its total length is 7.2 km.

The strongest earthquakes ($M \geq 5$) of the seismic sequence which occurred during the first forty-one days seem to be associated with the activation of three fault segments as illustrated in figure 2.4 b. These earthquakes correspond to the August 7 mainshock of M=5.4 (0 day on the time axis), the August 10 earthquake of M=5.0 (2nd day on the time axis) and the September 16 earthquake of M=5.3 (40th day on the time axis). The length of each segment is delimited by black rectangles which equals to 5.8 km, 4.2 km and 5.5 km.

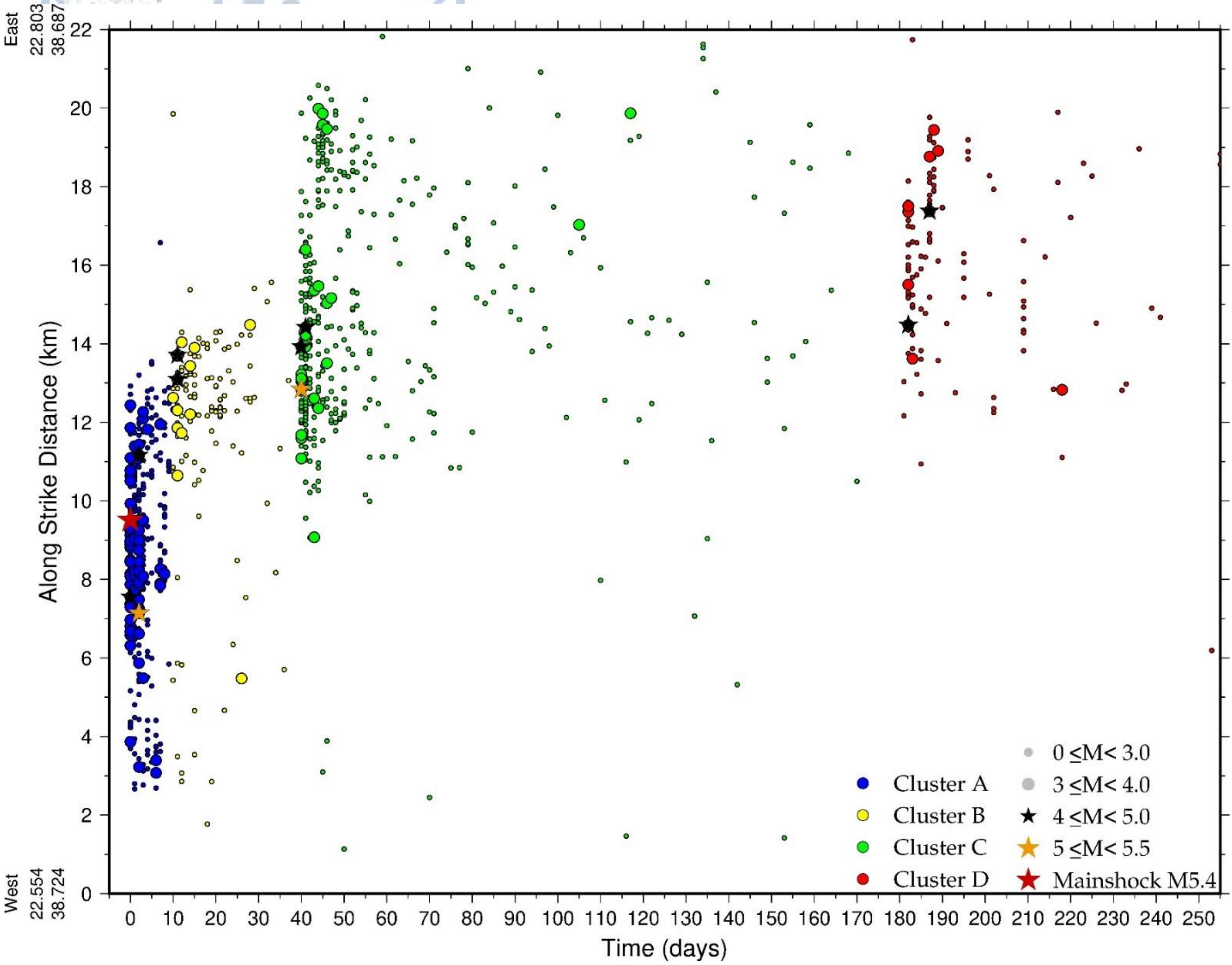
East
22.803
38.687
West
22.554
38.724
Along Strike Distance (km)
Time (days)
Cluster A
Cluster B
Cluster C
Cluster D
0 ≤M< 3.0
3 ≤M< 4.0
4 ≤M< 5.0
5 ≤M< 5.5
Mainshock M5.4

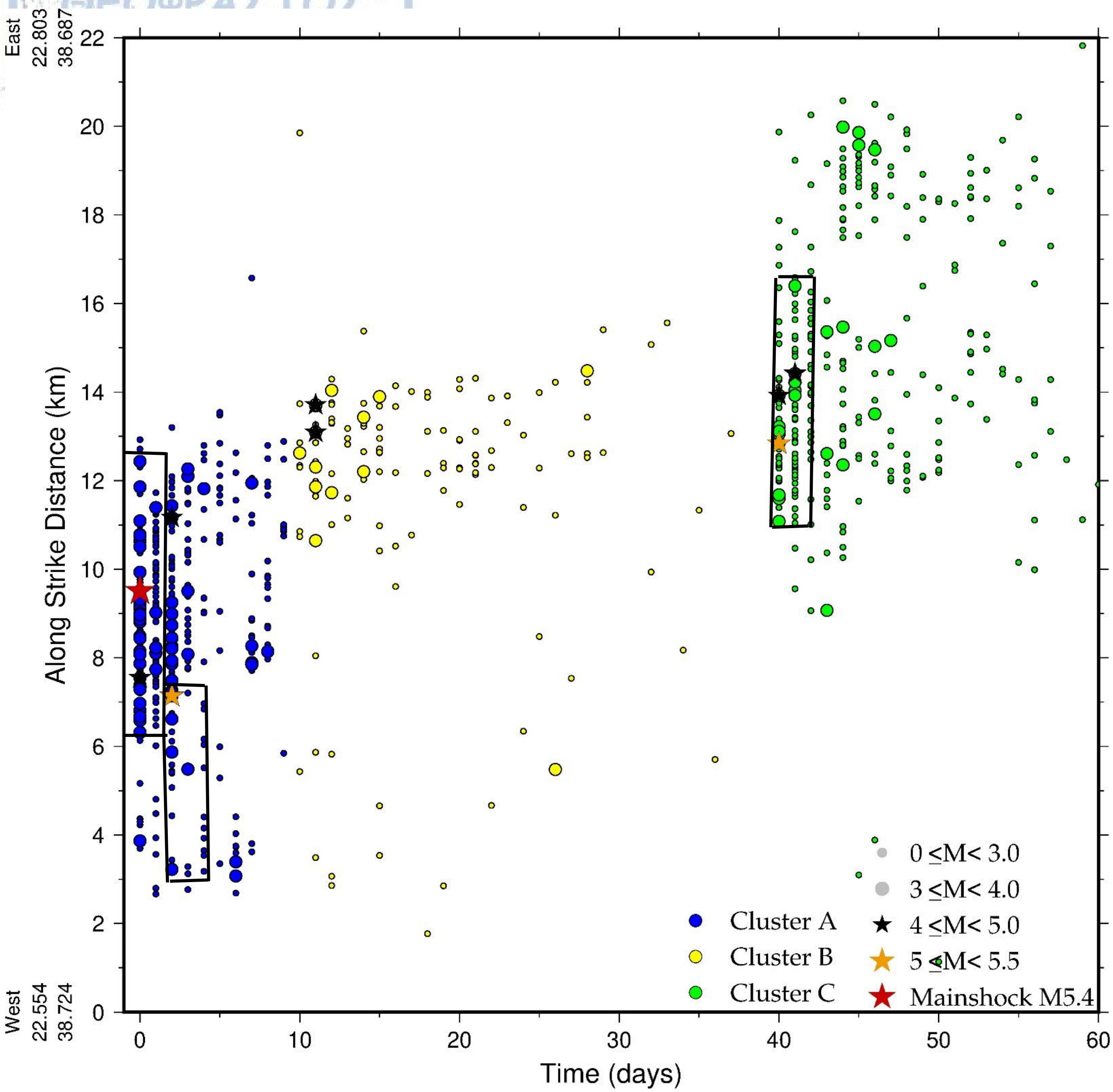

Figure 2.4 a., b. Space-time distribution of the Amfikleia sequence. The clusters and the earthquake magnitudes are plotted according to the symbols and colors shown in the legend, b. The length of each fault segment is delimited by black rectangles.

2.5 Magnitude distribution of the seismic sequence

2.5.1 b-value

The concept of determining the magnitudes of earthquakes was introduced by Richter in 1935. Most of the times, magnitude is expressed by the maximum recorded amplitude of the seismic wave and it is measured on the seismogram (Woessner et al., 2010). Ishimoto and Iida (1939) and Gutenberg and Richter (1944) proposed a relation that characterizes the distribution of the number of earthquakes by their magnitudes (FMD). This law has been above-mentioned (Eq.(2.1)) and it is:

$$\log N = a - bM$$

where N is the cumulative number of earthquakes with magnitude equal to and larger than M, a and b are constant coefficients that are identified by observations.

The b-value depends on the stress regime (Mogi, 1962, 1963, Scholz, 1968, Mori and Abercrombie, 1997, Wiemer and Wyss, 2002, Singh and Chadha, 2010), the mechanical structure of materials in the focal area (Mogi, 1962, Scholz, 1968, Tsapanos, 1990) and the tectonic characteristics of a region (Allen et al., 1965, Karnik, 1969, Hatzidimitriou et al., 1985, Tsapanos et al., 1994, Wiemer and Baer, 2000, Kalyoncuoglu, 2007). It expresses the rate at which the number of earthquakes is increased whilst their magnitudes are decreased (Papazachos et al., 1967).

b-values range from 0.4 to 1.8 (Miyamura, 1962) and according to Papazachos (1974) they can be used to characterize the type of a sequence. Relatively large b-values (>1.0) correspond to mainshock sequences, even larger values are typical for swarms whilst relatively small b-values (<0.7) characterize foreshock sequences.

Although the b-value has been observed to vary in space, time and depth, it is commonly found to be constant (~1.0) (Frohlich and Davis, 1993, Abercrombie, 1996, Wesnousky, 1999). Global and regional studies showed that the b-value varies considerably on a regional scale (Mogi, 1979, Tsapanos, 1990) but on a global scale the variation of this parameter is not significant (Frohlich and Davis, 1993).

The temporal variation of b-value has been studied by Mogi (1962) who has attempted to relate b-values to the mechanical properties of materials. From a series of laboratory tests based on the fracture of rocks he suggested that:

a) The experimental relation between magnitude and frequency of earthquakes was satisfied for the fracturing phenomena in heterogeneous materials. The b-value was decreased before the fracture of specimens and it was increased remarkably after it. This fracture could be attributed to a mainshock thus decreased b-values were associated with foreshocks and increased values were related to aftershocks.

b) The b-value was increased with the degree of the structural heterogeneity and the spatial distribution of stress.

The depth behavior of b-value has been studied by Mori and Abercombie (1997) in the California region. They have demonstrated that b-value becomes lower with increasing depth of earthquakes. Consistent results have also been found by other researchers who have shown an inverse proportion between the b-value and depth (Gutenberg and Richter, 1944, Papazachos et al., 1967, Curtis, 1973, Wyss, 1973, Heety 2011, Popandopoulos and Lukk, 2014).

The dependence of b-value on the seismotectonic characteristics of a region has been shown by Papazachos (1999) who divided Greece and the surrounding area into seismic zones according to the spatial distribution of the b-value. The data covered the period from 1911 to 1995. The results showed that b-values were decreased from the outer-arc to the back-arc area.

One more investigation of the spatial distribution of the b-value in the broader Aegean area has been performed by Vamvakaris et al. (2016). In this work the catalog covered the period from 550 BC to 2008 and according to seismotectonic criteria the area of interest was divided into 113 shallow seismic zones. b-values were estimated for each seismic zone (**Fig.2.5**) and the results were in good agreement with the above-mentioned zonation model (Papazachos, 1999). Older studies about the spatial variation of the b-value in the same area (Hatzidimitriou et al., 1985, 1994) are also in good agreement despite the different catalogs and the approaches that were used.

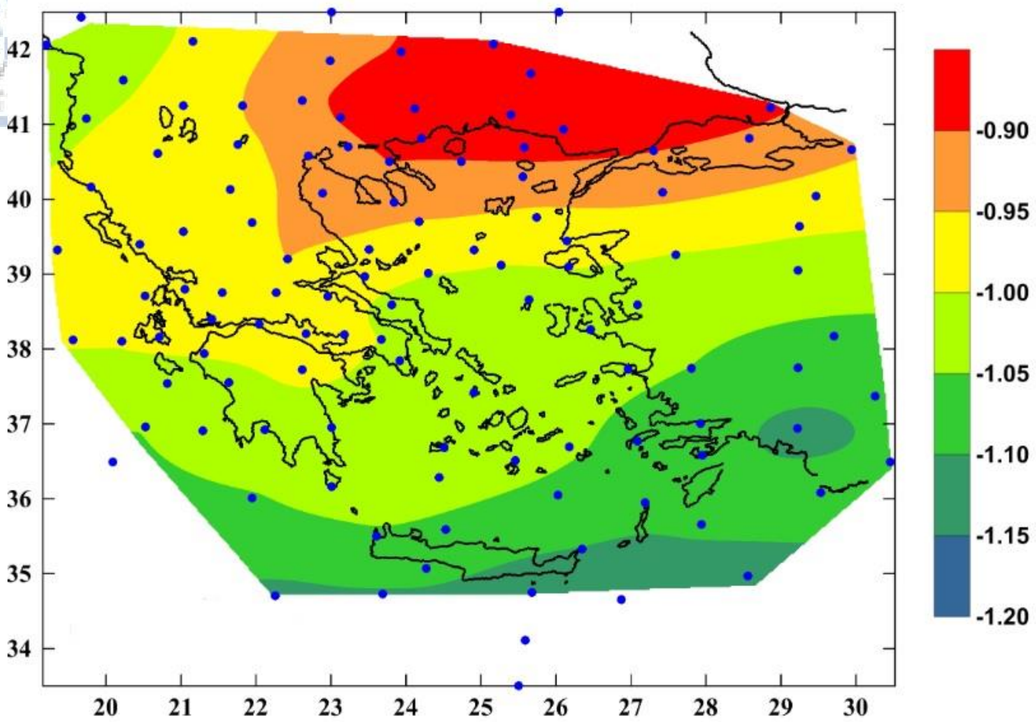

Figure 2.5 Spatial distribution of the b-value in the Aegean area and its surroundings (Vamvakaris et al., 2016)

2.5.2 Determination of completeness magnitude (M_c)

According to Wiemer and Wyss (2000) the determination of the magnitude of completeness (M_c) is essential for correctly calculating the b-value. The magnitude of completeness (M_c) is determined as the lowest magnitude above which all the earthquakes in a space-time window are detected (Rydelek and Sacks, 1989, Taylor et al., 1990, Mignan and Woessner, 2012). Bellow this value a fraction of events is missed by the seismological network because: a) network operators decided that events bellow a critical value are not to be processed, b) the events are too small to be recorded by a sufficient number of stations, c) the events are too small and their signals can't be distinguished from the background noise on the seismogram and d) the events in a case of a mainshock sequence are too small to be detected within the coda of larger ones (Mignan and Woessner, 2012).

A reliable M_c calculation is critical, a larger value decreases the number of available data due to smaller sample sizes. This could result to a reduced spatial and temporal resolution and an increased uncertainty rate. On the other hand, a lower M_c value could lead to incorrect determination of the seismic parameters a and b due to the incompleteness of a catalog (Huang et al., 2016).

The assessment of M_c of earthquake catalogs is required for any seismicity analysis since catalogs are not complete over the magnitude range that they cover. The data contained in earthquake catalogs are the result of signals that are recorded by spatially and temporally heterogeneous seismological networks. The records are processed by humans with the help of software that is based on assumptions (Zuniga and Wiemer, 1999). Thus, catalog data are usually heterogeneous and/or spatiotemporally inconsistent (Woessner, 2005, Yadav et al., 2009, Mignan and Woessner, 2012).

2.5.2.1 Methodology

The M_c value could be estimated by visual examination of the frequency-magnitude distribution (FMD) plot (**Fig.2.6**). M_c could be denoted as the magnitude increment at which the FMD deviates from a linear trend at small magnitudes. Deviations from theoretical linearity at small magnitudes are explained by the incompleteness of the catalog due to the defective detection capability of the networks as above-mentioned. At large magnitudes, deviations that are observed may be due to statistical fluctuations because of the under-sampling (Rydelek and Sacks, 1989). A quantitative criterion to estimate the M_c is usually preferable than visual examination (Wiemer and Wyss, 2000).

The magnitude of completeness (M_c) estimation depends on two different types of methods. The first type is based on the properties of the seismological network whilst the second one is catalog-based, which only uses catalog data. Network-based methods use waveform data to measure the signal-to-noise ratio (Sereno and Bratt, 1989, Gomberg, 1991, von Seggern, 2004) or phase-pick data (Schorlemmer et al., 2010b, Plenkers et al., 2011). The methods that depend on the earthquake catalog are divided into two different groups. On the first group it is assumed that during the night the earthquakes that are detected are less due to the decreased level of noise. On the contrary, during the day-time the level of noise is increased due to human activity thus the number earthquakes is higher. Therefore, the magnitude of completeness is estimated using the day-to-night ratio of earthquake frequency (Rydelek and Sacks, 1989, Taylor et al., 1990, Gorbatikov et al., 2004, Vassallo et al., 2008). The second group relies on the assumption of self-similarity of the earthquake process, which implies that the cumulative frequency-magnitude distribution (FMD) should be consistent with the Gutenberg-Richter Law (Eq.(2.1)). Some of the methods that assume self-similarity are presented below:

1) Entire-magnitude-range method (EMR) (Ogata and Katsura, 1993 modified by Woessner and Wiemmer, 2005)

2) Maximum curvature-method (MAXC) (Wiemer and Wyss, 2000)

3) M_c by b-value stability (MBS) (Cao and Gao, 2002)

4) Goodness-of-fit test (GFT) (Wiemer and Wyss, 2000)

In the present study, the last method will be applied.

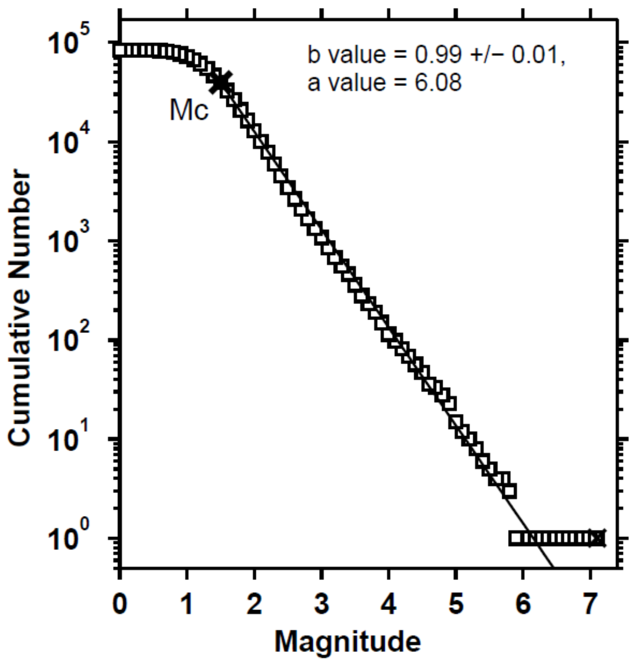

Figure 2.6 Cumulative frequency of earthquakes as a function of magnitude, the M_c value is 1.5. The slope and intercept of this straight line represent the b and a parameters of the G-R law, respectively. Example by Wiemer and Wyss (2002).

2.5.2.2 Goodness-of-Fit Test (GFT)

According to Wiemer and Wyss (2000), the magnitude of completeness (M_c) is found by comparing the observed frequency magnitude distribution (FMD) with the synthetic ones. Synthetic distributions are calculated with the maximum likelihood estimation of the a and b (Eq.(2.4)) parameters of the observed dataset for magnitudes greater than or equal to a cut-off (minimum) magnitude (M_{co}), as a function of the cut-off magnitude (M_{co}). The goodness-of-fit is evaluated by the parameter R which is the absolute difference of the cumulative number of events between the observed (B_i) and synthetic distributions (S_i). The absolute difference R is calculated for each magnitude bin as a function of the cut-off magnitude (M_{co}) (Eq.(2.4)). R is expressed in percentage and defines the confidence level at which the observed data can be modelled by respective power-law. A high R-value indicates that the dataset above a cut-off magnitude (M_{co}) is incomplete. Magnitude of completeness can be found at the first magnitude cut-off at which R falls below the line of 95% or 90% fit (Woessner, 2005, Yadav et al., 2009).

$$\mathrm{R}(\mathrm{a},\mathrm{b},\mathrm{M_{co}}) = 100 - \frac{\sum_{\mathrm{Mco}}^{\mathrm{Mmax}}|B_i - S_i|}{\sum_{\mathrm{i}}\mathrm{B_i}} \times 100 \qquad \text{Eq. (2.4).}$$

B-value is estimated by equation 2.5 (Aki, 1965, Bender, 1983, Lombardi, 2003, Kijko and Smit, 2012), where $\langle M \rangle$ is the mean magnitude of the sample and ΔM is the binning width of the catalog, here ΔM equals to 0.1.

$$\mathrm{b} = \frac{1}{\ln(10)\left[\langle \mathrm{M} \rangle - \left(\mathrm{M_c} - \frac{\Delta \mathrm{M}}{2}\right)\right]} \qquad \text{Eq. (2.5).}$$

Aki (1965) estimated the b-value accuracy (σ_b) (Eq.(2.6)), where N is the sample size.

$$\sigma_{\mathrm{b}} = \frac{\mathrm{b}}{\sqrt{\mathrm{N}}} \qquad \text{Eq. (2.6).}$$

2.5.3 Results

A seismic catalog containing 1079 events that occurred from 8 August 2013 to 5 August 2014 was used in order to determine the magnitude of completeness (M_c) and the b-value. Firstly, the completeness of magnitude was estimated by the goodness-of-fit test (GFT). The first magnitude cut-off at which the residual (R) was below the line of 95% confidence level was at 2.0. Thus, magnitude of completeness (M_c) is found equal to 2.0 and its corresponding residual (R) equals to 4.57. As shown in figure 2.7, residuals above an approximately value of M=2.9 are increased significantly. This could imply that theoretical distribution can't be sufficiently simulated at high magnitudes where there are less data.

As shown in figure 2.8, the cumulative frequency magnitude distribution (FMD) is modelled by a Gutenberg-Richter law (dashed line) and the b parameter of the power law was determined using the maximum-likelihood estimate (Eq.(2.5)). Cumulative distribution provides better linear fit instead of non-cumulative because numbers are larger and less degraded by statistics of small numbers (Kulhanek, 2005). As demonstrated in equation 2.5, the b-value depends on the choice of the completeness magnitude M_c. The b-value represents the slope of the cumulative frequency-magnitude distribution and it was found in the range $0.792<b<0.848$ with an average value of b= 0.82 ± 0.028. Figure 2.8 reveals that frequency above M= 3.5 decreases more rapidly than linearity and consequently the observed data doesn't modelled by a straight line. A possible explanation to this deviation could be an absence in continuity of faults capable to fail in earthquakes over a specific magnitude range (Console et al., 2015).

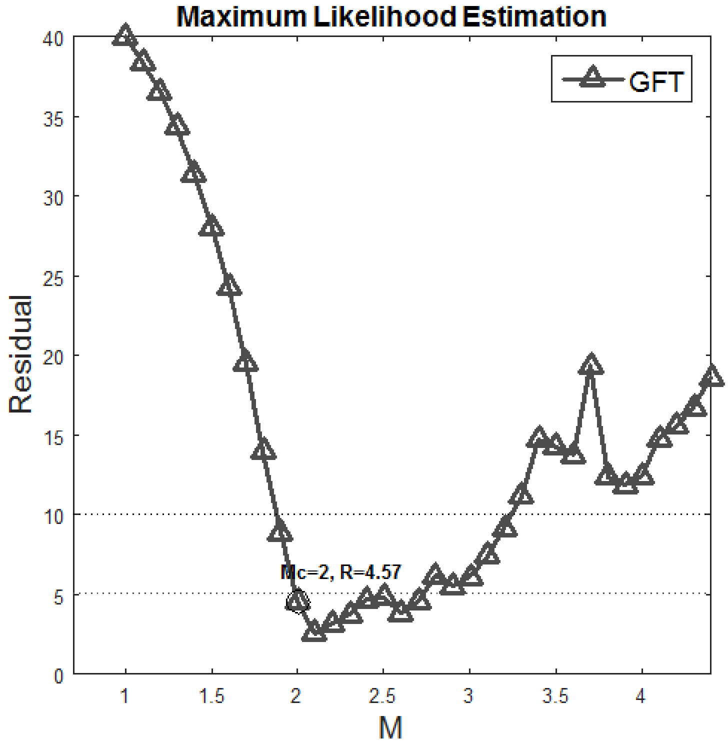

Figure 2.7 Residual plot which displays the absolute difference of the cumulative number of earthquakes between the observed and synthetic distributions. Black circle indicates the magnitude of completeness (M_c). The lower and upper dotted lines denote the 5% and 10% residuals, respectively.

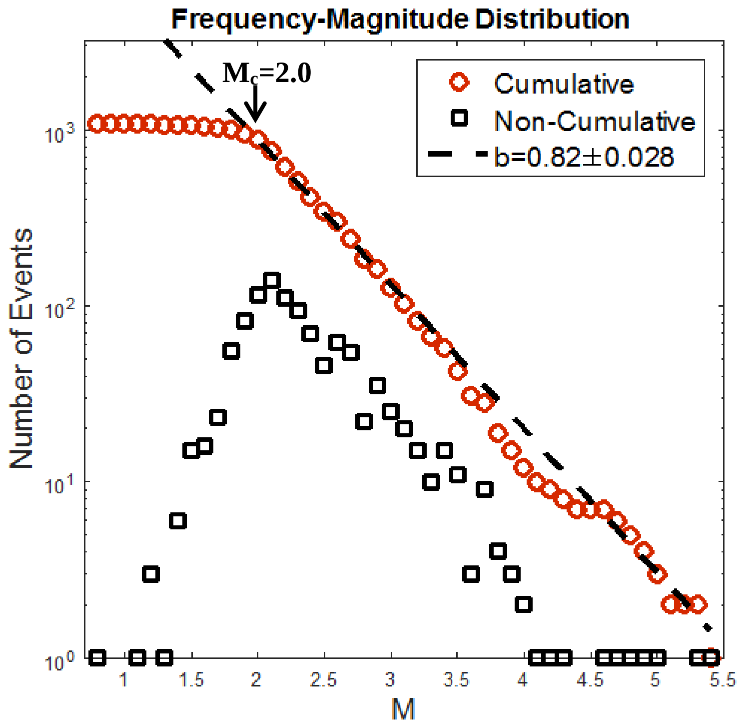

Figure 2.8 Frequency magnitude distribution of earthquake sequence of the 7, August, 2013 event. The b-value and its accuracy (σ_b) were calculated by the maximum likelihood estimation (Aki, 1965). Red circles and black squares indicate the cumulative and the non-cumulative number of events per magnitude bin, respectively.

2.5.4 Temporal and spatial variations of b-value

Temporal and spatial variations of the b-value have been employed in many seismicity studies. The drop in the b-value is interpreted by Scholz (1968) and Wyss (1973) as an increase in stress prior to an earthquake. Sammonds et al. (1992) showed that a large earthquake is frequently preceded by an increase in b-value which is followed by a decrease in weeks or months before the earthquake. Temporal variations within days and hours have been studied by Molchan and Dmitrieva (1990) and showed that b drops to half during a few hours before a mainshock. The hypothesis of b-value decrease prior to a large earthquake has been also supported by Monterroso (2003) and Nuannin et al. (2005) who used the temporal distribution of b-values in order to forecast major regional earthquakes. Spatial and temporal fluctuations of the b-value have been studied in order to determine the volume of active magma bodies (Wiemer et al., 1998) and to forecast mining tremors (Gibowicz, 1990, Holub, 1995, Gibowicz and Lasocki, 2001). Changes of b-values present statistical significance in seismically active areas such as subducting slabs (Wyss et al., 2001) and aftershock zones (Wiemer and Katsumata, 1999).

To examine temporal variations of b-value, a sliding time window with constant number of events technique was employed. A constant number of events in each window sample was used to avoid changes in sample size that could affect the analysis (Nuannin et al., 2005). A number of 50 events per sample was defined after several tests in order to achieve a reasonable compromise between required resolution and smoothing. The b-value was estimated for the first 50 events. Then, the time window was moved through the catalog event by event and the b-value was calculated for every window sample until the last event. The calculated values were plotted at the end of the considered time interval (Tormann et al., 2013).

Temporal variations of the b-value were computed with constant and fluctuated magnitude of completeness (M_c) per window sample (**Fig.2.9**). The M_c values could, as above mentioned, change in time and space due to a spatially and temporally heterogeneous seismic network. As can be noticed from the figures 2.9a) and 2.9b), there aren't any significant variations among them probably due to stability of the seismic network geometry since dataset covered a short period. In order to examine the temporal fluctuations of the b-value, the magnitude of completeness is considered constant.

Figure 2.9 exhibits the computed temporal variations of b during the evolution of the earthquake sequence. The horizontal axis displays time in days since mainshock (zero day), while the vertical axis shows the estimated b-values. Red asterisks illustrate events with M ≥4. The temporal variations of b (blue line) range from about 0.43 to 1.65. b-value peaks are easily observed in the plot by visual examination. There are four distinct drops (black arrows) in b-value, the first one is on the day of mainshock (zero day in time axis) while the others are observed after fourteen, forty and one hundred ninety days, respectively. All significant drops are in a good agreement with the events with M ≥4. The lowest peak in the b-value is discerned during the first day on which the mainshock occurred (M=5.4). After forty-one days the b parameter is successively increased, reaching the value of 1.65 which is the highest. Then it is gradually decreased and after about a hundred days it drops sharply (b=0.78). After two days, b-value is increased again and it is kept around 1.0 for the rest of the sequence.

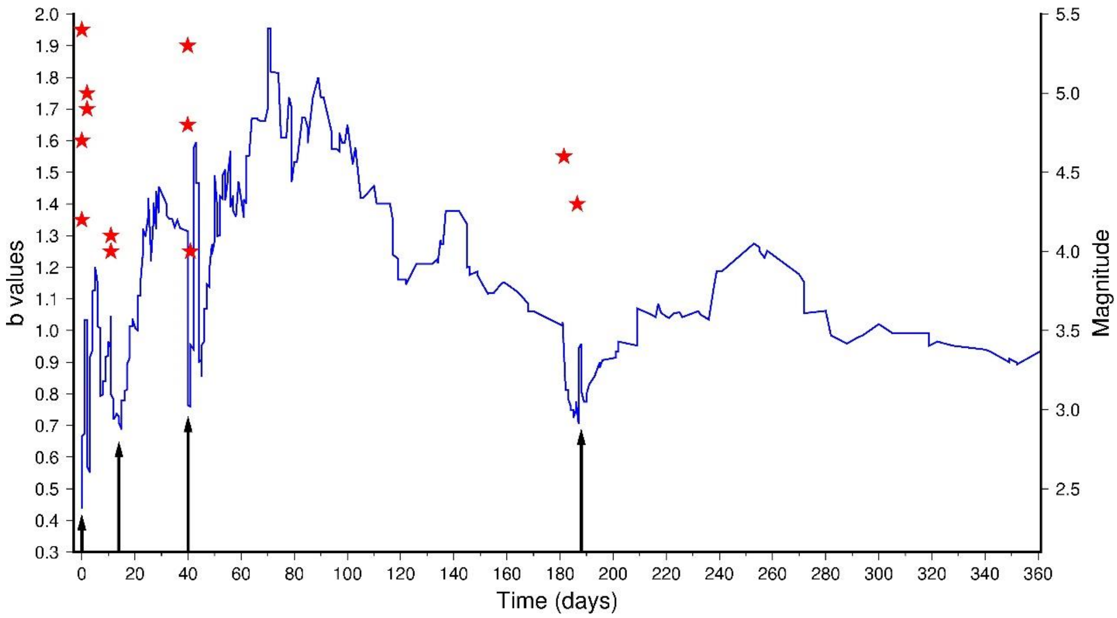

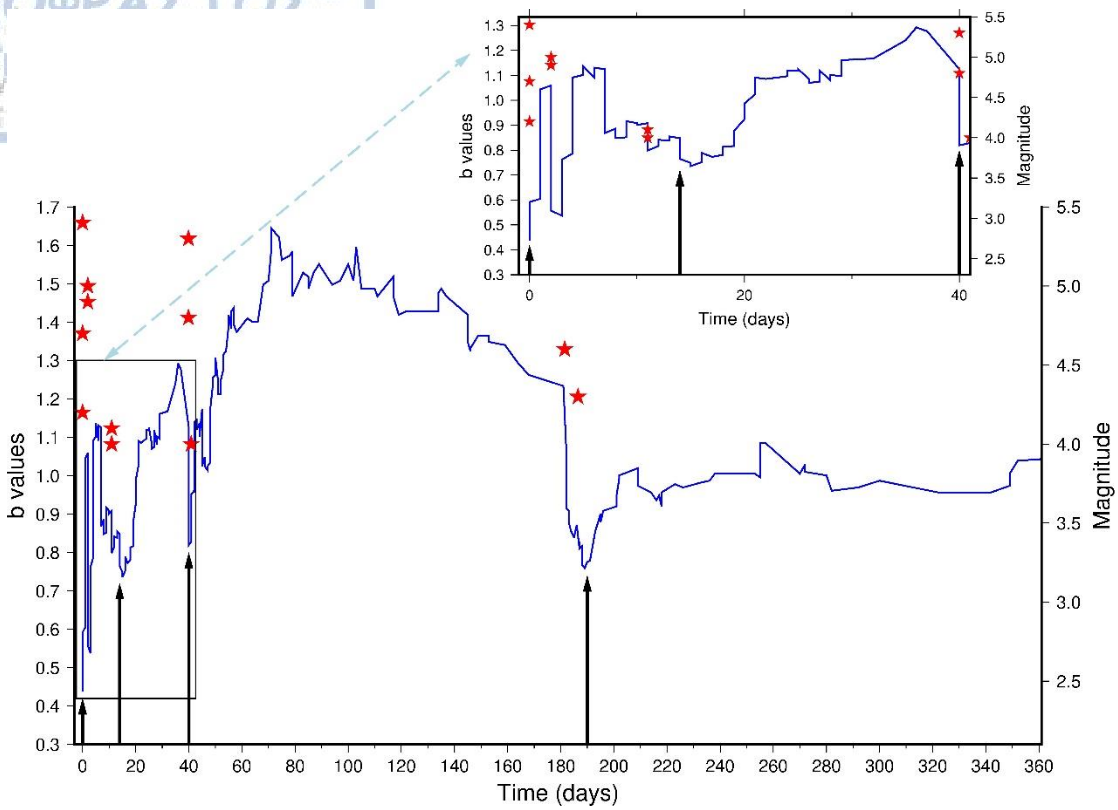

Figure 2.9 b-value as a function of time (days) for the study area a) with constant magnitude of completeness (M_c), (inset top) close-up view of the first forty days and b) with moving magnitude of completeness (M_c). The plots were calculated by sliding time windows comprising 50 events.

To map spatial variations of the b-values, the study area was subdivided into a 0.5km x 0.5km grid. Each grid node contained a circular epicentral area with a fixed radius that covered a number of events. For each grid node a minimum number (N_{min}) of 50 events was set in order to calculate the b-values. This threshold was selected because Monte Carlo sampling and bootstrapping showed large errors in b-values for data samples under 50 events (Shi and Bolt, 1982, Tormann et al., 2014). The sampling approach was based on the nearest neighbor algorithm which assigns an average value to every node that has a N_{min} of points. Therefore, b-values were determined by sampling the N_{min}= 50 nearest events for each grid node within a radius R=2.5 km (**Fig.2.10**). This radius value was chosen because it showed more details in b-value variations. According to Wiemer and Wyss (2002) the radius of the circle is inversely correlated with the density of the earthquakes, and therefore indicates the spatial resolution. The b parameters were calculated for $M>M_c$ using the maximum likelihood estimation (Eq.(2.5)) by Aki (1965). Finally, for each b-value a color was assigned.

Figure 2.10 shows the spatial distribution of b in the study area. Black asterisks illustrate events with M ≥ 4. The b-value ranges between 0.48 and 1.73. Two distinct areas of low b-values (red) are observed in the figure, one in the west, say, between 22.61^o and 22.68^o and the other at the center of the study area. It can be noticed that these areas have generally been developed around the epicenters of the M ≥4 earthquakes. The mainshock (M=5.4, August 7, 2013) occurred at the eastern edge of the western low b area. The second largest aftershock (M=5.3, September 16, 2013) took place at the northern edge of the central low b area. The spatial distribution map (**Fig.2.10**) displays three high b areas (blue) that they are less extensive. They concentrate close to the edges of the study area around the central low b area.

From the abovementioned spatial and temporal variations it follows that low b-values coincide with the occurrence of M ≥4 earthquakes.

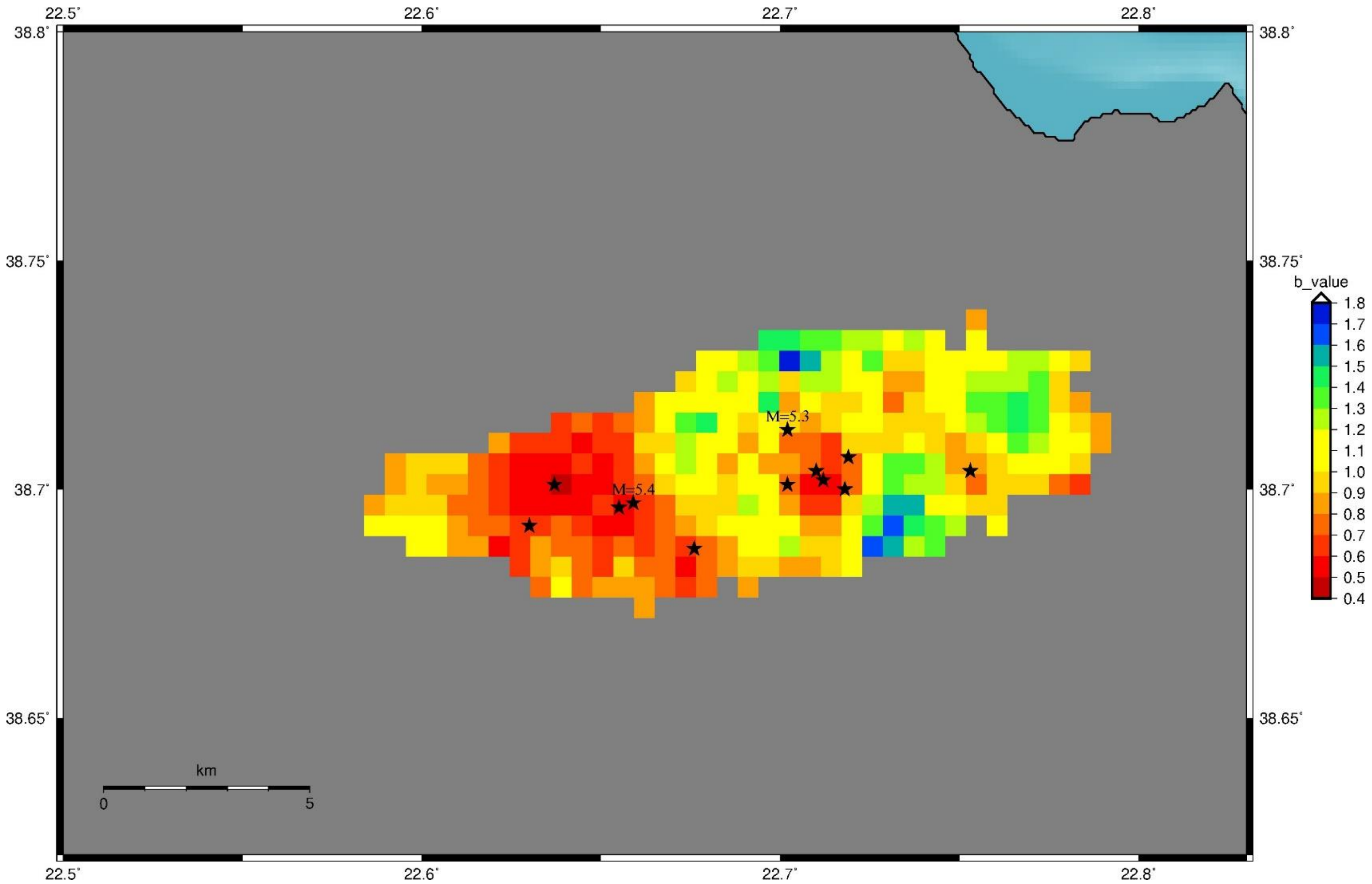

Figure 2.10 Spatial b distribution, grid spacing is 0.5 km, b-value at each grid node was computed by the maximum likelihood method (Aki, 1965). Black asterisks mark the epicentral locations (M ≥4). Red shows low b-values, whereas blue denotes high b-values.

2.6 Mean magnitude distribution

The mean magnitude distribution of earthquakes and its fluctuations are examined in order to indicate changes over time. These changes could reveal whether a seismic sequence evolves normally or not (Teza et al., 2013). According to Papazachos (2000), normal evolution is usually called the physical procedure of generation of a mainshock sequence. In a study of the 1952 Kern Country sequence (M=7.5), Lomnitz (1966) reported that the mean magnitude (M) of successive groups of earthquakes remained approximately constant. In his paper, Lomnitz (1966) proposed a hypothesis of magnitude stability, namely, stability of the magnitudes and their independence of the occurrence times. Utsu (1962) also supported this hypothesis in the analysis of three Alaskan mainshock sequences (Ogata, 1988). Observations (Papazachos et al., 1983) on the sequence of the Mygdonian basin (06/20/1978) showed an increase of the average magnitude ($\overline{\mathrm{M}}$) before the occurrence of the mainshock. The above mentioned sequences could be connected with a normal and a non-normal evolution, respectively. A non-normal evolution could be associated with the occurrence of a large oncoming event.

The mean magnitude has been calculated for the first 100 days of the sequence as:

$$\overline{\mathrm{M}} = \frac{1}{\mathrm{K}}\sum_{\mathrm{i}=1}^{\mathrm{K}} \mathrm{M_i} \quad , \qquad \mathrm{i} = 1,2,\dots,\mathrm{K} \qquad \text{Eq. (2.7)}$$

Where K is the total number of the aftershocks and M is the magnitude of each earthquake in the sequence. The calculation has based on the complete data for the first 100 days (Ranalli, 1969). The mean magnitude (M) of 10 successive earthquakes is estimated so as to eliminate large individual fluctuations.

Figure 2.11 shows the result of plotting the mean magnitude (purple line) of all aftershocks (M >2.0) as a function of time (days). Each dot is the average magnitude of 10 successive earthquakes which oscillates about a $\overline{\mathrm{M}}$ during the sequence. The purple dashed lines represent the 68% confidence limits ($\overline{\mathrm{M}}$ ± 1 standard deviaton). As it is seen (**Fig.2.11**) the average magnitude for the first 100 days is 2.55 and the confidence limits correspond to M ± 0.24.

Higher values of M are observed in the first hours after the mainshock which are characterized by high frequency and therefore small aftershocks cannot be detected. A notable increase is detected almost 40 days after the mainshock where it coincides with the largest aftershock (M=5.3) occurrence. Values of M exceed the confidence limits at noticeable aftershocks. It has estimated that 78.7% out of 61 dots are within the confidence limits (M ± 0.24) thus, the law of magnitude stability is not fully satisfied.

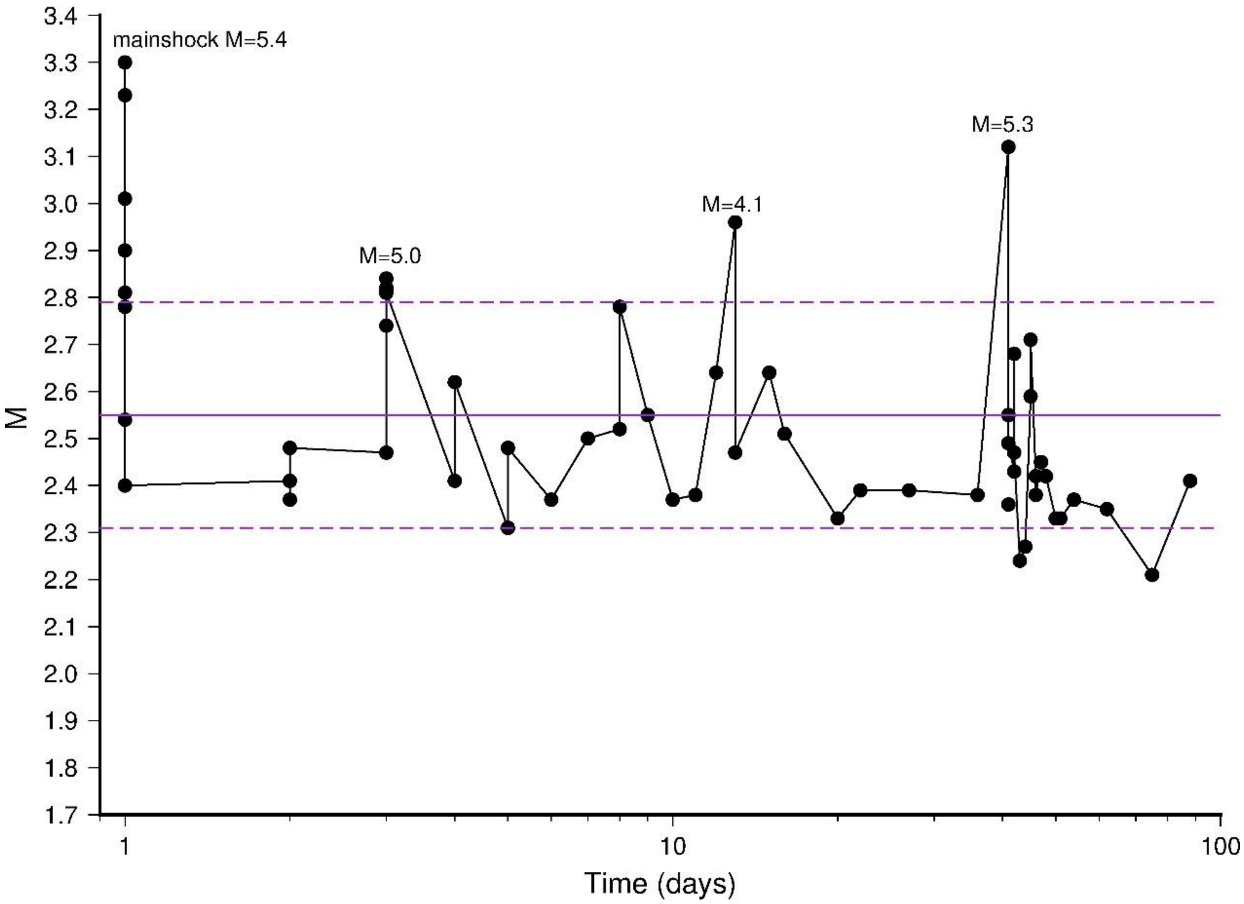

Figure 2.11 Temporal variation of mean magnitude for the first 100 days of the Amfikleia sequence. The purple line and the purple dashed lines show the value of average magnitude and its standard deviation, respectively.

2.7 Temporal distribution

The study of the time variation of a seismic sequence provides useful information about the evolution of an aftershock activity. An important feature in a temporal variation analysis is to find the decay rate in order to estimate the duration of a sequence. Another key aspect of this study is to predict the occurrence of the largest aftershock as a function of time which can sometimes cause more damage and loss of life than the mainshock (e.g, Prochazkova, 1973, Papazachos, 1974a, Kagan and Knopoff, 1978, Drakatos and Latoussakis, 2001).

Figure 2.12 shows the number of aftershocks per day (bars), their magnitude and the cumulative number with time (days) since 7 August 2013 (0 day on the time axis). In general, the seismicity rate of the complete catalog (M_c=2) decay with time, although there is an increasing number of earthquakes after a significant aftershock. It is noticeable that during the first three days there was a considerable number of aftershocks. About 212 aftershocks occurred within 72 hours and after that the activity was low.

In the time interval between the mainshock (0 day on the time axis) and the M=5.0 event which struck during the third day, more than 55 aftershocks occurred with magnitudes ≥ 3, including 3 events with M≥ 4. After that the activity was decreased up until the eleventh day where a small onset in seismicity is observed. The small onset corresponds to a magnitude 4.1 earthquake. The seismic activity in the following days remained low. Forty days after the mainshock, the second largest aftershock struck (M=5.3). About 124 events followed in five days, 16 of them with M≥ 3 and 2 of them with M≥ 4. Afterwards, the seismic rate declined progressively and one-hundred and eighty-two days after the beginning of the seismic sequence a M= 4.6 event struck. Forty-seven aftershocks followed in seven days, containing 7 M≥ 3 events and 1 M≥ 4 event.

The examination of the cumulative curve showed turning points that are associated with the steep rise the of daily earthquakes number. Noticeable turning points (red arrows) are observed on the fortieth day and on the one-hundred and eighty-two day where the second largest event (40 day on the time axis) and a M= 4.6 event occurred, respectively.

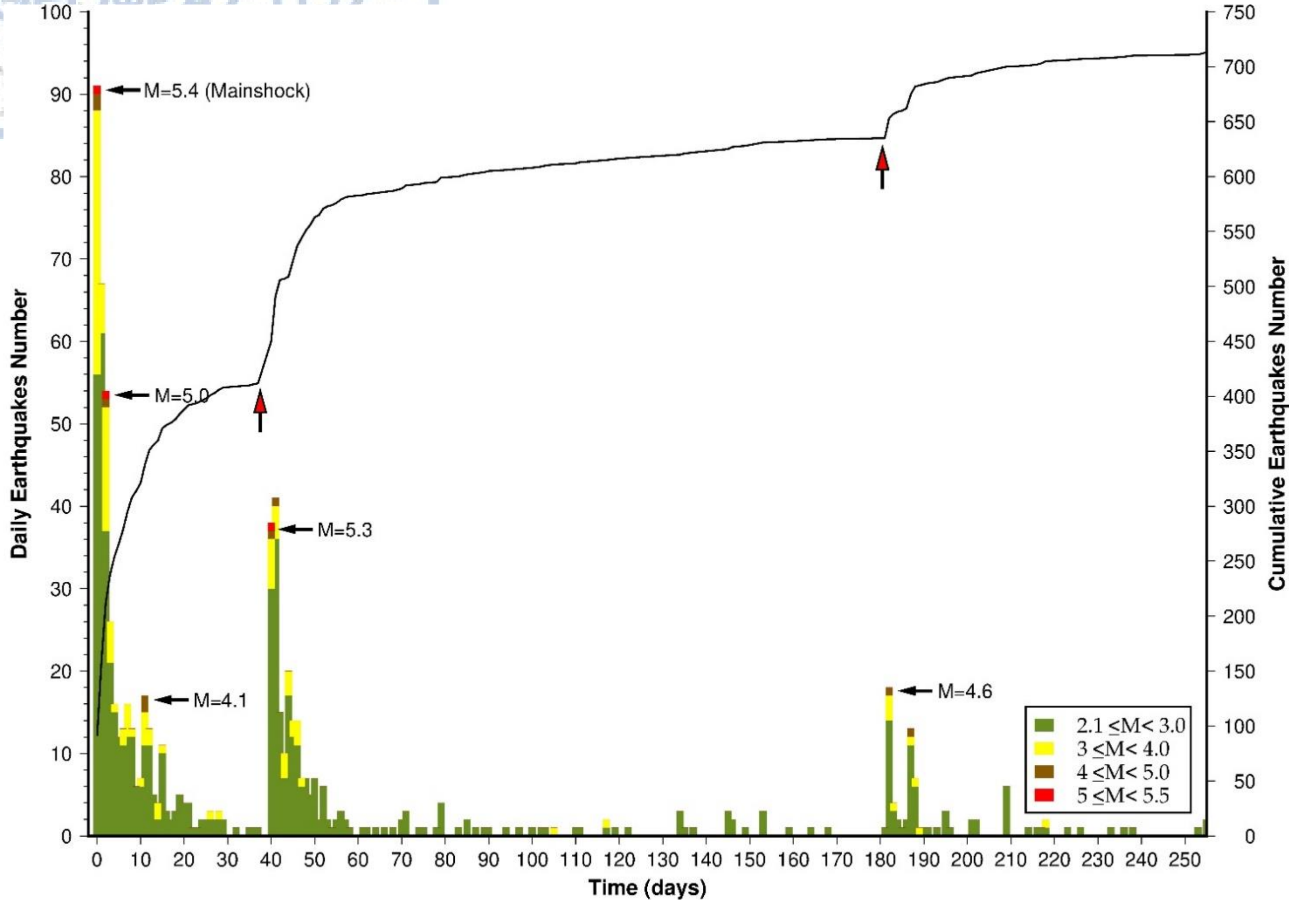
M=5.4 (Mainshock)
M=5.0
M=4.1
M=5.3
M=4.6
2.1 ≤M< 3.0
3 ≤M< 4.0
4 ≤M< 5.0
5 ≤M< 5.5
Daily Earthquakes Number
Cumulative Earthquakes Number
Time (days)

a.

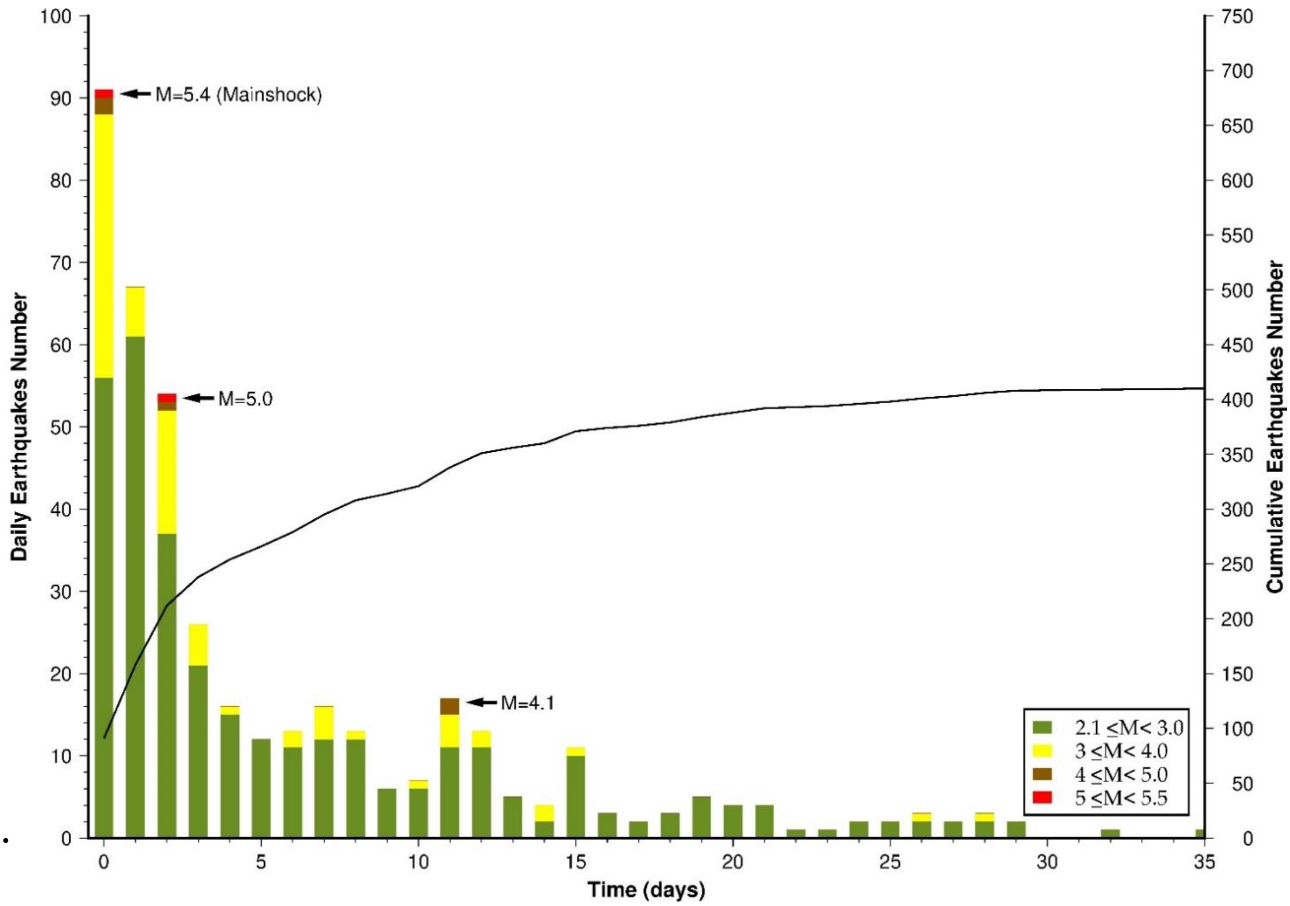
M=5.4 (Mainshock)
M=5.0
M=4.1
2.1 ≤M< 3.0
3 ≤M< 4.0
4 ≤M< 5.0
5 ≤M< 5.5
Daily Earthquakes Number
Cumulative Earthquakes Number
Time (days)

b.

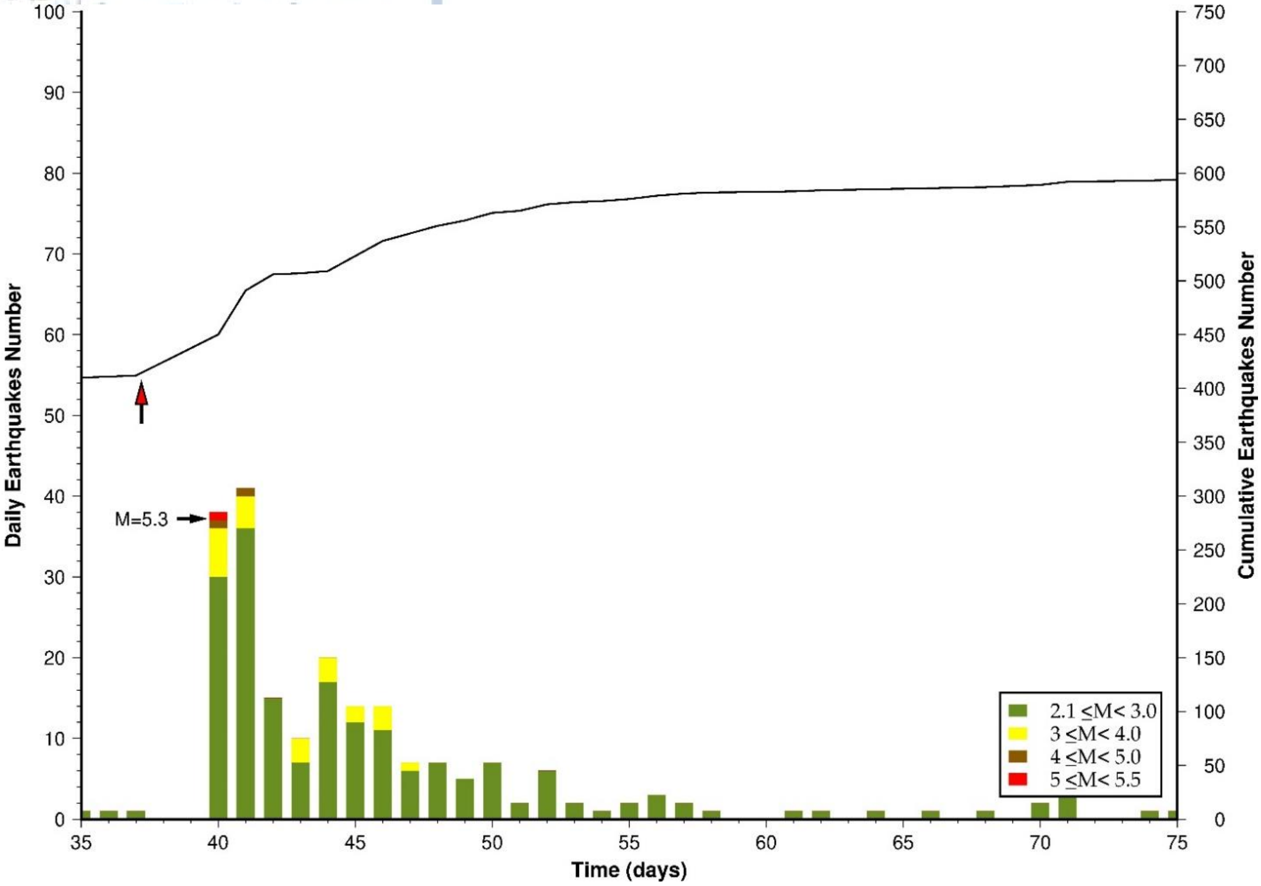

Figure 2.12 Seismicity pattern as a function of time indicating the daily number of events, their magnitude and the cumulative daily number of events, the turning points of the cumulative curve are shown by the red arrows, (a, b) close-up views of the seismicity pattern that cover the first forty days and the time period between thirty-five and seventy-five days.

Omori (1894) was the first to report that the aftershock frequency decays with time since the mainshock, according to the equation:

$$\mathrm{n(t)} = K(t+c)^{-1} \qquad \text{Eq. (2.8)}$$

where n(t) is the frequency of aftershocks per unit time interval, t is the time and it is usually measured in days from the origin time of the mainshock, K and c are constants. The observed frequency was deviated randomly from the above mentioned equation. Since then, many equations have been proposed to define the rate of aftershock decay (e.g, Hirano, 1924, Jeffreys, 1938, Otsuka, 1985, Yamashita and Knopoff, 1987, Gross and Kisslinger, 1994, Lolli and Gasperini, 2006). However, by comparing them as to their performance, the results were mixed relative to the Omori's equation (Kisslinger, 1993, Gross and Kisslinger, 1994, Narteau et al., 2002, Lolli and Gasperini, 2006). Utsu (1957) highlighted that the aftershock decay rate was faster than that expected from the

Omori relation (Eq.(2.8)). Thus, he proposed a relation that satisfies the occurrence rate of aftershocks which can be written as a power law.

$$n(t) = Kt^{-p} \qquad \text{Eq. (2.9)}$$

where p is a parameter that expresses the decay rate of aftershocks. P parameter varies from 0.9 to 1.9 and values between 1.1 and 1.4 are most common (Utsu, 1969). Utsu (1969) also suggested that there is not any correlation between the p parameter and the magnitude of the mainshock and p is independent of the magnitude of completeness (M_c). Thus, p values could characterize individual mainshock sequences (Utsu, 1961, 1969). Equation 2.9 diverged at t=0, and therefore, Utsu (1961) recommended equation (2.2) which he called the modified Omori formula. Omori's formula and its modified version have become widely acknowledged as one of a few established statistical laws in seismology.

In a study of the 1927 Tango, sequence in Japan, Jeffreys (1938) did not observe any mutual dependence between aftershocks apart from the common dependence upon the mainshock. It has since become accepted that the aftershocks are regarded as random events in time and their frequency is determined by the Omori's law.

Despite the random events, mainshock sequences are not represented by a stationary Poisson process. In a Poisson process the probability of a number of events occurring in a fixed interval of time is constant. Aftershocks' probability of occurrence depend on the time since the mainshock (Ranalli, 1969).

Omori's formula has been applied successfully to many earthquake sequences but some sequences could not be represented fully by this law. Some of these sequences contained secondary aftershock sequences, thus, the seismic activity did not decrease regularly as a function of time (Utsu, 1969, Utsu et al., 1995).

The relation that satisfies the occurrence rate of aftershocks (Eq.(2.9)) has been suggested by many researchers (e.g, Mogi, 1962, Ranalli, 1969, Papazachos, 1974, Teza, 2011, etc) and can be written as:

$$\log n = \log K - p \log t \qquad \text{Eq. (2.10).}$$

The parameters K and p have been estimated by the least squares method. The data have been grouped according to a method proposed by Ranalli (1969).

The origin time of the mainshock has been considered as t_0=0 and the origin times of the aftershocks have been expressed in days after the mainshock. The time axis has been subdivided into logarithmic intervals and their limits are computed by the relation:

$$\mathrm{logt_i} = 0.1\mathrm{i}, \quad \mathrm{i} = 0,1,2,\ldots,25 \qquad \text{Eq. (2.11)}.$$

If the number of aftershocks (N_i) occur in the time interval $\Delta t_i = t_{i+1} - t_i$ then the frequency of the aftershocks per time unit is represented by:

$$n_i = \frac{N_i}{\Delta t_i} \qquad \text{Eq. (2.12)}.$$

This frequency (n_i) is plotted against the centered value of the time interval (Δt_i) which is:

$$t_i = \frac{t_{i+1} + t_i}{2} \qquad \text{Eq. (2.13)}.$$

Equation 2.10 has been used to model the observed data (dots) by a straight line (**Fig.2.13**). K and p parameters have been calculated by using the least squares method. Then, the 95% confidence limits (dashed lines) have been estimated in order to detect any deviations prior to large aftershocks. Finally, the percentage of the number of points that falls outside the confidence band has been estimated in order to check if the data could be sufficiently simulated by the equation 2.10.

Figure 2.13 illustrates the temporal distribution of the Amfikleia sequence which appears to decay according to Omori's law. p and K values have been calculated and found equal to 1.64 and 190.5 (=$10^{2.28}$), respectively. It can be noticed that one data point (dot) exceeds the confidence limits. This deviation coincide with the occurrence of a large aftershock (M=4.6). The percentage of the data points that is not within the confidence limits (± 2σ) is 4%, thus the time frequency law is fully satisfied (Ranalli, 1969).

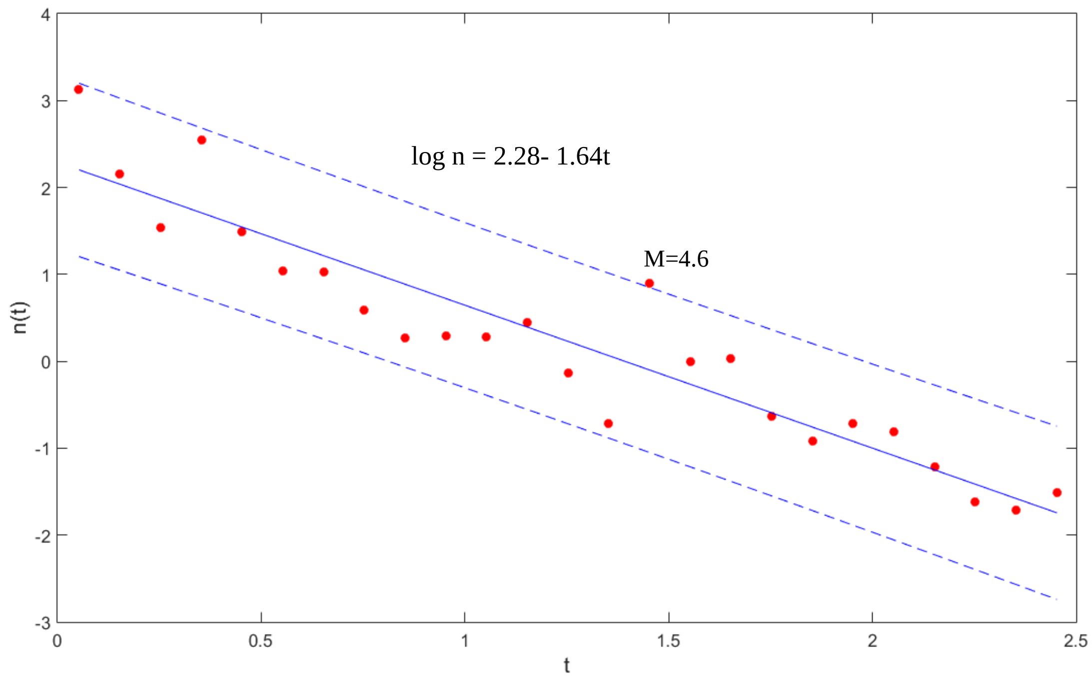

Figure 2.13 Time distribution plot with 95% confidence limits (dashed lines).

CHAPTER 3: FOCAL MECHANISMS

3.1 Introduction

Focal mechanisms or fault plane solutions provide useful information about the tectonic characteristics of a region (Reyners and McGinty, 1999, Scholz, 2019) and are necessary as inputs to the Coulomb stress calculations. Fault slip during an earthquake is geometrically represented by focal mechanisms using three angular parameters which are the strike, dip and rake.

The existing methods for the estimation of the fault plane solutions make use of the P-wave first motion polarities and S-wave information. Focal mechanisms of the 2013 Amfikleia sequence were calculated by P-wave first motion polarities using a wide range of events.

3.2 Computing focal mechanisms

Focal mechanisms were calculated and displayed using the FPFIT software (Reasenberg and Oppenheimer, 1985). FPFIT is a FORTRAN program which estimates the source model that is the optimal fit to the observed first P-wave polarities. The program considers the distribution of the first P-wave polarities and determines the two nodal planes. The determination of the nodal planes is achieved by the distinction of the compressional from the dilatational polarities. In order to determine the nodal planes, FPFIT uses a grid search to find a fault plane solution with the minimum misfit between all the observed and theoretical polarities (Hardebeck and Shearer, 2002). The misfit is a normalized, weighted sum of first P-wave polarity discrepancies. The weighted sum is expressed through the F parameter that lies in the range $0 \leq F \leq 1$. A F- value that is equivalent to 0 represents a perfect fit to the data whilst a value of 1 is a perfect misfit (Reasenberg and Oppenheimer, 1985, Kilb and Hardebeck, 2006).

A station distribution ratio (STDR) is calculated. STDR indicates how the seismic stations are distributed about the focal sphere. It lies in the range $0 \leq STDR \leq 1$, where a low ratio suggests that most of the data approach the nodal planes and a high ratio indicates that most of the data scatter from the nodal planes. A solution is considered less robust when STDR < 0.5 and therefore it should be examined carefully (Reasenberg and Oppenheimer, 1985, Kilb and Hardebeck, 2006).

FPFIT uses polarity pick information contained in an archive (.arc) file in order to search for focal mechanisms with the minimum misfit. An archive file contains all of the data about the earthquake and it is generated by the HypoInverse-2000 software (Klein, 2002). The HypoInverse-2000 software processes seismic station data to determine the epicenter location and the event magnitude. In order to locate earthquakes, the HypoInverse-2000 software uses a 1D velocity model along with a V_p/V_s ratio. The 1D velocity model used was stemmed from a previous study in the broader area (Karakostas et al., 2006). The velocity model and the V_p/V_s ratio are provided in Table 1.

Karakostas et al., 2006	
V_p/V_s ratio	1.76
P-wave velocity (km/sec)	**Ceiling Depth (km)**
5.73	0.00
6.11	4.07
6.76	8.83
6.89	8.27
7.90	31.00

Table 1 1D velocity model along with the V_p/V_s ratio used in the present study.

FPFIT requires at least six polarity observations to include in focal mechanism computation. Generally, a large number of polarity observations leads to a better constrained fault plane solution.

3.3 Results

Focal mechanisms of 62 events with magnitudes M>2.5 were determined. All results of focal mechanisms are presented graphically as beach ball diagrams in figure 3.7. Information on sixty-two focal mechanisms that were estimated is provided in Table 2.

Most of the focal mechanisms exhibit normal faulting while some of them demonstrate an oblique normal faulting type. The focal mechanisms of most of the events have a WNW or SE strike. The fault plane solution of the mainshock (**Fig.3.1** red asterisk) exhibits normal faulting on WNW or SE striking nodal planes. These nodal planes are inconsistent with the epicentral distribution of the aftershocks.

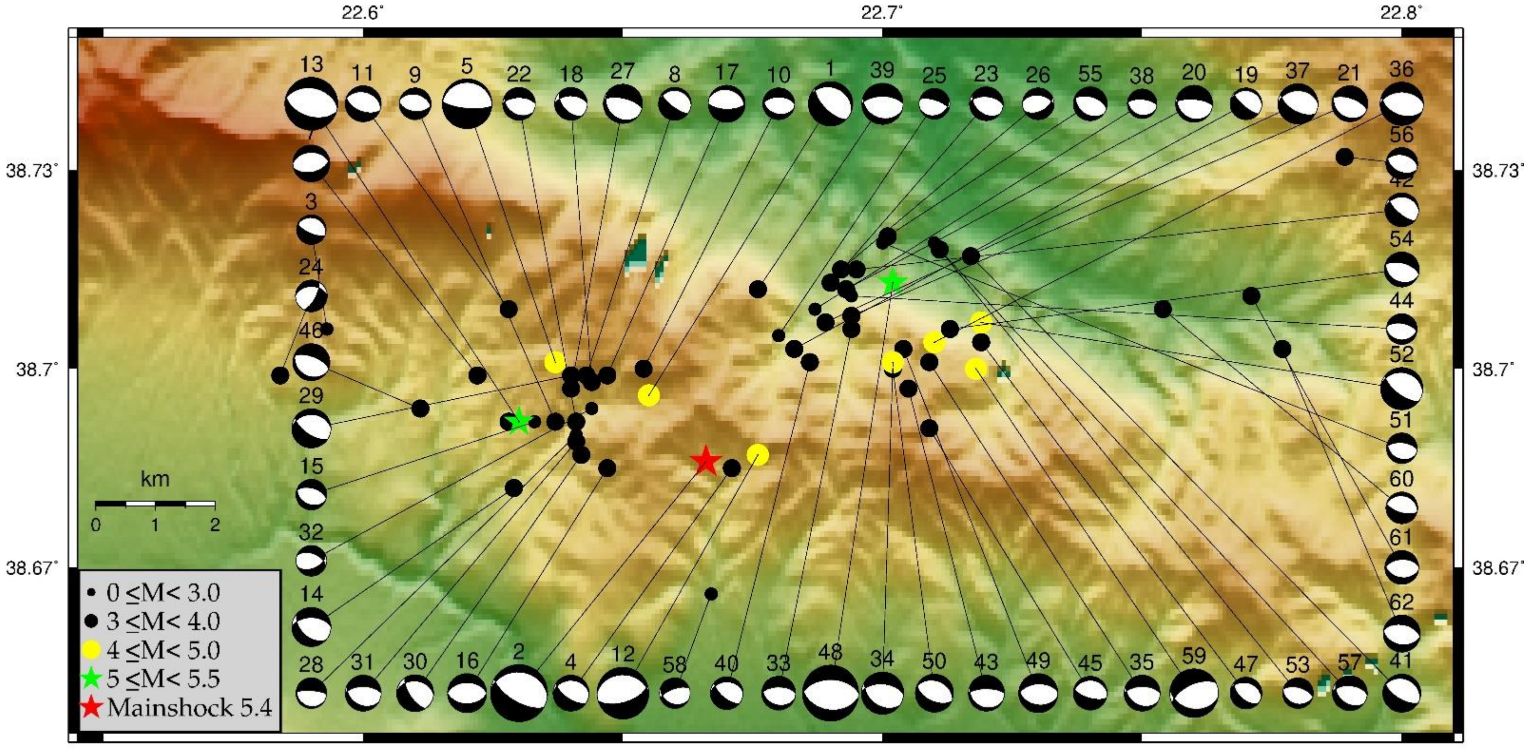

Figure 3.1 Fault plane solutions depicted as *beachball* diagrams, along with the corresponded epicenters. The compressional quadrants are shown in black. The numbers on the top of each solution correspond to the chronological order of the earthquake occurrence provided in Table 2. The beachball size is a function of the earthquake magnitude.

Table 2 Information on the fault plane solutions determined in the present study.

n	Date	Occurrence time	Lat (ºN)	Lon (ºE)	Depth (km)	M_L	Nodal Plane 1			Nodal Plane 2		
							Strike (º)	Dip (º)	Rake (º)	Strike (º)	Dip (º)	Rake (º)
1.	07/08/13	9:02:45	38.696	22.655	10	4.2	292	27	-110	135	65	-80
2.	07/08/13	9:06:51	38.686	22.666	9.93	5.4	277	27	-110	120	65	-80
3.	07/08/13	10:19:37	38.706	22.593	3.81	2.8	283	20	-100	114	70	-84
4.	07/08/13	10:44:37	38.685	22.671	9.39	3.4	270	30	-120	124	64	-74
5.	07/08/13	13:44:32	38.701	22.637	10.27	4.7	270	15	-95	95	75	-89
6.	07/08/13	16:03:45	38.692	22.628	6.9	3.7	270	40	-125	132	58	-64
7.	07/08/13	20:04:50	38.699	22.622	5.43	3.5	270	40	-80	77	51	-98
8.	08/08/13	0:04:54	38.699	22.643	5.89	3.1	275	20	-120	127	73	-80
9.	08/08/13	12:08:11	38.692	22.637	5.59	3	283	40	-85	96	50	-94
10.	08/08/13	19:41:35	38.7	22.654	0.71	3	270	55	-100	107	36	-76
11.	09/08/13	3:51:31	38.709	22.628	8.06	3.4	285	35	-95	111	55	-87
12.	09/08/13	11:49:24	38.687	22.676	4.52	4.9	270	30	-75	73	61	-98
13.	09/08/13	13:10:10	38.692	22.63	10.97	5	280	40	-95	107	50	-86
14.	09/08/13	13:43:44	38.682	22.629	7.49	3.7	270	50	-120	132	48	-59
15.	09/08/13	15:58:41	38.692	22.633	4.54	2.9	285	55	-95	114	35	-83
16.	09/08/13	19:26:51	38.685	22.647	6.27	3.7	270	45	-90	90	45	-90
17.	09/08/13	19:49:48	38.699	22.647	5.67	3.5	287	25	-75	91	66	-97
18.	09/08/13	20:30:59	38.698	22.644	6.96	3.1	270	50	-125	137	51	-56
19.	09/08/13	23:02:50	38.703	22.683	4.62	3	276	18	-123	130	75	-80
20.	10/08/13	0:19:59	38.712	22.693	7.16	3.5	275	70	-100	122	22	-64
21.	10/08/13	8:40:23	38.708	22.694	6.15	3.4	289	65	-95	121	25	-79
22.	10/08/13	11:11:36	38.692	22.641	7.01	3.1	270	59	-106	120	35	-65
23.	11/08/13	12:48:25	38.713	22.69	5.6	3.2	275	55	-110	127	40	-64
24.	13/08/13	9:01:40	38.699	22.584	6.43	3	270	40	-35	28	68	-125
25.	13/08/13	20:51:48	38.705	22.68	7.35	2.9	288	70	-75	70	25	-125
26.	14/08/13	3:27:03	38.715	22.692	6.09	3	277	45	-65	64	50	-113
27.	14/08/13	16:41:27	38.697	22.64	8.04	3.7	283	67	-101	130	25	-65
28.	14/08/13	17:08:27	38.69	22.641	7.27	2.9	274	76	-95	115	15	-70
29.	14/08/13	17:12:58	38.699	22.64	7.88	3.7	270	30	-120	124	64	-74
30.	14/08/13	22:58:01	38.687	22.642	8.87	3.5	275	35	-135	146	66	-64

31.	15/08/13	1:03:31	38.689	22.641	7.29	3.4	270	60	-105	118	33	-66
32.	15/08/13	2:05:57	38.694	22.644	5.14	2.9	290	50	-60	68	48	-121
33.	18/08/13	4:28:57	38.706	22.694	8.34	3.2	270	60	-100	109	31	-73
34.	18/08/13	10:42:55	38.701	22.702	10.98	4	274	54	-110	125	40	-65
35.	18/08/13	13:42:26	38.701	22.709	10.63	3.4	270	60	-105	118	33	-66
36.	18/08/13	16:39:22	38.704	22.71	8.93	4.1	270	45	-105	111	47	-75
37.	18/08/13	20:08:44	38.707	22.689	8.89	3.8	270	35	-115	120	59	-74
38.	18/08/13	20:41:25	38.709	22.687	7.17	2.8	275	65	-95	107	25	-79
39.	18/08/13	22:16:19	38.712	22.676	9.8	3.9	270	60	-100	109	31	-73
40.	19/08/13	1:29:25	38.701	22.686	5.31	3.1	269	32	-126	130	65	-70
41.	19/08/13	3:32:31	38.717	22.717	6.82	3.6	290	25	-100	121	65	-85
42.	21/08/13	7:09:23	38.715	22.695	5.47	3.2	272	25	-125	130	70	-75
43.	21/08/13	22:20:00	38.697	22.705	9.1	3.4	270	70	-100	117	22	-64
44.	22/08/13	1:18:01	38.711	22.694	4.71	2.9	280	60	-85	90	30	-99
45.	22/08/13	17:45:16	38.691	22.709	7.22	3.2	270	25	-105	106	66	-83
46.	02/09/13	4:40:21	38.694	22.611	9.1	3.5	290	65	-95	122	25	-79
47.	04/09/13	0:16:48	38.704	22.719	5.24	3	287	35	-110	131	57	-77
48.	16/09/13	15:01:14	38.713	22.702	9.54	5.3	270	50	-95	98	40	-84
49.	16/09/13	15:15:46	38.703	22.704	7.99	3.7	267	51	-98	100	40	-80
50.	16/09/13	16:13:09	38.7	22.702	10.34	3.6	289	35	-95	115	55	-87
51.	16/09/13	20:42:11	38.719	22.7	8.68	2.9	275	60	-100	114	31	-73
52.	17/09/13	7:39:44	38.707	22.719	10.39	4	280	25	-115	127	67	-79
53.	17/09/13	16:11:49	38.719	22.71	5.51	2.9	285	60	-90	105	30	-90
54.	17/09/13	17:35:19	38.706	22.713	7.49	3.3	285	60	-95	115	30	-81
55.	19/09/13	18:30:17	38.72	22.701	11.37	3.2	287	56	-100	125	35	-75
56.	21/09/13	7:30:48	38.732	22.789	7.28	3	281	45	-100	115	46	-80
57.	22/09/13	4:05:45	38.718	22.711	8.71	3.3	275	55	-110	127	40	-64
58.	21/10/13	1:28:39	38.666	22.667	9.71	2.9	251	67	-110	115	30	-50
59.	01/02/14	8:14:03	38.7	22.718	10.54	4.6	245	60	-109	100	35	-60
60.	01/02/14	9:24:34	38.709	22.754	9.34	3	280	25	-95	106	65	-88
61.	06/02/14	8:48:01	38.711	22.771	4.1	3.2	267	51	-98	100	40	-80
62.	07/02/14	6:59:59	38.703	22.777	6.91	3.5	280	50	-90	100	40	-90

As discussed in the previous chapter, the spatiotemporal evolution of the Amfikleia sequence (**Fig.2.4**) indicates an eastward activation pattern of fault segments. The events can be distinguished into clusters that are probably related to different fault segments. In order to constrain the geometry of the fault segments, cross sections normal to the strike of each cluster were constructed. Well-constrained focal depths provided by a relocated earthquake catalog that contains the first 80 days of the seismic sequence.

Figure 3.2 presents the spatiotemporal analysis of the Amfikleia sequence for the first 80 days. Cluster A (blue dots) occupies the first 8 days and includes the mainshock (red asterisk). Cluster B (yellow dots) is observed between the 9th and 38th day of activity. Cluster C (green dots) occupies the last 41 days and is associated with the largest aftershock (orange asterisk).

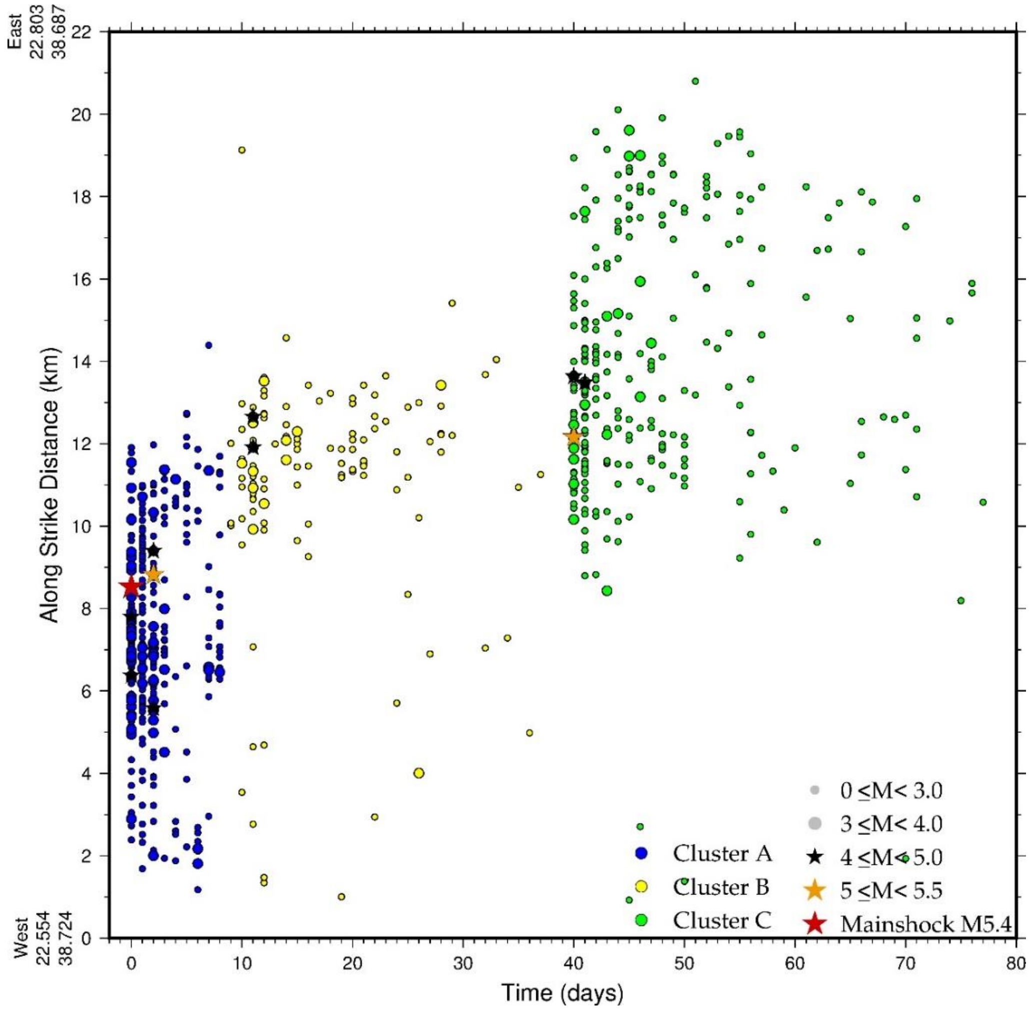

Figure 3.2 Spatiotemporal plot of the Amfikleia sequence for the first 80 days. The clusters and the earthquake magnitudes are plotted in accordance with the legend's symbols and colors.

Several cross sections were constructed normal to a strike range between 250° and 280° in order to define the optimal orientation of each cluster. The cross sections that were chosen displayed the narrowest aftershock zones. Eleven cross sections were made across the three clusters with a width of 1.5 km in either side of each section. The surface projections of the cross sections are illustrated by the lines in figure 3.9. There are overlaps between two pairs of lines, the B9B10 with Y1Y2 and the Y3Y4 with G1G2, which correspond to different clusters. Lines B1B2 to G3G4 oriented in a NNW-SSE direction whilst lines G5G6 and G7G8 have a NNE-SSW orientation. (**Fig.3.3**).

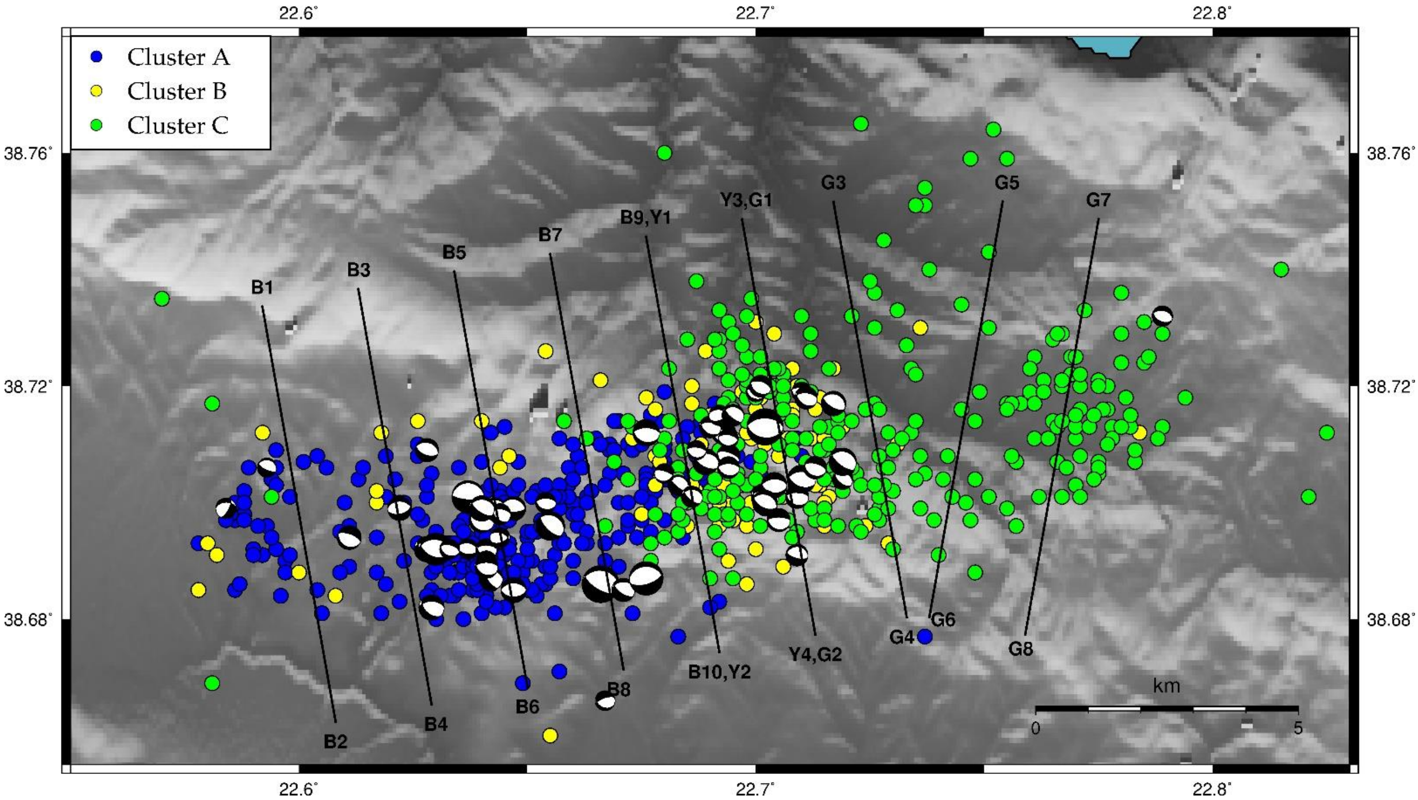

Figure 3.3 Epicentral distribution of the three clusters, plotted with different colors, along with the fault plane solutions. The lines represent the locations of cross sections. Lines B1-B10, Y1-Y4 and G1-G8 correspond to clusters A, B and C respectively

Figure 3.4 depicts the cross sections of cluster A. The mainshock is encompassed in cluster A and is shown in section B7B8 at a focal depth of 9.93 km, it is displayed with red compression quadrants. This cluster includes the majority of M ≥ 3 events. The hypocentral distribution along these sections indicates an active structure dipping to the SSE. This is more evident in sections B3B4 and B7B8. The focal mechanisms agree with this orientation. The dip average of the south dipping nodal planes in cluster A (61°) are consistent with the dip angle of the mainshock (65°) fault plane solution. The seismogenic layer in this cluster was found to be in the range of 4-10 km

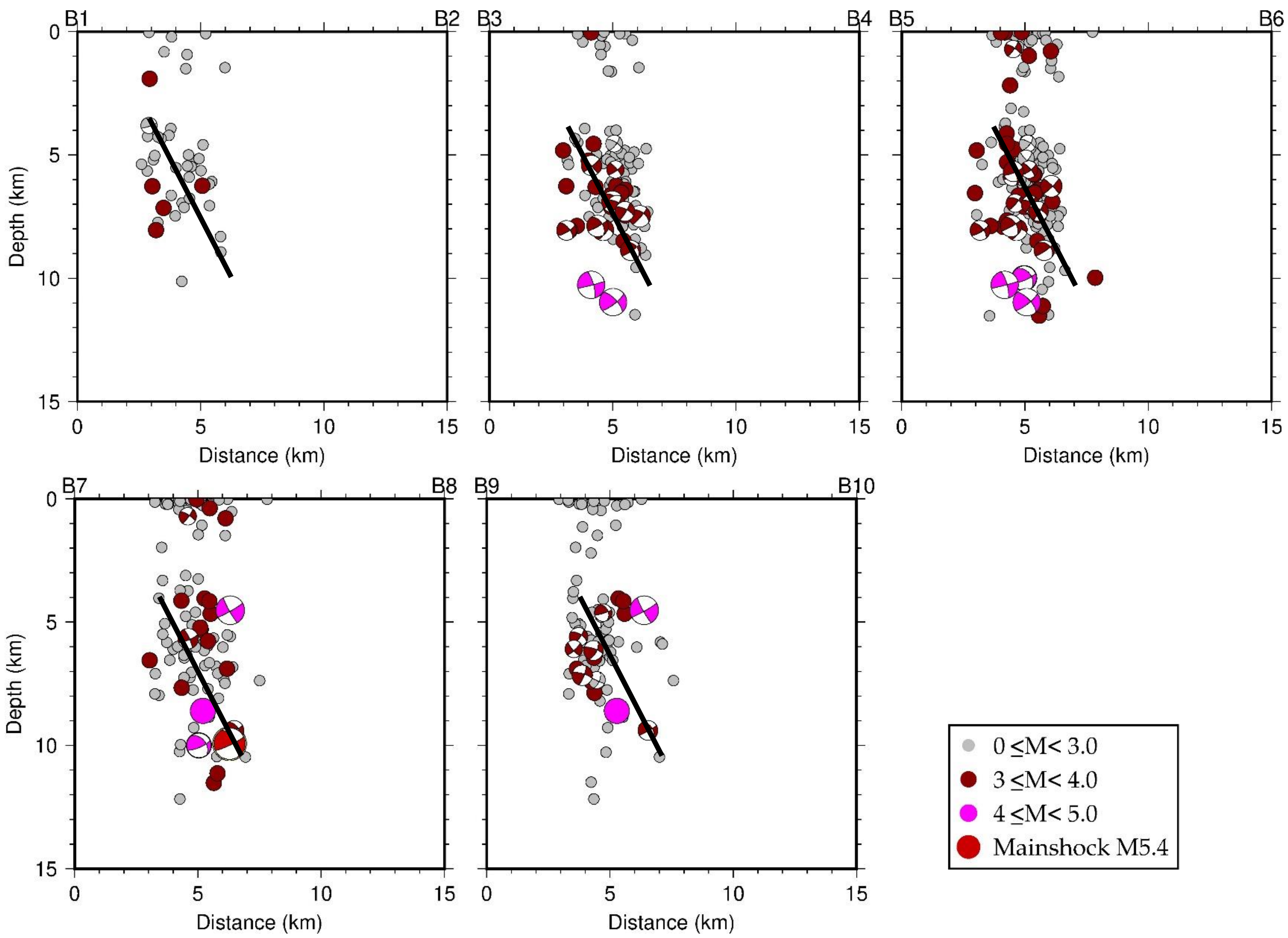

Figure 3.4 Cross sections of the cluster A. The hypocenters are plotted as circles with different diameters and colors according to their magnitude. The focal mechanisms are depicted as beachball diagrams having the same color and size as their hypocenters. Black lines illustrate the fault dip according to the dip average of the nodal planes.

Cross sections normal to the strike of the cluster B are presented in figure 3.5. The cluster B is positioned at the center of the study area overlapping with clusters A and C (**Fig.3.3**). Two $M \geq 4$ earthquakes, with focal depths of 8.93 km and 10.98 km, occurred at the western part of this cluster. These earthquakes are represented by their focal mechanisms in section Y3Y4 and are displayed with magenta compression quadrants.

The cross sections denote an active structure that dips at the same direction as the cluster A (SSE). The mean value of the dip of the south dipping planes in this cluster (58º) agrees with the average dip of the two M ≥ 4 events (50º) focal mechanisms. The seismogenic layer in this cluster range from 4 km to 11 km.

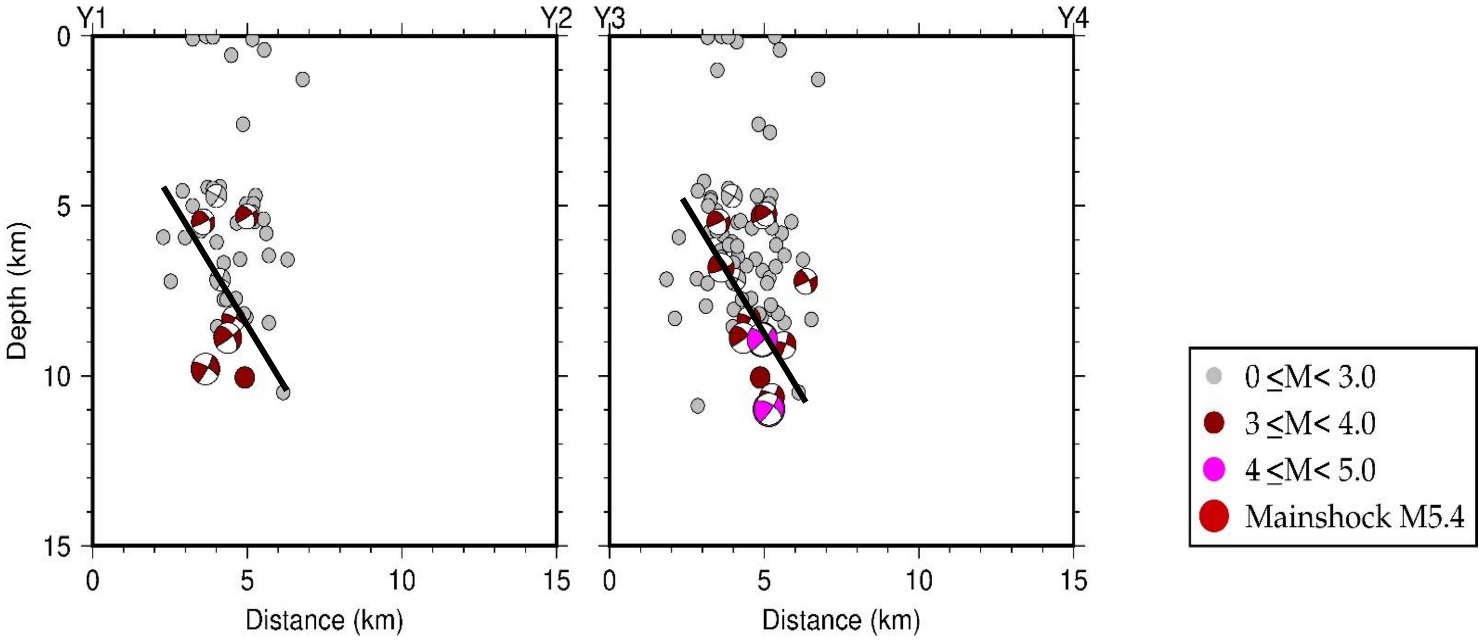

Figure 3.5 Cross sections of the cluster B. The hypocenters are plotted as circles with different diameters and colors according to their magnitude. The focal mechanisms are depicted as beachball diagrams having the same color and size as their hypocenters. Black lines illustrate the fault dip according to the dip average of the nodal planes.

Figure 3.6 illustrates the cross sections normal to the strike of the cluster C. The strongest aftershock (M=5.3) occurred in this cluster at a focal depth of 9.54 km. This aftershock is represented in section G1G2 as a beachball diagram with yellow compression quadrants. This cluster comprises two M ≥ 4 earthquakes at the focal depths of 10.37 km and 10.88 km (colored with magenta).

The section G1G2 illustrates a thick seismic zone which is probably due to location uncertainties. Although, the nodal planes of the focal mechanisms along with the M ≥ 3 events ascertain the SSE dipping structure. On section G3G4 an antithetic NNW dipping fault segment seems to be activated. The sections G5G6 and G7G8 are characterized by a sparser distribution of the earthquake foci and a lower magnitude activity thus the rupture properties cannot be easily distinguished. The dip average of the south dipping nodal planes in cluster C (58°) are consistent with the dip angle of the strongest aftershock (50°). The mean value of the dip of the north dipping planes (34°) is in agreement with the dip of the M= 4.0 event (25°) focal mechanism, which is depicted in section G3G4. The seismogenic layer extends between 4 km and 11.5 km.

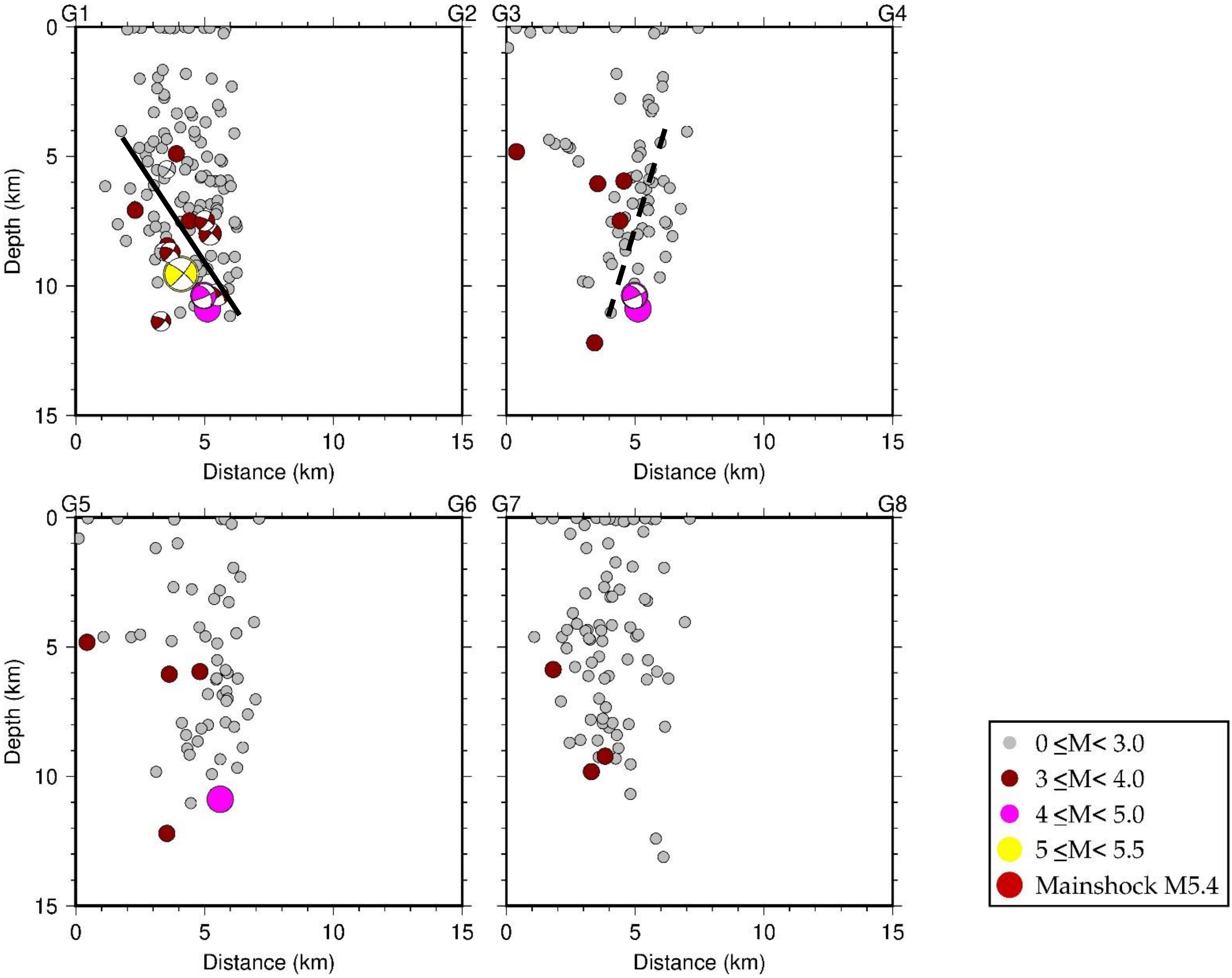

Figure 3.6 Cross sections of the cluster C. The hypocenters are plotted as circles with different diameters and colors according to their magnitude. The focal mechanisms are depicted as beachball diagrams having the same color and size as their hypocenters. Black lines illustrate the fault dip according to the dip average of the nodal planes.

3.3.1 T-axis orientation

The "FaultKin" software (Marrett and Allmendinger, 1990, Allmendinger et al., 2012) was used in order to determine the minimum compressive axis (T-axis) orientation of each focal mechanism. The strike, dip and rake were input for one nodal plane from each focal mechanism, following the Aki and Richards (2002) terminology. A positive rake defines a fault with a thrust component whilst a negative rake defines a fault with a normal component (Allmendinger, 2016).

Figure 3.7 depicts the T-axis orientation onto a stereonet produced by the Faultkin program. The T-axes are characterized by a NNE-SSW orientation with an average strike at N12^{o}E (black arrows). It can be estimated (**Fig.3.7**) that 90% of them, display a NNE-SSW orientation whilst 10% show a NNW-SSE orientation. The T-axis orientation is consistent with the nearly N-S extensional regime identified for the study area (Karamanos et al., 2010). The map of the study area in figure 3.8 illustrates the T-axes as vectors displaying mainly a NNE-SSW orientation.

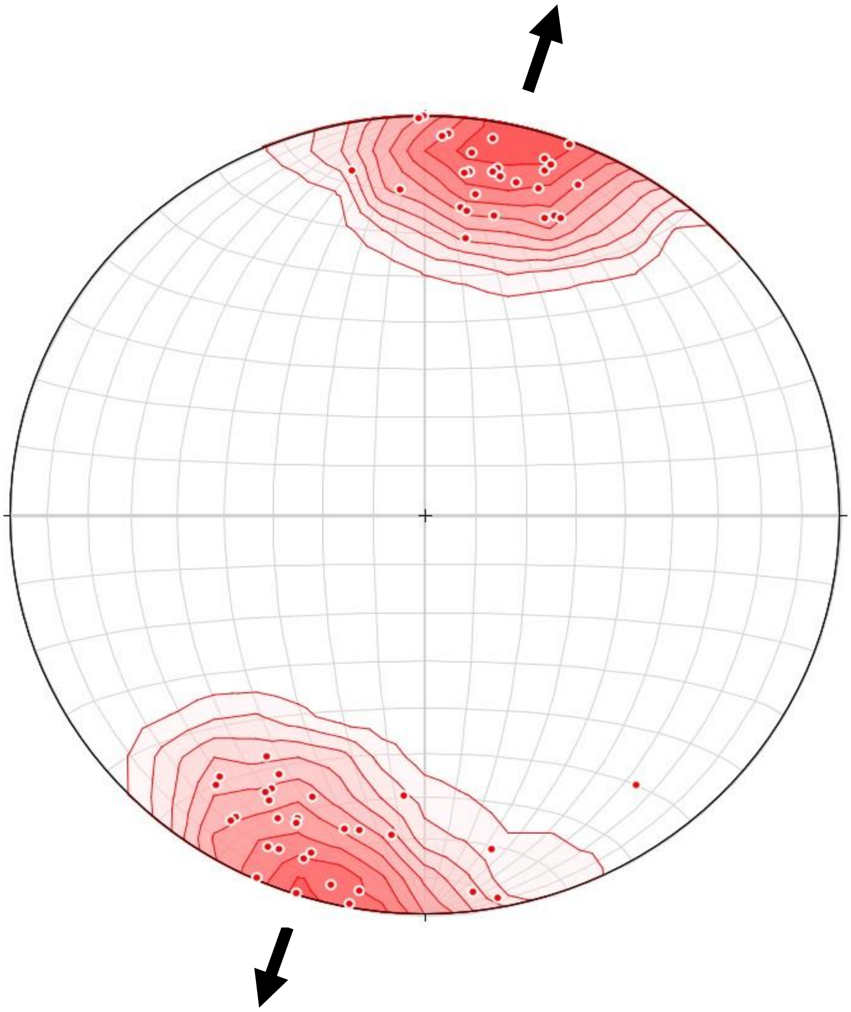

Figure 3.7 Stereonet produced by FaultKin, illustrating the distribution of the T-axes orientations. The T-axes were plotted as points and as contours. The average T-axis orientation is N12°E (black arrows).

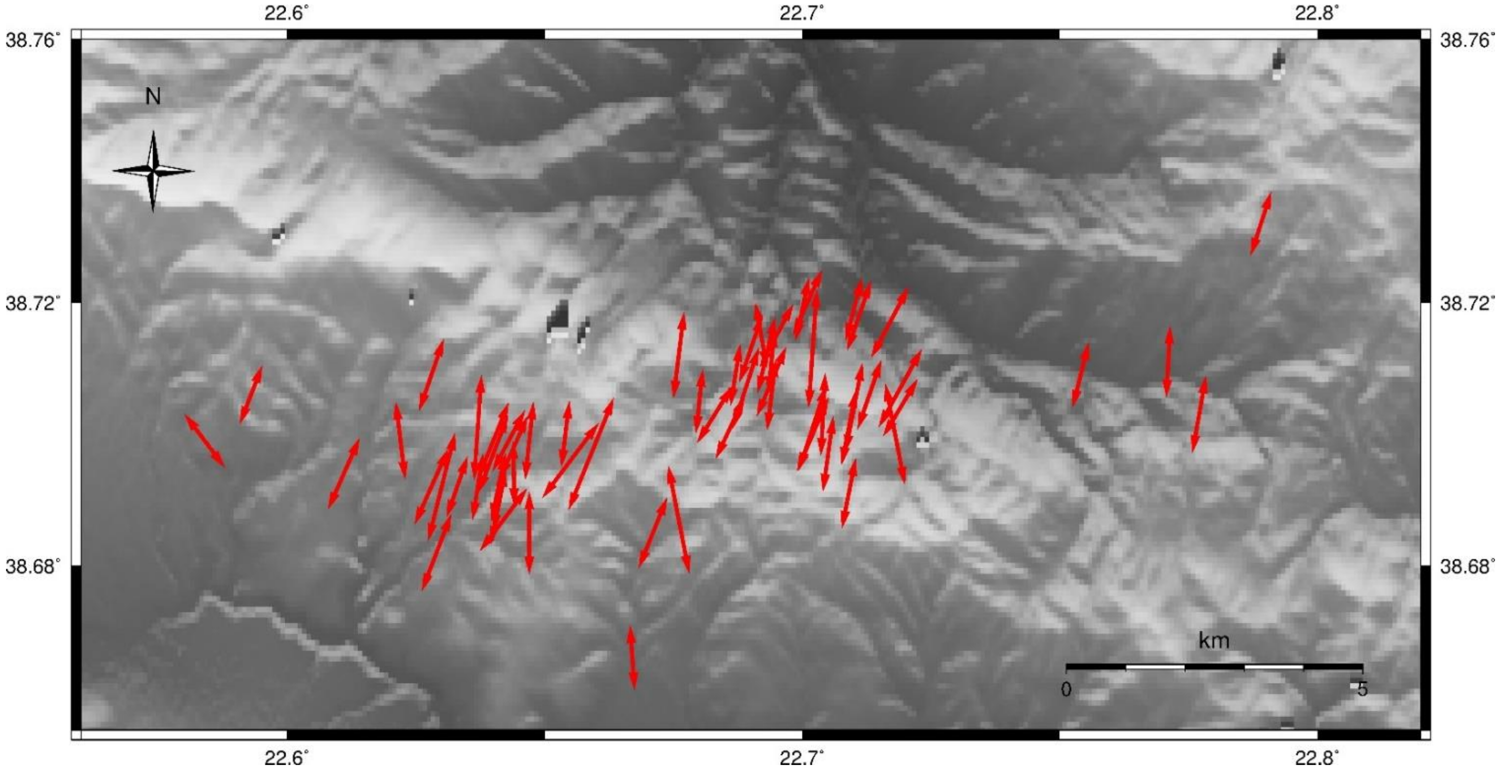

Figure 3.8 Map of the study area illustrating the results of the "FaultKin" software. The T-axes (red vectors) are inferred from the focal mechanisms and they show a sub-horizontal orientation.

CHAPTER 4: COULOMB STRESS CALCULATIONS

4.1 Introduction

Coulomb stress calculations are used in seismological studies in order to understand how earthquakes interact among each other. As explained in section 2.1.2, after the occurrence of a mainshock, stresses in the Earth's crust are released and redistributed. These stress changes can alter the mechanical conditions of active faults inducing aftershocks (Toki and Miura, 1985, King et al., 1994, Belardinelli et al., 2003, Hardebeck and Okada, 2018). The perturbations in the stress field can be static and dynamic. Static stress changes are permanent and they can advance or delay an induced aftershock. Dynamic stress changes are transient and they instantly trigger aftershocks. They are related to the propagation of seismic waves and they have been proposed to interpret triggered seismicity at large distances (Brodsky et al., 2000, Belardinelli et al., 2003, Bizzari and Belardinelli, 2008). According to Brodsky et al. (2000), dynamic stress changes induced by the M=7.4 Izmit, Turkey earthquake in 1999, triggered widespread remote seismicity in Greece. Dynamic stress changes will not be discussed further in the present thesis. The stress on a fault cannot be measured directly and the absolute value of stress is often unknown, however, it is possible to estimate the stress changes after an earthquake.

A fault is brought closer to failure when shear stress on a fault exceeds its strength. The closeness to failure can be quantitatively evaluated using the static Coulomb failure stress change (ΔCFS) as defined by:

$$\Delta \mathrm{CFS} = \Delta\tau_s - \mu(\Delta\sigma_n - \Delta p) \qquad \text{Eq. (4.1)}$$

$$\approx \Delta\tau_s - \mu'(\Delta\sigma_n) \qquad \text{Eq. (4.2).}$$

Where $\Delta\tau_s$ is the change in shear stress, $\Delta\sigma_n$ is the change in normal stress, Δp is the change in pore pressure and μ is the friction coefficient (Mignan, 2008, Scholz, 2019).

The pore pressure changes (Δp) depend on the normal stress changes ($\Delta\sigma_n$). A sudden change in normal stress under undrained conditions will induce a change in pore pressure. According to Rice and Cleary (1976) the relation between Δp and $\Delta\sigma_n$ is defined by:

$$\Delta p = -B\frac{\Delta\sigma_{kk}}{3} \qquad \text{Eq. (4.3).}$$

Where B is the Skempton's coefficient and $\Delta\sigma_{kk}$ is the sum of the diagonal elements of the stress tensor. The Skempton's coefficient varies between 0, for dry soil, and 1, for fully saturated soil (Skempton, 1954). According to Simpson and Reasenberg (1994) the materials inside the fault zone are more ductile than the surrounding materials, so that $\sigma_{xx} = \sigma_{yy} = \sigma_{zz}$, and so $\frac{\Delta\sigma_{kk}}{3} = \Delta\sigma_n$ (Harris, 1998). In that case equation 4.2 can be used, where $\mu' = \mu(1 - B)$ is the apparent (or effective) friction coefficient. The apparent friction coefficient (μ') includes the effects of pore pressure of the fault zone and ranges between 0.0 and 0.75 (King et al., 1994, Harris, 1998, Cocco and Rice, 2002, Ruiz-Barajas et al., 2019). A typical value of the apparent friction coefficient (μ') is 0.4 (King et al., 1994, Nalbant et al., 1998, Pollitz et al., 2006, Ryder et al., 2012a, Nalbant et al., 2013, Toda and Stein, 2013, Wang et al., 2014).

Coulomb stress changes produced by the 1992 M=7.4 Landers earthquake in California were calculated for a range of μ' values between 0.0 and 0.75. The results showed that there is a modest dependence between the Coulomb stress changes and the μ' parameter and a μ' = 0.4 was best fit (King et al., 1994). These results have been confirmed by several studies in different regions (Stein et al., 1992, Nalbant et al., 1998, King and Cocco, 2000, Nalbant et al., 2002, Papadimitriou, 2002, Wan and Shen, 2010). Karakostas et al. (2003) calculated Coulomb stress changes, due to 2001 M=6.4 Skyros mainshock in North Aegean region, for a range of μ' values between 0.2 and 0.9. They evidenced that triggering is not very sensitive on μ' variations and μ' = 0.6 was assumed. Rhoades et al. (2010) correlated Coulomb stress changes with earthquake (M≥5.2) occurrence in the North Aegean region. They selected a μ' = 0.4 which was sufficient to show the correlation of Coulomb stress changes to earthquake occurrence. Ganas et al. (2006) computed the Coulomb stress changes associated with the 1894 M=6.4 and M=6.6 Atalanti (central Greece) earthquakes occurred in the broader study area and they adopted a value of μ' equals 0.4.

Papadimitriou and Karakostas (2003) selected a value of μ′= 0.4 in order to calculate the Coulomb stress changes related to strong earthquakes (M≥6.2) occurred between 1954 and 1957 in Thessalia area (central Greece). Considering the value of the apparent friction coefficient (μ′) of the broader study area (central Greece) a μ′ = 0.4 was adopted in this study.

Areas with positive values of ΔCFS present an increase in seismic activity whereas areas with negative ΔCFS values show a decrease in seismicity. The increase in seismic activity suggests that the fault with positive ΔCFS values is brought closer to failure and vice versa (King et al., 1994). Areas with negative values of ΔCFS are called stress shadow areas and they indicate decreased likelihood of slip in future earthquakes (Harris and Simpson, 1996, Deng and Sykes, 1997a,b, Papadimitriou et al., 2007). Earthquakes that are located in areas of positive ΔCFS values due to the coseismic slip of previous earthquakes are possibly triggered and they are called advanced events whilst earthquakes located in stress shadow areas (ΔCFS<0) are delayed (**Fig.4.1**) (King et al., 1994). Figure 4.1 shows that around the main rupture (white line) there are four lobes of positive ΔCFS (red) and four lobes of negative ΔCFS (blue). The pattern of ΔCFS in the figure, is a typical spatial pattern for a strike slip faulting.

The calculation of ΔCFS depends on the geometry and slip distribution of an earthquake rupture, the apparent friction coefficient (μ΄), the orientation and magnitude of the regional stress (Scholz, 2019). The effect of geometry and slip distribution is less important farther from the rupture (Aki and Richards, 1980, Harris, 1998, Papadimitriou and Sykes, 2001). King and Cocco (2000) showed that the calculation of ΔCFS is highly depended on the orientation of the regional stress, independent to the magnitude of the regional stress and moderately dependent on the apparent friction coefficient (μ΄).

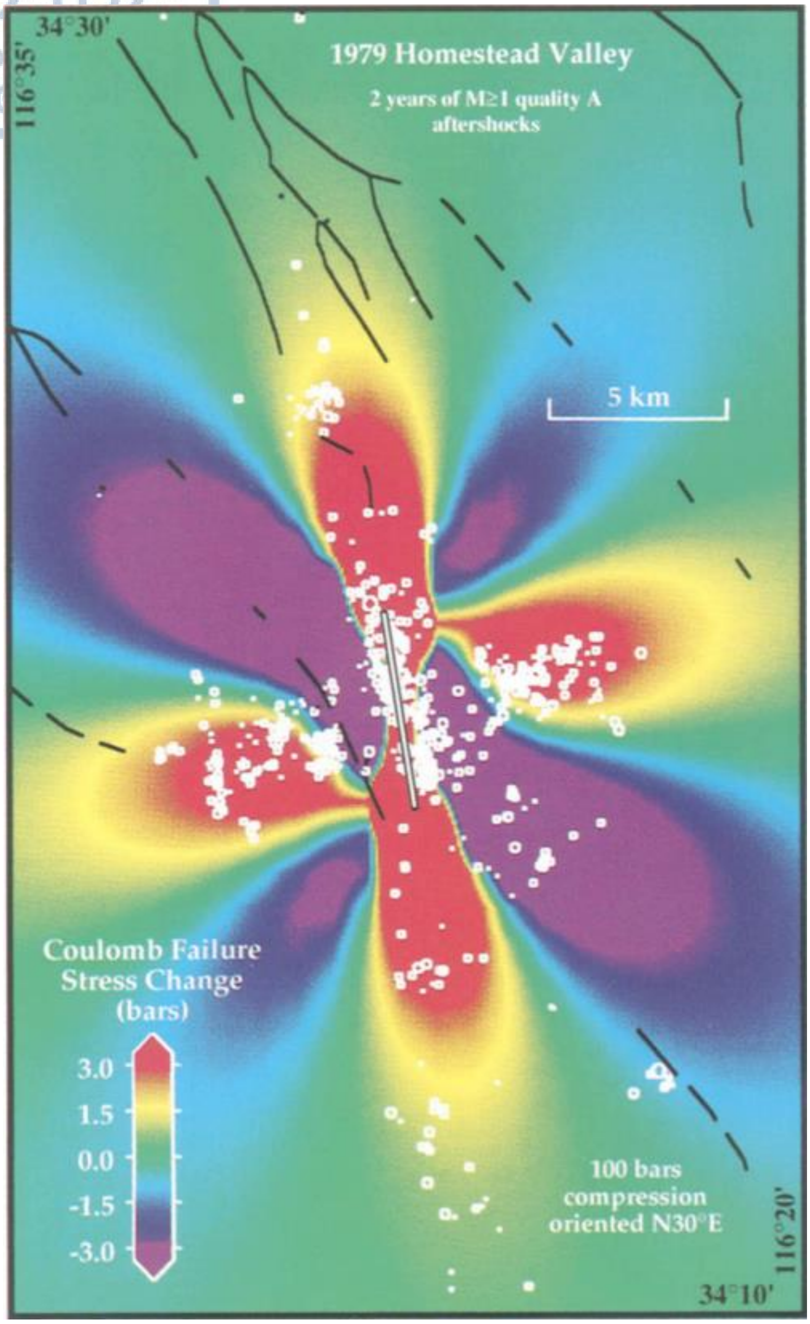

Figure 4.1 Coulomb stress changes on a strike slip fault (white line) induced by the 1979 Homestead Valley earthquake. Future events (white symbols) can be advanced or delayed depending on whether they are located in areas of positive (red) or negative (purple) ΔCFS values. The areas of negative ΔCFS values are called stress shadows. Four lobes of positive and negative ΔCFS are noticeable (King et al., 1994).

4.2 ΔCFS calculations

To calculate the static Coulomb failure stress changes (ΔCFS), the computer program Dis3dop (Erickson, 1986) was used. Dis3dop calculates stress changes, strains and displacements due to slip on one or more dislocation planes embedded in an elastic half-space. The elastic half-space is considered as a homogeneous and isotropic material that is characterized by the Poisson's ratio (PR) and the shear modulus (G). These elastic constants are input by the user, and the calculations are made at observational points located at the half-space. These observational points can be specified either as single points or grids of such points defining any number of dislocation planes in various orientations. When grids of observational points are chosen, the Coulomb stress changes can be calculated and can be represented at any plane in 3D. When single observational points are specified, the Coulomb stress changes will be calculated on a specific rectangular fault plane.

In order to calculate any ΔCFS, the Dis3dop software requires a set of control parameters which are:

1. the number of observational points (NP),
2. the number of rectangular dislocation planes (NF),
3. the Poisson's ratio (PR) and
4. the shear modulus (G).

The computed stress changes will have the same units as the shear modulus (G). The dislocation planes represent faults which are determined by their geometry, slip and position. The position is given in global coordinates. Dis3dop transforms the observational point's coordinates from the global reference frame to the local reference frame. The parameters needed to specify every dislocation plane are (**Fig.4.2**):

1. the dislocation plane's identification number (K),
2. the half-length of the dislocation plane (H in km),
3. the distance measured down-dip from the local coordinate origin to the upper edge of the dislocation plane (DU),
4. the distance measured down-dip from the local coordinate origin to the lower edge of the dislocation plane (DL),
5. the dip of the dislocation plane (θ in degrees),

6. the strike of the dislocation plane (φ in degrees),
7. the distance measured at the N-S direction, between the local and global coordinate origins (x_1^c in km),
8. the distance measured at the E-W direction, between the local and global coordinate origins (x_2^c in km),
9. the horizontal component of the slip (SS in m) and
10. the vertical component of the slip (DS in m).

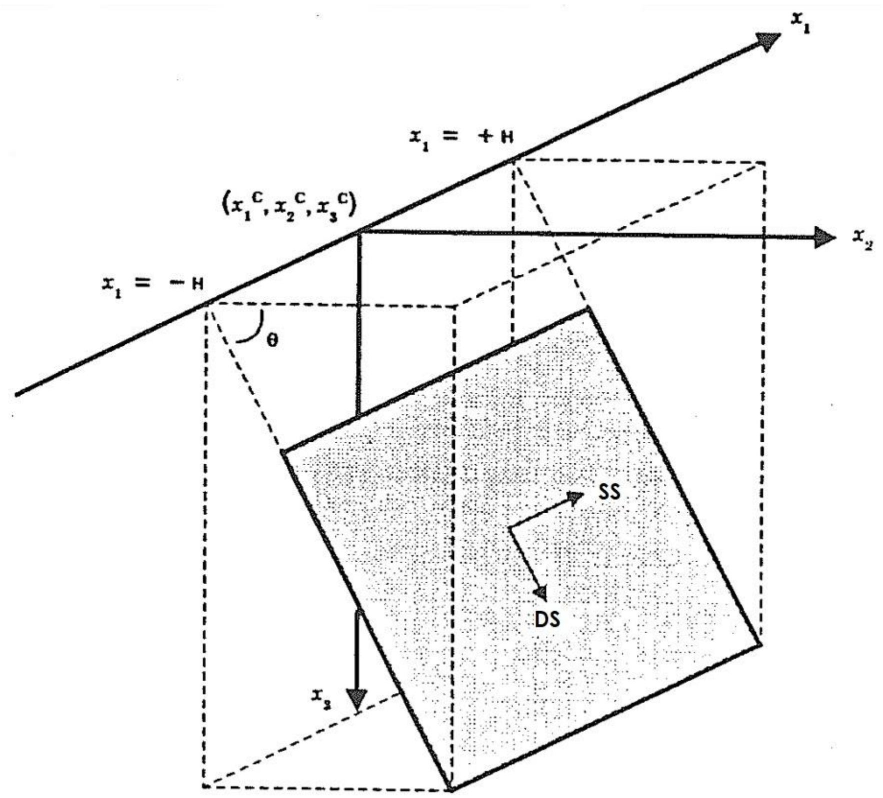

(a)

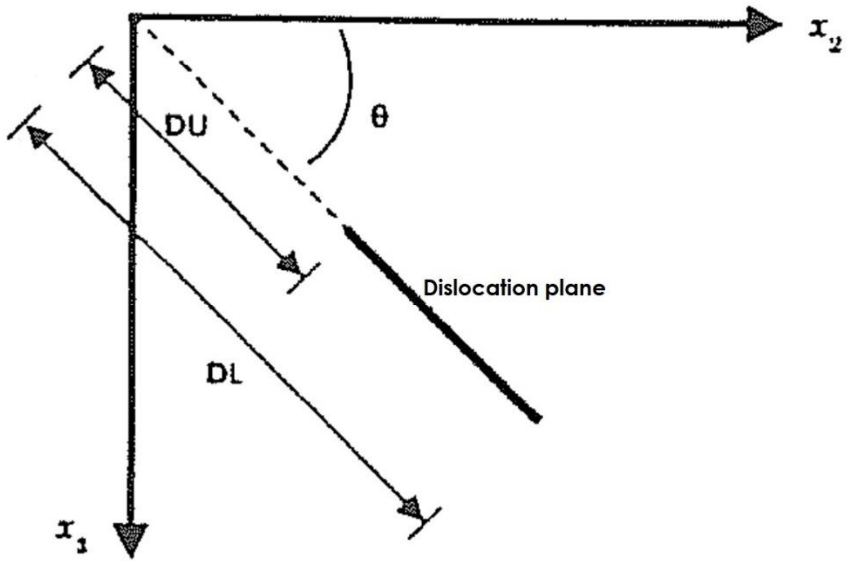

(b)

Figure 4.2 Parameters used to describe a dislocation plane according to the Dis3dop software. (a) The directions of the local coordinate axes are indicated (x_1^c, x_2^c, x_3^c). The strike of the dislocation plane is parallel to the x_1 axis. The endpoints of the dislocation are positioned at $x_1 = \pm$H, where H is the half-length of the dislocation. The parameters SS and DS correspond to the horizontal and vertical components of the slip respectively. The angle θ is the dip of the dislocation plane. (b) Vertical cross section of the dislocation plane. The distances measured down-dip from the local coordinate origin to the upper and lower edges of the dislocation plane are given by DU and DL respectively (Erickson, 1986).

In order to define the fault parameters, the focal mechanism (strike - φ, dip – θ, rake - λ) and the magnitude ($\mathrm{M_w}$) of the corresponding earthquake should be known. The length of the fault can be estimated from the aftershock distribution and scaling laws (Wells and Coppersmith, 1994, Papazachos et al., 2004). The parameters DU and DL are calculated from the depth range of the seismogenic layer using the following equations:

$$\mathrm{DU} = \frac{\mathrm{h_1}}{\sin\theta} \qquad \text{Eq. (4.4)}$$

$$\mathrm{DL} = \frac{\mathrm{h_2}}{\sin\theta} \qquad \text{Eq. (4.5)}$$

where h_1 and h_2 are the upper and lower boundaries of the seismogenic layer, respectively. The two components of slip (SS, DS) are determined by:

$$\mathrm{SS} = \cos\lambda \cdot \vec{\mathrm{u}} \qquad \text{Eq. (4.6)}$$

$$\mathrm{DS} = \sin\lambda \cdot \vec{\mathrm{u}} \qquad \text{Eq. (4.7)}$$

where λ is the rake angle and $\vec{u}$ is the average slip or of the fault. A positive SS value represents left-lateral slip whilst a positive DS value represents normal faulting. The average slip ($\vec{u}$) is defined by the relation (Aki, 1966):

$$\vec{u} = \frac{\mathrm{M}_0}{\mu \cdot \mathrm{L} \cdot \mathrm{w}} \qquad \text{Eq. (4.8)}$$

where M_0 is the scalar seismic moment, μ is the rigidity, L is the fault length and w is the fault width. The scalar seismic moment (M_0) can be found either from the GCMT solutions or from published results. Alternatively, M_0 is calculated from the following equation (Kanamori, 1977):

$$\log_{10}(M_o) = 1.5 \cdot M_w + 16.1 \qquad \text{Eq. (4.9).}$$

Coulomb stress changes associated with the coseismic slips of the three strongest events ($M \geq 5$) of the seismic sequence were calculated and are shown in map views at a depth of 7.5 km (**Fig.4.4**). The calculations were performed in order to evaluate a possible interaction between the adjacent fault segments (**Fig.4.3**) associated with the strongest events. The parameters used for the calculations are presented in Table 3. The fault plane solutions of the three strongest earthquakes were adopted from the Global CMT Project. The Poisson's ratio (PR) and the shear modulus (G) were fixed equal to 0.25 and $3.3 \cdot 10^5$ bars, respectively.

Table 3 Parameters of the fault segments used for the ΔCFS computation.

Nº	Date	Mw	M_0 (dyn·cm)	Strike (º)	Dip (º)	Rake (º)	Length (km)	Width (km)	DU (km)	DL (km)	SS (m)	DS (m)
1.	7/8/13	5.4	$1.58 \cdot 10^{24}$	73	64	-96	5.8	5.8	4.45	11.68	0.0148	0.1415
2.	10/8/13	5.0	$3.98 \cdot 10^{23}$	74	44	-121	4.2	4.2	5.75	15.11	0.0351	0.0585
3.	16/9/13	5.3	$1.12 \cdot 10^{24}$	87	43	-110	5.5	5.5	5.86	16.12	0.0383	0.1053

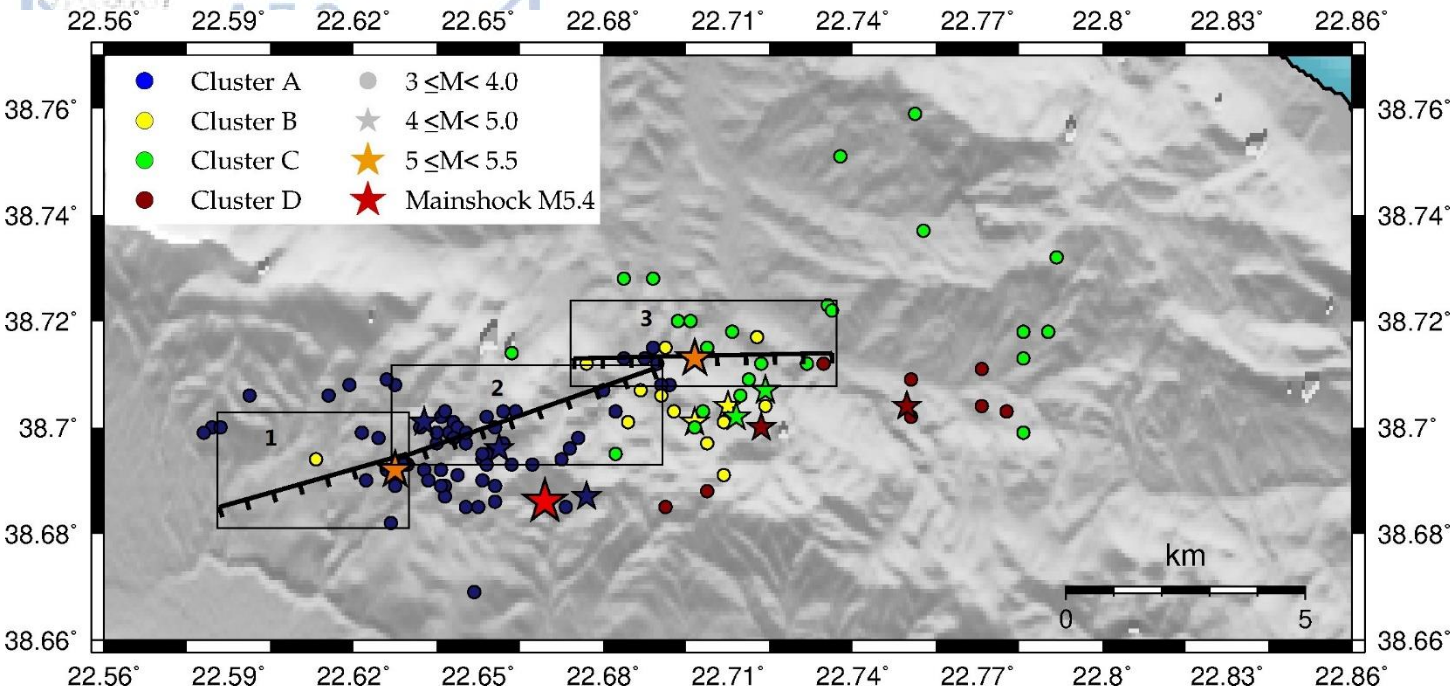

Figure 4.3 Fault segments of the study area along with M ≥ 3 earthquakes. Earthquake epicenters are plotted according to the symbols shown in the legend. Earthquake clusters are indicated by their color coding as shown in figure 2.4. The fault segments are associated with the three major earthquakes (M ≥ 5) of the Amfikleia sequence and are shown by black lines with spikes on the down thrown side.

4.3 Results

Figure 4.4 illustrates the stress pattern associated with the coseismic slips of the three major events (M ≥ 5) of the seismic sequence as well as the cumulative stress pattern prior to the September 16, earthquake (M=5.3). The first major event (M=5.4) (or mainshock) occurred on August 7, the second (M=5.0) struck two days later (10/8) and the third major event (M=5.3) occurred on September 16, almost forty-one days since the mainshock. Fault plane solutions of these earthquakes are also plotted. The Coulomb stress changes are displayed by a color scale. Warm colors indicate positive ΔCFS values whereas cold colors represent negative values of ΔCFS.

Figure 4.4 a) shows the Coulomb stress changes associated with the occurrence of the August 7, mainshock (M=5.4) along with the epicenters of the two major earthquakes (orange stars) of the seismic sequence. Both of these earthquakes are located in areas where the highest positive ΔCFS (1 bar) were calculated. The epicenters of the aftershocks (M ≥ 3) that occurred prior to the August 10 earthquake (M=5.0) are displayed by grey color. The majority of these aftershocks is located in the central negative ΔCFS area (-1 bar).

Figure 4.4 b) illustrates the stress perturbations due to coseismic slip of the August 10 (M=5.0) earthquake. This earthquake is located inside the highest negative ΔCFS area, close to the boundary between stress shadow and bright zones. On September 16, a major earthquake (M=5.3) occurred in an area where positive ΔCFS values were calculated at the eastern part of the study area. In the same figure the aftershocks of M ≥ 3 that occurred from August 10 prior to September 16 earthquake are shown. The majority of them is located in bright zones. Blue and yellow epicenters correspond to Clusters A and B, respectively.

In figure 4.4 c) the accumulated Coulomb stress changes just before the 16 September earthquake are shown. The calculations were made according to the fault parameters of the 16 September earthquake. This earthquake occurred in an area where the highest positive ΔCFS (1 bar) were computed. The aftershocks that occurred from the beginning of the seismic sequence prior to the 16 September earthquake are also plotted The majority of the aftershocks which correspond to Cluster B (yellow symbols) are located either in stress enhanced zones or close to the boundary between negative and positive ΔCFS area. The aftershocks of Cluster A (blue symbols) are located in stress shadow zones.

Figure 4.4 d) shows the coseismic stress changes related to the 16 September earthquake (M=5.3). This earthquake created a shadow zone at the eastern part of the study area. The epicenters of aftershocks with M ≥ 3 that occurred from the day of this earthquake (16/9/13) until the end of the Amfikleia sequence are denoted. These aftershocks belong to Clusters C (green symbols) and D (red symbols). Three out of four aftershocks with M ≥ 4 (red stars) are located close to the 16 September earthquake inside the highest negative ΔCFS area. One aftershock that belongs to Cluster D with

M ≥ 4 is located inside the highest positive ΔCFS area at the easternmost part of the study area.

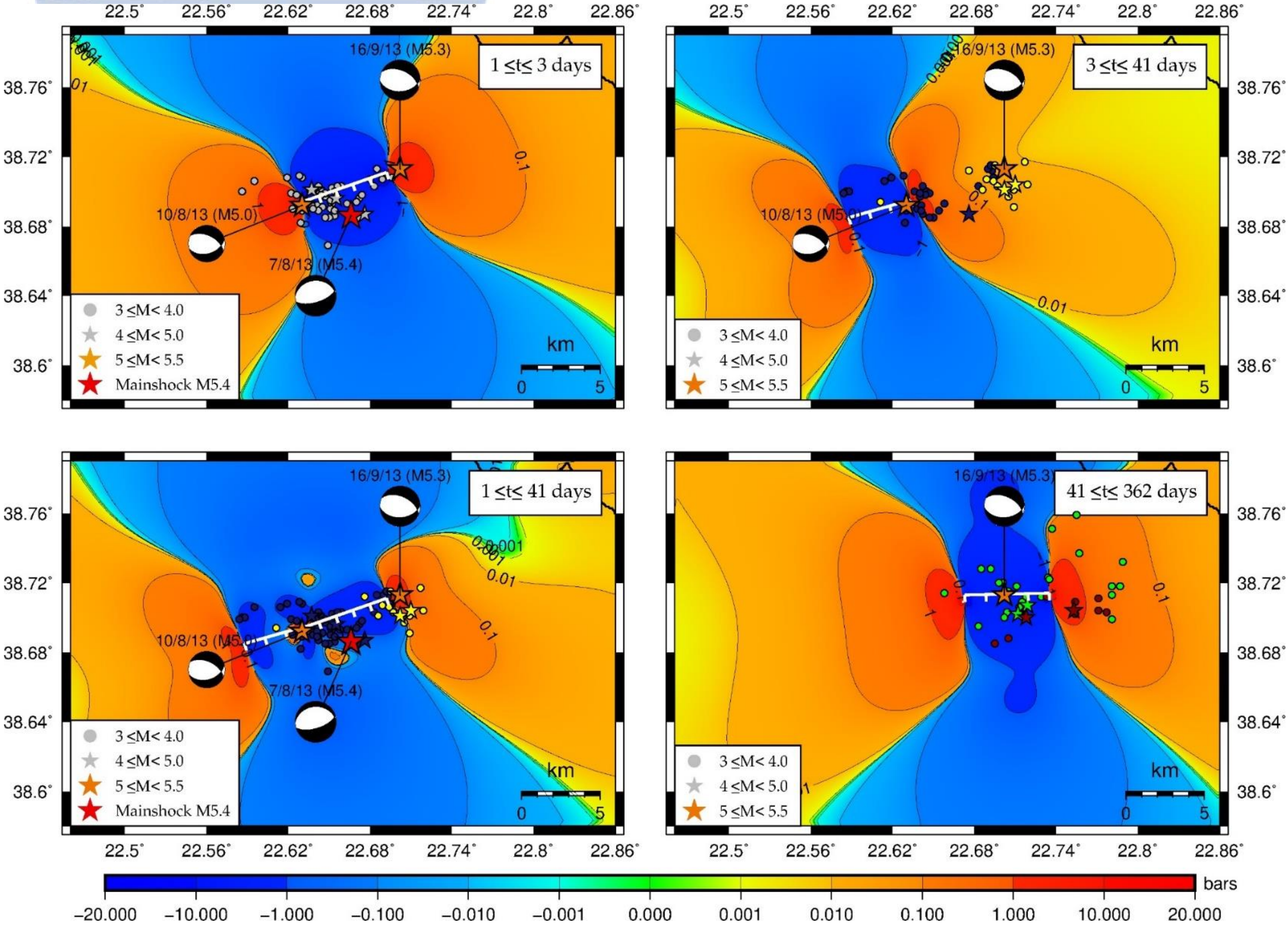

Figure 4.4 Coulomb stress changes caused by the three major events (M ≥ 5) of the Amfikleia sequence. The calculations were made for normal faults at a depth of 7.5 km for dates shown. Fault traces are shown by white lines with spikes on the down thrown side. The fault plane solutions of the three major events (M ≥ 5) are displayed as lower-hemisphere equal-area stereographic projections. The epicenters are colored according to the clusters of their occurrence as they have been shown in figure 2.4. The color scale at the bottom of this figure denotes the Coulomb stress changes in bars. a) Coseismic changes in stress associated with the August 7 mainshock (M=5.4). b) Coseismic stress changes associated with the August 10 earthquake (M=5.0). c) Accumulative ΔCFS just before the September 16 earthquake (M=5.3). d) Coseismic stress changes caused by the September 16 earthquake (M=5.3).

CHAPTER 5: CONCLUSIONS

The seismotectonic properties of the 2013 Amfikleia sequence in central Greece were investigated in order to define the activated fault segments and to examine the evolution of the seismic activity as well as the possible triggering between fault segments due to Coulomb stress transfer. To achieve this target, the seismic activity is assessed by its spatiotemporal and magnitude distribution along with the state of stress.

Four clusters of earthquakes are distinguished which may be attributed to the activation of adjacent fault segments. Throughout the seismic sequence the seismicity migrated to the east. The seismic sequence initiated with a 4.2 earthquake followed by the mainshock (M=5.4) and a 5.8 km rupture on a fault segment. After two days a M = 5.0 earthquake struck and the seismic activity migrated to the west on an adjacent fault segment which has a length of 4.2 km. Forty- one days since the mainshock the strongest aftershock (M=5.3) of the sequence struck. The seismic activity propagated to the east, the length of this segment is 5.5 km.

The examination of temporal (**Fig.2.9**) and spatial variations (**Fig.2.10**) of the b-value shows distinct drops in b-values which are associated with the occurrence of $M \geq 4$ earthquakes. Particularly, at the temporal variations of the b-value there four distinct drops in b-values that coincide with the time of occurrence of each cluster.

The magnitude distribution of earthquakes revealed a non-normal evolution of the seismic sequence which is attributed to the occurrence of the largest events of the sequence.

The pattern of seismicity based on time indicates the daily number of events, their magnitude and the cumulative daily number of events. All the previously mentioned showed an increasing number of earthquakes after a significant aftershock that can be related to the occurrence of four clusters mentioned at the spatiotemporal distribution. The cumulative curve showed remarkable turning points after quiescence periods. In addition the temporal distribution of the sequence was found to decay according to the Omori's law ($n(t) = Kt-p$) while 96% of the earthquakes are within the 95% confidence limits.

Most of the fault plane solutions exhibit normal faulting on WNW or SE striking nodal planes. Cross sections made normal to the strike of each cluster revealed that seismicity is concentrated at 4-11 km depth and distributed on activated structures dipping to the SSE. The minimum compressive axis (T-axis) orientation of the focal mechanisms indicated a NNE-SSW orientation which is in agreement with the nearly N-S extensional regime identified for the study area (Karamanos et al., 2010).

Coulomb stress changes have demonstrated success in identifying retrospectively the locations of the strongest earthquakes ($M \geq 5$) of the sequence which occurred three ($M=5.0$) and forty-one days ($M=5.3$) since the mainshock.

As a future perspective, detailed studies about the determination of the activated faults in the study area should be conducted for further analysis of future seismicity.

References

Abercrombie, R. E. (1996). The magnitude-frequency distribution of earthquakes recorded with deep seismometers at Cajon Pass, southern California. *Tectonophysics*, *261*(1-3), 1-7.

Aki, K. (1965). Maximum likelihood estimate of b in the formula log N= a-bM and its confidence limits. *Bull. Earthq. Res. Inst., Tokyo Univ.*, *43*, 237-239.

Aki, K. (1966). Generation and propagation of G waves from the Niigata Earthquake of June 16, 1964. Part 2. Estimation of earthquake movement, released energy, and stress-strain drop from the G wave spectrum. *Bull. Earthq. Res. Inst.*, *44*, 73-88.

Aki, K. (1979). Characterization of barriers on an earthquake fault. *Journal of Geophysical Research: Solid Earth*, *84*(B11), 6140-6148.

Aki, K., & Richards, P. G. (1980). Quantative seismology: Theory and methods. *Vol. 1-2 WH Freeman & Co. New York*.

Aki, K. (1984). Asperities, barriers, characteristic earthquakes and strong motion prediction. *Journal of Geophysical Research: Solid Earth*, *89*(B7), 5867-5872.

Aki, K., & Richards, P. G. (2002). Quantitative seismology. Second edition. *University Science Books, Sausalito, California* 700pp.

Allen, C. R., St. Amand, P., Richter, C. F., & Nordquist, J. M. (1965). Relationship between seismicity and geologic structure in the southern California region. *Bulletin of the Seismological Society of America*, *55*(4), 753-797.

Heety, E. (2011). Variation of b-value in the earthquake frequency-magnitude distribution with depth in the intraplate regions. *International Journal of Basic & Applied Sciences*, *11*(6), 29-37.

Allmendinger, Richard & Cardozo, Nestor & Fisher, Donald. (2012). Structural geology algorithms: Vectors and tensors. Structural Geology Algorithms: Vectors and Tensors. 10.1017/CBO9780511920202.

Allmendinger, R. W. (2016). Faultkin (version 8.0): Ithaca. *New York, Department of Geological Sciences, Cornell University*.

Ambraseys, N. N., & Jackson, J. A. (1990). Seismicity and associated strain of central Greece between 1890 and 1988. *Geophysical Journal International*, *101*(3), 663-708.

Ambraseys, N. N., & Jackson, J. A. (1997). Seismicity and strain in the Gulf of Corinth (Greece) since 1694. *Journal of Earthquake Engineering*, *1*(03), 433-474.

Antonioli, A., Piccinini, D., Chiaraluce, L., & Cocco, M. (2005). Fluid flow and seismicity pattern: Evidence from the 1997 Umbria-Marche (central Italy) seismic sequence. *Geophysical Research Letters*, *32*(10).

Anderson, H., & Jackson, J. (1987). Active tectonics of the Adriatic region. *Geophysical Journal International*, *91*(3), 937-983.

Armijo, R., Meyer, B. G. C. P., King, G. C. P., Rigo, A., & Papanastassiou, D. (1996). Quaternary evolution of the Corinth Rift and its implications for the Late Cenozoic evolution of the Aegean. *Geophysical Journal International*, *126*(1), 11-53.

Båth, M. (1965). Lateral inhomogeneities of the upper mantle. *Tectonophysics*, *2*(6), 483-514.

Βαλκανιώτης, Σ. (2009). *Συσχέτιση νεοτεκτονικών δομών και σεισμικότητας στην ευρύτερη περιοχή του Κορινθιακού Κόλπου (Κεντρική Ελλάδα)* (No. GRI-2010-4133). Aristotle University of Thessaloniki.

Bender, B. (1983). Maximum likelihood estimation of b values for magnitude grouped data. *Bulletin of the Seismological Society of America*, *73*(3), 831-851.

Belardinelli, M. E., Bizzarri, A., & Cocco, M. (2003). Earthquake triggering by static and dynamic stress changes. *Journal of Geophysical Research: Solid Earth*, *108*(B3), 2135.

Bizzarri, A., & Belardinelli, M. E. (2008). Modelling instantaneous dynamic triggering in a 3-D fault system: application to the 2000 June South Iceland seismic sequence. *Geophysical Journal International*, *173*(3), 906-921.

Brodsky, E. E., Karakostas, V., & Kanamori, H. (2000). A new observation of dynamically triggered regional seismicity: Earthquakes in Greece following the August 1999 Izmit, Turkey earthquake. *Geophysical Research Letters*, *27*(17), 2741-2744.

Burchfiel, B. C. (2004). New technology; new geological challenges. *Geol. Soc. Amer. Today*, *14*(2), 4-10.

Cao, A., & Gao, S. S. (2002). Temporal variation of seismic b-values beneath northeastern Japan island arc. *Geophysical research letters*, *29*(9), 48-1.

Carver, D. L., & Henrisey, R. (1978). *Preliminary report on the aftershocks of the June 20, 1978, Thessaloniki, Greece, earthquake* (No. 78-1099). US Geological Survey.

Carver, D., & Bollinger, G. A. (1981). Aftershocks of the June 20, 1978, Greece earthquake: a multimode faulting sequence. *Tectonophysics*, *73*(4), 343-363.

Cocco, M., & Rice, J. R. (2002). Pore pressure and poroelasticity effects in Coulomb stress analysis of earthquake interactions. *Journal of Geophysical Research: Solid Earth*, *107*(B2), ESE-2.

Comninakis, P., Drakopoulos, J., Moumoulidis, G., & Papazachos, B. (1968). Foreshock and aftershock sequences of the Cremasta earthquake and their relation to the waterloading of the Cremasta artificial lake. *Annals of Geophysics*, *21*(1), 39-71.

Console, R., Carluccio, R., Papadimitriou, E., & Karakostas, V. (2015). Synthetic earthquake catalogs simulating seismic activity in the Corinth Gulf, Greece, fault system. *Journal of Geophysical Research: Solid Earth*, *120*(1), 326-343.

Curtis, J. W. (1973). A magnitude domain study of the seismicity of Papua, New Guinea, and the Solomon Islands. *Bulletin of the Seismological Society of America*, *63*(3), 787-806.

Daniel, G., Prono, E., Renard, F., Thouvenot, F., Hainzl, S., Marsan, D., ... & Guiguet, R. (2011). Changes in effective stress during the 2003–2004 Ubaye seismic swarm, France. *Journal of Geophysical Research: Solid Earth*, *116*(B1).

Das, S., & Scholz, C. H. (1981). Theory of time-dependent rupture in the Earth. *Journal of Geophysical Research: Solid Earth*, *86*(B7), 6039-6051.

DeMets, C., Gordon, R. G., Argus, D. F., & Stein, S. (1990). Current plate motions. *Geophysical journal international*, *101*(2), 425-478.

Deng, J., & Sykes, L. R. (1997). Evolution of the stress field in southern California and triggering of moderate-size earthquakes: A 200-year perspective. *Journal of Geophysical Research: Solid Earth*, *102*(B5), 9859-9886.

Deng, J., & Sykes, L. R. (1997). Stress evolution in southern California and triggering of moderate-, small-, and micro-size earthquakes. *Journal of Geophysical Research: Solid Earth*, *102*(B11), 24411-24435.

Dewey, J. F. (1988). Extensional collapse of orogens. *Tectonics*, *7*(6), 1123-1139.

Δελαπόρτας Γ. (2016). Σεισμός Αυγούστου 2013 στο ρεγκίνι Φθιώτιδας. ζημιές και πορεία αποκατάστασης της περιοχής. σεισμική επικινδυνότητα και προετοιμασία του κρατικού μηχανισμού. *Masters Thesis, National and Kapodistrian University of Athens.*

Doutsos, T., & Kokkalas, S. (2001). Stress and deformation patterns in the Aegean region. *Journal of Structural Geology*, *23*(2-3), 455-472.

Drakatos, G., & Latoussakis, J. (2001). A catalog of aftershock sequences in Greece (1971–1997): Their spatial and temporal characteristics. *Journal of Seismology*, *5*(2), 137-145.

Eneva, M., & Hamburger, M. W. (1989). Spatial and temporal patterns of earthquake distribution in Soviet Central Asia: Application of pair analysis statistics. *Bulletin of the Seismological Society of America*, *79*(5), 1457-1476.

Erickson, L. (1986). User's Manual for DIS3D: A Three-dimensional Dislocation Program With Applications to Faulting in the Earth. *Masters Thesis, Stanford Univ., Stanford, Calif*, 167.

Fintel, M. (1978). Report of the earthquakes of May 24 and June 20. 1978, Salonika, Greece. *Journal of the American Concrete Institute*, *75*(10), N9-N15.

Frohlich, C., & Davis, S. D. (1993). Teleseismic b values; or, much ado about 1.0. *Journal of Geophysical Research: Solid Earth*, *98*(B1), 631-644.

Galanopoulos, A. G. (1955). The seismic geography of Greece. *Ann. Geol. Pays Hellen.*, *6*, 83-121.

Ganas, A., & White, K. (1996). Neotectonic fault segments and footwall geomorphology in Eastern Central Greece from Landsat TM data. *Geological Society of Greece Special Publication*, *6*, 169-175.

Ganas, A. (1997). Fault segmentation and seismic hazard assessment in the Gulf of Evia Rift, central Greece. *Doctoral dissertation, University of Reading, UK*, 369pp .

Ganas, A., Roberts, G. P., & Memou, T. (1998). Segment boundaries, the 1894 ruptures and strain patterns along the Atalanti Fault, central Greece. *Journal of Geodynamics*, *26*(2-4), 461-486.

Ganas, A., Sokos, E., Agalos, A., Leontakianakos, G., & Pavlides, S. (2006). Coulomb stress triggering of earthquakes along the Atalanti Fault, central Greece: Two April 1894 M6+ events and stress change patterns. *Tectonophysics*, *420*(3-4), 357-369.

Ganas, A., & Parsons, T. (2009). Three-dimensional model of Hellenic Arc deformation and origin of the Cretan uplift. *Journal of Geophysical Research: Solid Earth*, *114*(B6).

Ganas, A., Karastathis, V., Moshou, A., Valkaniotis, S., Mouzakiotis, E., & Papathanassiou, G. (2014). Aftershock relocation and frequency–size distribution, stress inversion and seismotectonic setting of the 7 August 2013 M= 5.4 earthquake in Kallidromon Mountain, central Greece. *Tectonophysics*, *617*, 101-113.

Gibowicz, S. J. (1990). Seismicity induced by mining. In *Advances in geophysics* (Vol. 32, pp. 1-74). Elsevier.

Gibowicz, S. J., & Lasocki, S. (2001). Seismicity induced by mining: Ten years later. *Advances in geophysics*, *44*, 39-181.

Goldsworthy, M., Jackson, J., & Haines, J. (2002). The continuity of active fault systems in Greece. *Geophysical Journal International*, *148*(3), 596-618.

Goldsworthy, M., & Jackson, J. (2001). Migration of activity within normal fault systems: examples from the Quaternary of mainland Greece. *Journal of Structural Geology*, *23*(2-3), 489-506.

Gomberg, J. (1991). Seismicity and detection/location threshold in the southern Great Basin seismic network. *Journal of Geophysical Research: Solid Earth*, *96*(B10), 16401-16414.

Gorbatikov, A. V., Kalinina, A. V., Volkov, V. A., Arnoso, J., Vieira, R., & Velez, E. (2004). Results of analysis of the data of microseismic survey at Lanzarote Island, Canary, Spain. In *Geodetic and Geophysical Effects Associated with Seismic and Volcanic Hazards* (pp. 1561-1578). Birkhäuser, Basel.

Gross, S. J., & Kisslinger, C. (1994). Tests of models of aftershock rate decay. *Bulletin of the Seismological Society of America*, *84*(5), 1571-1579.

Gutenberg, B., & Richter, C. F. (1944). Frequency of earthquakes in California. *Bulletin of the Seismological society of America*, *34*(4), 185-188.

Gutenberg, B. and Richter, C.F. (1954) *Seismicity of the Earth and Associated Phenomena*. 2nd Edition, Princeton Univ. Press, N.J., 310p.

Guidoboni, E., Comastri, A., & Traina, G. (1994). Catalogue of Ancient Earthquakes in the Mediterranean Area up to the 10th Century Rome. *Istituto nazionale di geofisica*, p. 504.

Gupta, H. K., Rastogi, B. K., & Narain, H. (1972). Some discriminatory characteristics of earthquakes near the Kariba, Kremasta, and Koyna artificial lakes. *Bulletin of the Seismological Society of America*, *62*(2), 493-507.

Hardebeck, J., & Shearer, P. (2002). A New Method for Determining First-Motion Focal Mechanisms. Bulletin of the Seismological Society of America. 92. 2264-2276. 10.1785/0120010200.

Hardebeck, J. L., & Okada, T. (2018). Temporal stress changes caused by earthquakes: A review. *Journal of Geophysical Research: Solid Earth*, *123*(2), 1350-1365.

Harris, R. A., & Simpson, R. W. (1996). In the shadow of 1857-the effect of the great Ft. Tejon earthquake on subsequent earthquakes in southern California. *Geophysical Research Letters*, *23*(3), 229-232.

Harris, R. A. (1998). Introduction to special section: Stress triggers, stress shadows, and implications for seismic hazard. *Journal of Geophysical Research: Solid Earth*, *103*(B10), 24347-24358.

Hashemi, M., & Karimi, H. A. (2016). Seismic source modeling by clustering earthquakes and predicting earthquake magnitudes. In *Smart City 360°* (pp. 468-478). Springer International Publishing, Cham, Switzerland.

Hatzfeld, D., Nord, J., Paul, A., Guiguet, R., Briole, P., Ruegg, J. C., ... & Veis, G. (1995). The Kozani-Grevena (Greece) earthquake of May 13, 1995, Ms= 6.6, Preliminary results of a field multidisciplinary survey. *Seismological Research Letters*, *66*, 61-70.

Hatzfeld, D., Karakostas, V., Ziazia, M., Selvaggi, G., Leborgne, S., Berge, C., ... & Papaioannou, C. (1997). The Kozani-Grevena (Greece) earthquake of 13 May 1995 revisited from a detailed seismological study. *Bulletin of the Seismological Society of America*, *87*(2), 463-473.

Hatzfeld, D., Karakostas, V., Ziazia, M., Selvaggi, G., Leborgne, S., Berge, C., & Makropoulos, K. (1998). The Kozani-Grevena (Greece) earthquake of May 13, 1995, a seismological study. *Journal of Geodynamics*, *26*(2-4), 245-254.

Hatzidimitriou, P. M., Papadimitriou, E. E., Mountrakis, D. M., & Papazachos, B. C. (1985). The seismic parameter b of the frequency-magnitude relation and its association with the geological zones in the area of Greece. *Tectonophysics*, *120*(1-2), 141-151.

Hatzidimitriou, P. M., Papazachos, B. C., & Karakaisis, G. F. (1994). Quantitative seismicity of the Aegean and surrounding area. *Proc. of the XXIV Gen. Assembly of ESC, Athens*, 19-24.

Hirano, R. (1924). An Investigation in After Shocks felt at Kumagai accompanying the Great Kwanto Earthquake of September Ist, 1923. *Journal of the Meteorological Society of Japan. Ser. II*, *2*(3), 77-83.

Holub, K. (1995). Preliminary results of b-values analysis for mining-induced seismic events. *Acta Montana IRSM AS CR, Ser A*, (6), 27-31.

Huang, Y. L., Zhou, S. Y., & Zhuang J. C. (2016). Numerical tests on catalog-based methods to estimate magnitude of completeness. *Chinese Journal of Geophysics*, *59*(3), 266-275.

Ishimoto, M. (1936). Observations of earthquakes registered with the microseismograph constructed recently. *Bull. Earthquake Res. Inst. Univ. Tokyo*, *17*, 443-478.

Jackson, J., & McKenzie, D. (1988). The relationship between plate motions and seismic moment tensors, and the rates of active deformation in the Mediterranean and Middle East. *Geophysical Journal International*, *93*(1), 45-73.

Jackson, J. (1994). Active tectonics of the Aegean region. *Annual Review of Earth and Planetary Sciences*, *22*(1), 239-271.

Jeffreys, H. (1938). Aftershock and periodicity in earthquakes. *Gerlands Beitr. Geophys.*, *56*, 111-139.

Jolivet, L., Faccenna, C., Huet, B., Labrousse, L., Le Pourhiet, L., Lacombe, O., Lecomte, E., Burov, E., Denèle, Y., Brun, J.-P., Philippon, M., Paul, A., Salaün, G.,Karabulut, H., Piromallo, C., Monié, P., Gueydan, F., Okay, A.I., Oberhänsli, R., Pourteau, A., Augier, R., Gadenne, L., & Driussi, O. (2013). Aegean tectonics: Strain localization, slab tearing and trench retreat. *Tectonophysics*, *597*, 1-33.

Kagan, Y., & Knopoff, L. (1978). Statistical study of the occurrence of shallow earthquakes. *Geophysical Journal International*, *55*(1), 67-86.

Kagan, Y. Y. (2004). Short-term properties of earthquake catalogs and models of earthquake source. *Bulletin of the Seismological Society of America*, *94*(4), 1207-1228.

Kalligeris, N., Flouri, E., Okal, E., & Synolakis, C. (2012). The AD 365 earthquake: high resolution tsunami inundation for Crete and full scale simulation exercise. In *EGU General Assembly Conference Abstracts* (p. 11787).

Kalyoncuoglu, U. Y. (2007). Evaluation of seismicity and seismic hazard parameters in Turkey and surrounding area using a new approach to the Gutenberg–Richter relation. *Journal of Seismology*, *11*(2), 131-148.

Kanamori, H. (1977). The energy release in great earthquakes. *Journal of geophysical research*, *82*(20), 2981-2987.

Kanamori, H., & Stewart, G. S. (1978). Seismological aspects of the Guatemala earthquake of February 4, 1976. *Journal of Geophysical Research: Solid Earth*, *83*(B7), 3427-3434.

Karamanos, C. K., Karakostas, V. G., Seeber, L., Papadimitriou, E. E., & Kilias, A. A. (2010). Recent seismic activity in Central Greece revealing local seismotectonic properties. *Bulletin of the Geological Society of Greece*, *43*(4), 2075-2083.

Karnik, V. (1969). Seismicity of the European area. *Washington DC American Geophysical Union Geophysical Monograph Series*, *13*, 139-144.

Karakaisis, G. F. (1984). Contribution to the Study of the Seismic Sequences in the Aegean and Surrounding Areas. *Ph. D. Thesis, Univ. of Thessaloniki*, pp. 192.

Karakaisis, G. F., Hatzidimitriou, P. M., Scordilis, E. M., & Panagiotopoulos, D. G. (1998). Seismicity of western Macedonia, Greece. *Journal of Geodynamics*, *26*(2-4), 297-307.

Karakostas, V. G., Papadimitriou, E. E., Karakaisis, G. F., Papazachos, C. B., Scordilis, E. M., Vargemezis, G., & Aidona, E. (2003). The 2001 Skyros, Northern Aegean, Greece, earthquake sequence: off-fault aftershocks, tectonic implications, and seismicity triggering. *Geophysical Research Letters*, *30*(1), 12-1.

Karakostas, V. G., Papadimitriou, E. E., & Papazachos, C. B. (2004). Properties of the 2003 Lefkada, Ionian Islands, Greece, earthquake seismic sequence and seismicity triggering. *Bulletin of the Seismological Society of America*, *94*(5), 1976-1981.

Karakostas, V., Karamanos, C., Papadimitriou, E., Kassaras, I., & Makropoulos, K. (2006). Microseismicity and faulting geometry in central Greece. *1st European Conference on Earthquake Engineering and Seismology: 1-10, Geneva.*

Karakostas, V., Papadimitriou, E., & Gospodinov, D. (2014). Modelling the 2013 North Aegean (Greece) seismic sequence: geometrical and frictional constraints, and aftershock probabilities. *Geophysical Journal International*, *197*(1), 525-541.

Karakostas, V., Papadimitriou, E., Mesimeri, M., Gkarlaouni, C., & Paradisopoulou, P. (2015). The 2014 Kefalonia doublet (Mw 6.1 and Mw 6.0), central Ionian Islands, Greece: Seismotectonic implications along the Kefalonia transform fault zone. *Acta Geophysica*, *63*(1), 1-16.

Kato, A., Fukuda, J. I., Nakagawa, S., & Obara, K. (2016). Foreshock migration preceding the 2016 Mw 7.0 Kumamoto earthquake, Japan. *Geophysical Research Letters, 43*(17), 8945-8953.

Kijko, A., & Smit, A. (2012). Extension of the Aki-Utsu b-value estimator for incomplete catalogs. *Bulletin of the Seismological Society of America*, *102*(3), 1283-1287.

Kilias, A. A., Tranos, M. D., Papadimitriou, E. E., & Karakostas, V. G. (2008). The recent crustal deformation of the Hellenic orogen in Central Greece; the Kremasta and Sperchios Fault Systems and their relationship with the adjacent large structural features. *Zeitschrift der Deutschen Gesellschaft fur Geowissenschaften*, *159*(3), 533.

Kilb, D., & Hardebeck, J. L. (2006). Fault parameter constraints using relocated earthquakes: a validation of first-motion focal-mechanism data. *Bulletin of the Seismological Society of America*, *96*(3), 1140-1158.

King, G. C., Stein, R. S., & Lin, J. (1994). Static stress changes and the triggering of earthquakes. *Bulletin of the Seismological Society of America*, *84*(3), 935-953.

King, G. C. P., & Cocco, M. (2001). Fault interaction by elastic stress changes: New clues from earthquake sequences. *Adv. Geophys.*, *44*, 1-38.

Kiratzi, A., & Louvari, E. (2003). Focal mechanisms of shallow earthquakes in the Aegean Sea and the surrounding lands determined by waveform modelling: a new database. *Journal of Geodynamics*, *36*(1-2), 251-274.

Kisslinger, C. (1993). The stretched exponential function as an alternative model for aftershock decay rate. *Journal of Geophysical Research: Solid Earth*, *98*(B2), 1913-1921.

Klein, F. W. (2002). User's guide to HYPOINVERSE-2000, a Fortran program to solve for earthquake locations and magnitudes. *U. S. Geol. Surv. Open File Report 02–171 Version 1.0.*

Kostoglou, A., Karakostas, V., Bountzis, P., & Papadimitriou, E. (2020). The February-March 2019 Seismic Swarm Offshore North Lefkada Island, Greece: Microseismicity Analysis and Geodynamic Implications. *Applied Sciences*, *10*(13), 4491.

Kranis, H. D. (1999). Neotectonic activity of fault zones in Lokris, central-eastern mainland Greece. *PhD t hesis, Faculty of Geology, National and Kapodistrian University of Athens,(GAIA publ. No. 10).*

Kranis, H. D., & Papanikolaou, D. I. (2001). Evidence for detachment faulting on the NE Parnassos mountain front (Central Greece). *Bulletin of the Geological Society of Greece*, *34*(1), 281-287.

Kranis, H. (2007). Neotectonic basin evolution in central-eastern mainland Greece: an overview. *Bulletin of the Geological Society of Greece*, *40*(1), 360-373.

Kulhánek, O., & Meyer, K. (1979). Source parameters of the Volvi-Langadhas earthquake of June 20, 1978 deduced from body-wave spectra at stations Uppsala and Kiruna. *Bulletin of the Seismological Society of America*, *69*(4), 1289-1294.

Kulhanek, O. (2005). Seminar on b-value. *Dept. of Geophysics, Charles University, Prague*, 10-190.

Leeder, M. R., & Jackson, J. A. (1993). The interaction between normal faulting and drainage in active extensional basins, with examples from the western United States and central Greece. *Basin research*, *5*(2), 79-102.

Le Pichon, X., & Angelier, J. (1979). The Hellenic arc and trench system: a key to the neotectonic evolution of the eastern Mediterranean area. *Tectonophysics*, *60*(1-2), 1-42.

Le Pichon, X., Chamot-Rooke, N., Lallemant, S., Noomen, R., & Veis, G. (1995). Geodetic determination of the kinematics of central Greece with respect to Europe: Implications for eastern Mediterranean tectonics. *Journal of Geophysical Research: Solid Earth*, *100*(B7), 12675-12690.

Lippiello, E., De Arcangelis, L., & Godano, C. (2009). Role of static stress diffusion in the spatiotemporal organization of aftershocks. *Physical review letters*, *103*(3), 038501.

Llenos, A. L., & McGuire, J. J. (2011). Detecting aseismic strain transients from seismicity data. *Journal of Geophysical Research: Solid Earth*, *116*, B06305.

Lombardi, A. M. (2003). The maximum likelihood estimator of b-value for mainshocks. *Bulletin of the Seismological Society of America*, *93*(5), 2082-2088.

Lombardi, A. M., Cocco, M., & Marzocchi, W. (2010). On the increase of background seismicity rate during the 1997–1998 Umbria-Marche, Central Italy, sequence: apparent variation or fluid-driven triggering?. *Bulletin of the Seismological Society of America*, *100*(3), 1138-1152.

Lomnitz, C. (1966). Magnitude stability in earthquake sequences. *Bulletin of the Seismological Society of America*, *56*(1), 247-249.

Lolli, B., & Gasperini, P. (2006). Comparing different models of aftershock rate decay: The role of catalog incompleteness in the first times after main shock. *Tectonophysics*, *423*(1-4), 43-59.

Louvari, E., Kiratzi, A. A., & Papazachos, B. C. (1999). The Cephalonia transform fault and its extension to western Lefkada Island (Greece). *Tectonophysics*, *308*(1-2), 223-236.

Main, I. G., & Meredith, P. G. (1991). Stress corrosion constitutive laws as a possible mechanism of intermediate-term and short-term seismic quiescence. *Geophysical journal international*, *107*(2), 363-372.

Marrett, R., & Allmendinger, R. W. (1990). Kinematic analysis of fault-slip data. *Journal of structural geology*, *12*(8), 973-986.

Mariolakos, I., & Papanikolaou, D. (1987). Deformation patters and relation between deformation and seismicity in the Hellenic *Arc. Proc. 2nd Cong., Geol.Soc.Greece, Athens, 1984. Bull.geol.Soc.Greece, XIX*, 59-76.

Mariolakos, I., Fountoulis, I., & Kranis, H. (2001). Geology and tectonics: Sterea Hellas area. *Engineering Geology and the Environment, Marines, Koukis, Tsiambaos & Stournaras (Eds.)*, 3971-3986.

Marsan, D., Prono, E., & Helmstetter, A. (2013). Monitoring aseismic forcing in fault zones using earthquake time series. *Bulletin of the Seismological Society of America*, *103*(1), 169-179.

McClusky, S., Balassanian, S., Barka, A., Demir, C., Ergintav, S., Georgiev, I., ... & Veis, G. (2000). Global Positioning System constraints on plate kinematics and dynamics in the eastern Mediterranean and Caucasus. *Journal of Geophysical Research: Solid Earth*, *105*(B3), 5695-5719.

McKenzie, D. P. (1970). Plate tectonics of the Mediterranean region. *Nature*, *226*(5242), 239-243.

McKenzie, D. (1972). Active tectonics of the Mediterranean region. *Geophysical Journal International*, *30*(2), 109-185.

McKenzie, D. (1978). Active tectonics of the Alpine—Himalayan belt: the Aegean Sea and surrounding regions. *Geophysical Journal International*, *55*(1), 217-254.

Mercier, J., Delibassis, N., Gauthier, A., Jarrige, J., & Lemeille, F. (1979). La néotectonique de l'Arc Egéen. *Revue de géologie dynamique et de géographie physique Paris*, *21*(1), 67-92.

Mercier, J. L., Sorel, D., Vergely, P., & Simeakis, K. (1989). Extensional tectonic regimes in the Aegean basins during the Cenozoic. *Basin research*, *2*(1), 49-71.

Migiros, G., Antoniou, V., Papanikolaou, I., & Antoniou, V. (2010). Tectonic setting and deformation of the Kallidromo Mt, Central Greece. *Bulletin of the Geological Society of Greece*, *43*(1), 320-330.

Minster, J. B., & Jordan, T. H. (1978). Present-day plate motions. *Journal of Geophysical Research: Solid Earth*, *83*(B11), 5331-5354.

Mignan, A. (2008). The stress accumulation model: Accelerating moment release and seismic hazard. *Advances in geophysics*, *49*, 67-201.

Mignan, A., & Woessner, J. (2012). Estimating the magnitude of completeness for earthquake catalogs. *Community Online Resource for Statistical Seismicity Analysis*. 10.5078/corssa-00180805.

Mitsakaki, C., Sakellariou, M., Tsinas, D., & Marinou, A. (2006). Assessment of Coulomb stress changes associated with the 1995 Aigion earthquake in the Gulf of Corinth (Greece). In *Geodetic Deformation Monitoring: From Geophysical to Engineering Roles*, pp. 172-180.

Miyamura, S. (1962). Magnitude-frequency relation of earthquakes and its bearing on geotectonics. *Proceedings of the Japan Academy*, *38*(1), 27-30.

Mogi, K. (1962). On the time distribution of aftershocks accompanying the recent major earthquakes in and near Japan. *Bull. Earthq. Res. Inst., Univ. Tokyo*, *40*, 107-124.

Mogi, K. (1963). Some discussions on aftershocks, foreshocks and earthquake swarms-the fracture of a semi-infinite body caused by an inner stress origin and its relation the earthquake phenomena. *Bull. Earthq. Res. Inst.*, *41*, 615-658.

Mogi, K. (1979). Global variation of seismic activity. *Tectonophysics*, *57*(2-4), T43-T50.

Mori, J., & Abercrombie, R. E. (1997). Depth dependence of earthquake frequency-magnitude distributions in California: Implications for rupture initiation. *Journal of Geophysical Research: Solid Earth*, *102*(B7), 15081-15090.

Morales-Esteban, A., Martínez-Álvarez, F., Troncoso, A., Justo, J. L., & Rubio-Escudero, C. (2010). Pattern recognition to forecast seismic time series. *Expert systems with applications*, *37*(12), 8333-8342.

Molchan, G. M., & Dmitrieva, O. E. (1990). Dynamics of the magnitude—frequency relation for foreshocks. *Physics of the earth and planetary interiors*, *61*(1-2), 99-112.

Mountrakis, D., Pavlides, S., Zouros, N., Astaras, T., & Chatzipetros, A. (1998). Seismic fault geometry and kinematics of the 13 May 1995 Western Macedonia (Greece) earthquake. *Journal of Geodynamics*, *26*(2-4), 175-196.

Monterroso, D. (2003). Seismic precursory potential of temporal variation of b-value: five case studies in Central America. *Comprehensive Summaries of Uppsala Dissertations from the Faculty of Science and Technology*, *897*, 17.

Nalbant, S. S., Hubert, A., & King, G. C. (1998). Stress coupling between earthquakes in northwest Turkey and the north Aegean Sea. *Journal of Geophysical Research: Solid Earth*, *103*(B10), 24469-24486.

Nalbant, S. S., McCloskey, J., Steacy, S., & Barka, A. A. (2002). Stress accumulation and increased seismic risk in eastern Turkey. *Earth and Planetary Science Letters*, *195*(3-4), 291-298.

Nalbant, S., McCloskey, J., Steacy, S., NicBhloscaidh, M., & Murphy, S. (2013). Interseismic coupling, stress evolution, and earthquake slip on the Sunda megathrust. *Geophysical Research Letters*, *40*(16), 4204-4208.

Narteau, C., Shebalin, P., & Holschneider, M. (2002). Temporal limits of the power law aftershock decay rate. *Journal of Geophysical Research: Solid Earth*, *107*, 2359.

Nuannin, P., Kulhanek, O., & Persson, L. (2005). Spatial and temporal b value anomalies preceding the devastating off coast of NW Sumatra earthquake of December 26, 2004. *Geophysical research letters*, *32*(11), L11307-1.

Ogata, Y. (1988). Statistical models for earthquake occurrences and residual analysis for point processes. *Journal of the American Statistical association*, *83*(401), 9-27.

Ogata, Y., & Katsura, K. (1993). Analysis of temporal and spatial heterogeneity of magnitude frequency distribution inferred from earthquake catalogues. *Geophysical Journal International*, *113*(3), 727-738.

Omori, F. (1894). On the after-shocks of earthquakes. *J. Coll. Sci., Imp. Univ., Japan*, *7*, 111-200.

Oral, M. B., Reilinger, R. E., Toksoz, M. N., King, R. W., Barka, A. A., & Kinik, I. (1995). Coherent plate motion in the eastern Mediterranean continental collision zone. *Eos Trans. AGU*, 76, 9-11.

Otsuka, M. (1985). Studies on aftershock sequences-Part 1. Physical interpretation of Omori's formula. *Sci. Rep. Shimabara Earthq. Volcano Obs*, *13*, 11-20.

Pacchiani, F., & Lyon-Caen, H. (2010). Geometry and spatio-temporal evolution of the 2001 Agios Ioanis earthquake swarm (Corinth Rift, Greece). *Geophysical Journal International*, *180*(1), 59-72.

Palyvos, N. (2001). Geomorphological study of the broader Atalanti area (Fthiotis, Central Greece), Doctoral dissertation, PhD Thesis, Univ. of Athens. Dep. of Geology, 233 pp. (in Greek).

Papadimitriou, E. (1993). Focal mechanism along the convex side of the Hellenic Arc. *Bollettino di Geofisica Teorica ed Applicata*, *35*(140), 401-426.

Papadimitriou, E. E., & Sykes, L. R. (2001). Evolution of the stress field in the northern Aegean Sea (Greece). *Geophysical Journal International*, *146*(3), 747-759.

Papadimitriou, E., Karakostas, V., & Baba, A. (2001). Possible triggering of strong earthquakes in a seismic sequence due to Coulomb stress changes generated by the occurrence of previous strong shocks. *Bulletin of the Geological Society of Greece*, *34*(4), 1539-1546.

Papadimitriou, E. E. (2002). Mode of strong earthquake recurrence in the central Ionian Islands (Greece): possible triggering due to Coulomb stress changes generated by the occurrence of previous strong shocks. *Bulletin of the Seismological Society of America*, *92*(8), 3293-3308.

Papadimitriou, E. E., & Karakostas, V. G. (2003). Episodic occurrence of strong (Mw≥ 6.2) earthquakes in Thessalia area (central Greece). *Earth and Planetary Science Letters, 215*(3-4), 395-409.

Papadimitriou, E., Karakostas, V., Tranos, M., Ranguelov, B., & Gospodinov, D. (2007). Static stress changes associated with normal faulting earthquakes in South Balkan area. *International Journal of Earth Sciences*, *96*(5), 911-924.

Papadimitriou, E., Karakostas, V., Mesimeri, M., Chouliaras, G., & Kourouklas, C. (2017). The Mw6. 5 17 November 2015 Lefkada (Greece) earthquake: structural interpretation by means of the aftershock analysis. *Pure and Applied Geophysics*, *174*(10), 3869-3888.

Papanikolaou, D. J., & Royden, L. H. (2007). Disruption of the Hellenic arc: Late Miocene extensional detachment faults and steep Pliocene-Quaternary normal faults—Or what happened at Corinth?. *Tectonics*, *26*(5), TC5003.

Papazachos, B., Delibasis, N., Liapis, N., Moumoulidis, G., & Purcaru, G. (1967). Aftershock sequences of some large earthquakes in the region of Greece. *Annals of Geophysics*, *20*(1), 1-93.

Papazachos, B. C., & Comninakis, P. E. (1971). Geophysical and tectonic features of the Aegean arc. *Journal of Geophysical Research*, *76*(35), 8517-8533.

Papazachos, B. C. (1971). Aftershock activity and aftershock risk in the area of Greece. *Annals of Geophysics*, *24*(4), 439-456.

Papazachos, B. C. (1974). On the relation between certain artificial lakes and the associated seismic sequences. *Engineering Geology*, *8*(1-2), 39-48.

Papazachos, B. C. (1974). Dependence of the seismic parameter b on the magnitude range. *Pure and Applied Geophysics*, *112*(6), 1059-1065.

Papazachos, B. C. (1975). On certain aftershock and foreshock parameters in the area of Greece. *Annals of Geophysics*, *28,* 497-515.

Papazachos, B. C. (1975). Foreshocks and earthquake prediction. *Tectonophysics*, *28*(4), 213-226.

Papazachos, B. C., Tsapanos, T. M., & Panagiotopoulos, D. (1983). The time, magnitude and space distributions of the 1978 Thessaloniki seismic sequence. *The Thessaloniki Northern Greece Earthquake of June20, 1978 and Its Seismic Sequence*, Technical Chamber of Greece, Section of Central Macedonia, 117–131.

Papazachos, B. C. (1990). Seismicity of the Aegean and surrounding area. *Tectonophysics*, *178*(2-4), 287-308.

Papazachos, B., Kiratzi, A., & Papadimitriou, E. (1991). Regional focal mechanisms for earthquakes in the Aegean area. *Pure and Applied Geophysics*, *136*(4), 405-420.

Papazachos, B. C., Karakaisis, G. F., & Hatzidimitriou, P. P. (1994). Further information on the transform fault of the Ionian sea. *XXIV General Assembly of the European Seismology Commission*, Athens, 19–24 September, 12 pp.

Papazachos, C. B., & Kiratzi, A. A. (1996). A detailed study of the active crustal deformation in the Aegean and surrounding area. *Tectonophysics*, *253*(1-2), 129-153.

Papazachos, B. C., Papadimitriou, E. E., Kiratzi, A. A., Papazachos, C. B., & Louvari, E. K. (1998). Fault plane solutions in the Aegean Sea and the surrounding area and their tectonic implication. *Bollettino di Geofisica Teorica ed Applicata*, *39*(3), 199-218.

Papazachos, B. C., Karakostas, B. G., Kiratzi, A. A., Papadimitriou, E. E., & Papazachos, C. B. (1998). A model for the 1995 Kozani-Grevena seismic sequence. *Journal of Geodynamics*, *26*(2-4), 217-231.

Papazachos, C. (1999). An alternative method for a reliable estimation of seismicity with an application in Greece and the surrounding area. *Bulletin of the seismological society of America*, *89*(1), 111-119.

Papazachos, B., Karakaisis, G., Hatzidimitriou, P., Karakostas, B., Kiratzi, A., Leventakis, G., Margaris, B., Panagiotopoulos, D., Papadimitriou, E., Papaioannou, Ch., Papazachos, C., Savvaidis, A., Theodoulidis, N., Tsanos, T. and P. Dimitriou (2000). A procedure to assess the evolution of a seismic sequence. *Annales Geologiques des Pays Helleniques, XXXVIII*, p.119-128.

Papazachos, B. C., Mountrakis, D. M., Papazachos, C. B., Tranos, M. D., Karakaisis, G. F., & Savvaidis, A. S. (2001). The faults which have caused the known major earthquakes in Greece and surrounding region between the 5th century BC and today. *2nd Greek Conference on Earthquake Engineering and Engineering Seismology*, 1, 17-26.

Papazachos, B. C., & Papazachou, C.B. (2003). The earthquakes of Greece. Ziti publications, Thessaloniki, 273pp.

Papazachos, B. C., Scordilis, E. M., Panagiotopoulos, D. G., Papazachos, C. B., & Karakaisis, G. F. (2004). Global relations between seismic fault parameters and moment magnitude of earthquakes. *Bulletin of the Geological Society of Greece*, *36*(3), 1482-1489.

Paradisopoulou, P. M., Karakostas, V. G., Papadimitriou, E. E., Tranos, M. D., Papazachos, C. B., & Karakaisis, G. F. (2006). Microearthquake study of the broader Thessaloniki area (Northern Greece). *Annals of Geophysics*, *49*(4-5).

Παυλίδης, Σ. Β., Βαλκανιώτης, Σ., Γκανάς, Α., Κεραμυδάς, Δ., & Σμπόρας, Σ. (2004). The Atalanti active fault: Re-evaluation using new geological data. *Bulletin of the Geological Society of Greece*, *36*(4), 1560-1567.

Peng, Z., Vidale, J. E., Ishii, M., & Helmstetter, A. (2007). Seismicity rate immediately before and after main shock rupture from high-frequency waveforms in Japan. *Journal of Geophysical Research: Solid Earth*, *112*(B3).

Permanent Regional Seismological Network operated by the Aristotle University of Thessaloniki, doi:10.7914/SN/HT.

Popandopoulos, G. A., & Lukk, A. A. (2014). The depth variations in the b-value of frequency-magnitude distribution of the earthquakes in the Garm region of Tajikistan. *Izvestiya, Physics of the Solid Earth*, *50*(2), 273-288.

Philip, H. (1974). Etude Neotectonique des Rivages Egeenes en Locride et en Eubee Nord Occidentale (Grececentrale). *PhD thesis, University of Montpellier, France*, p. 90.

Plenkers, K., Schorlemmer, D., Kwiatek, G., & JAGUARS Research Group. (2011). On the probability of detecting picoseismicity. *Bulletin of the Seismological Society of America*, *101*(6), 2579-2591.

Procházková, D. (1973). Properties of earthquake sequences in Europe. *Trav. Inst. Geophys. Acad. Czech. Sci., Geofys., No. 402*, *XXI*, p. 8.

Pollitz, F. F., Banerjee, P., Bürgmann, R., Hashimoto, M., & Choosakul, N. (2006). Stress changes along the Sunda trench following the 26 December 2004 Sumatra-Andaman and 28 March 2005 Nias earthquakes. *Geophysical research letters*, *33*(6).

Ranalli, G. (1969). A statistical study of aftershock sequences. *Annals of Geophysics*, *22*(4), 359-397.

Reasenberg, P., & Oppenheimer, D. (1985). FPFIT, FPPLOT, and FPPAGE: Fortran computer programs for calculating and displaying earthquake fault-plane solutions. *US Geol. Surv. Open-File Rep.*, 85-739, 109pp.

Reid, H. (1910). The mechanism of the earthquake, The California earthquake of April 18, 1906. *Report of the Research Senatorial Commission, Carnegie Institution, Washington, DC*, *2*, 16-18.

Reyners, M., & McGinty, P. (1999). Shallow subduction tectonics in the Raukumara Peninsula, New Zealand, as illuminated by earthquake focal mechanisms. *Journal of Geophysical Research: Solid Earth*, *104*(B2), 3025-3034.

Reverso, T., Marsan, D., & Helmstetter, A. (2015). Detection and characterization of transient forcing episodes affecting earthquake activity in the Aleutian Arc system. *Earth and Planetary Science Letters*, *412*, 25-34.

Rhoades, D. A., Papadimitriou, E. E., Karakostas, V. G., Console, R., & Murru, M. (2010). Correlation of Static Stress Changes and Earthquake Occurrence in the North Aegean Region. *Pure & Applied Geophysics*, *167*(8-9), 1049.

Rice, J. R., & Cleary, M. P. (1976). Some basic stress diffusion solutions for fluid-saturated elastic porous media with compressible constituents. *Reviews of Geophysics*, *14*(2), 227-241.

Richter, C. F. (1935). An instrumental earthquake magnitude scale. *Bulletin of the seismological society of America*, *25*(1), 1-32.

Roberts, S., & Jackson, J. (1991). Active normal faulting in central Greece: an overview. *Geological Society, London, Special Publications*, *56*(1), 125-142.

Roumelioti, Z., & Kiratzi, A. (2010). Moderate magnitude earthquake sequences in central Greece (for the year 2008). *Bulletin of the Geological Society of Greece*, *43*(4), 2144-2153.

Roumelioti, Z., Theodulidis, N., & Kiratzi, A. (2007). The 20 June 1978 Thessaloniki (Northern Greece) earthquake revisited: slip distribution and forward modelling of geodetic and seismological observations. In *Conf. Earthq. Geotech. Eng.*, (pp. 25-28).

Ruiz-Barajas, S., Santoyo, M. A., Oterino, M. B., Alvarado, G. E., & Climent, A. (2019). Stress transfer patterns and local seismicity related to reservoir water-level variations. A case study in central Costa Rica. *Scientific reports*, *9*(1), 1-16.

Rydelek, P. A., & Sacks, I. S. (1989). Testing the completeness of earthquake catalogues and the hypothesis of self-similarity. *Nature*, *337*(6204), 251-253.

Ryder, I., Bürgmann, R., & Fielding, E. (2012). Static stress interactions in extensional earthquake sequences: An example from the South Lunggar Rift, Tibet. *Journal of Geophysical Research: Solid Earth*, *117*(B9).

Sammonds, P. R., Meredith, P. G., & Main, I. G. (1992). Role of pore fluids in the generation of seismic precursors to shear fracture. *Nature*, *359*(6392), 228-230.

Savvaidis, A., Smirnov, M. Y., Tranos, M. D., Pedersen, L. B., & Chouliaras, G. (2012). The seismically active Atalanti fault in Central Greece: A steeply dipping fault zone imaged from magnetotelluric data. *Tectonophysics*, *554*, 105-113.

Scholz, C. H. (1988). Mechanisms of seismic quiescences. *Pure and Applied Geophysics*, *126*(2), 701-718.

Scholz, C. H (1990). Mechanics of Earthquakes and Faulting. Cambridge university press.

Scholz, C. H. (1968). The frequency-magnitude relation of microfracturing in rock and its relation to earthquakes. *Bulletin of the seismological society of America*, *58*(1), 399-415.

Scholz, C. H. (2019). The mechanics of earthquakes and faulting. Cambridge university press.

Schorlemmer, D., Zechar, J. D., Werner, M. J., Field, E. H., Jackson, D. D., & Jordan, T. H. (2010). First Results of the Regional Earthquake Likelihood Models Experiment. *Pure and Applied Geophysics*, *167*(8-9), 859-876.

Schäfer, A. M. (2014). State-of-the-Art Review and Analysis in Earthquake Forecasting (Doctoral dissertation, Ludwig-Maximilians-Universität München).

Shi, Y., & Bolt, B. A. (1982). The standard error of the magnitude-frequency b value. *Bulletin of the Seismological Society of America*, *72*(5), 1677-1687.

Scordilis, E. M., Karakaisis, G. F., Karacostas, B. G., Panagiotopoulos, D. G., Comninakis, P. E., & Papazachos, B. C. (1985). Evidence for transform faulting in the Ionian Sea: the Cephalonia island earthquake sequence of 1983. *Pure and Applied Geophysics*, *123*(3), 388-397.

Sereno Jr, T. J., & Bratt, S. R. (1989). Seismic detection capability at NORESS and implications for the detection threshold of a hypothetical network in the Soviet Union. *Journal of Geophysical Research: Solid Earth*, *94*(B8), 10397-10414.

Simpson R.W., & Reasenberg P.A. (1994). Earthquake-induced static stress changes. *US Geological Survey Professional Paper* 1550-F.

Singh, C., & Chadha, R. K. (2010). Variations in the frequency–magnitude distribution of earthquakes with depth in the Koyna–Warna region, India. *Journal of Asian Earth Sciences*, *39*(4), 331-334.

Sokos, E., Kiratzi, A., Gallovič, F., Zahradník, J., Serpetsidaki, A., Plicka, V., ... & Tselentis, G. A. (2015). Rupture process of the 2014 Cephalonia, Greece, earthquake doublet (Mw6) as inferred from regional and local seismic data. *Tectonophysics*, *656*, 131-141.

Sornette, A., & Sornette, D. (1990). Earthquake rupture as a critical point: Consequences for telluric precursors. *Tectonophysics*, *179*(3-4), 327-334.

Soufleris, C., & Stewart, G. S. (1981). A source study of the Thessaloniki (northern Greece) 1978 earthquake sequence. *Geophysical Journal International*, *67*(2), 343-358.

Skempton, A. W. (1954). The pore-pressure coefficients A and B. *Geotechnique*, *4*(4), 143-147.

Stein, R. S., King, G. C., & Lin, J. (1992). Change in failure stress on the southern San Andreas fault system caused by the 1992 magnitude= 7.4 Landers earthquake. *Science*, *258*(5086), 1328-1332.

Swanson, E. (2008). Cenozoic extensional features in the geology of central mainland Greece (Doctoral dissertation, Massachusetts Institute of Technology).

Tamaribuchi, K., Yagi, Y., Enescu, B., & Hirano, S. (2018). Characteristics of foreshock activity inferred from the JMA earthquake catalog. *Earth, Planets and Space*, *70*(1), 1-13.

Taylor, D. W. A., Snoke, J. A., Sacks, I. S., & Takanami, T. (1990). Nonlinear frequency-magnitude relationships for the Hokkaido Corner, Japan. *Bulletin of the Seismological Society of America*, *80*(2), 340-353.

Τέζα, E. N. (2011). *Αυτοματοποιημένη διαδικασία παρακολούθησης και εκτίμησης της εξέλιξης σεισμικών εξάρσεων* (No. GRI-2011-7619). Aristotle University of Thessaloniki.

Teza, E., Scordilis, E. M., Papazachos, C. B., & Karakaisis, G. F. (2013). Near-real-time evaluation of the evolution of a seismic excitation: Application to the January 8, 2013 Lemnos seismic sequence. *Bulletin of the Geological Society of Greece*, *47*(3), 1298-1307.

Toda, S., & Stein, R. S. (2013). The 2011 M= 9.0 Tohoku oki earthquake more than doubled the probability of large shocks beneath Tokyo. *Geophysical Research Letters*, *40*(11), 2562-2566.

Tormann, T., Wiemer, S., Metzger, S., Michael, A., & Hardebeck, J. L. (2013). Size distribution of Parkfield's microearthquakes reflects changes in surface creep rate. *Geophysical Journal International*, *193*(3), 1474-1478.

Tormann, T., Wiemer, S., & Mignan, A. (2014). Systematic survey of high-resolution b value imaging along Californian faults: Inference on asperities. *Journal of Geophysical Research: Solid Earth*, *119*(3), 2029-2054.

Toki, K., & Miura, F. (1985). Simulation of a fault rupture mechanism by a two-dimensional finite element method. *Journal of Physics of the Earth*, *33*(6), 485-511.

Tsapanos, T. M. (1990). b-values of two tectonic parts in the circum-Pacific belt. *pure and applied geophysics*, *134*(2), 229-242.

Tsapanos, T. M., Galanopoulos, D., & Burton, P. W. (1994). Seismicity in the Hellenic Volcanic Arc: relation between seismic parameters and the geophysical fields in the region. *Geophysical Journal International*, *117*(3), 677-694.

Tzanis, A., Kranis, H., & Chailas, S. (2010). An investigation of the active tectonics in central-eastern mainland Greece with imaging and decomposition of topographic and aeromagnetic data. *Journal of Geodynamics*, *49*(2), 55-67.

Utsu, T. (1957). Magnitudes of earthquakes and occurrence of their aftershocks. *Zisin, Ser. 2*, *10*, 35-45.

Utsu, T. (1961). A statistical study on the occurrence of aftershocks. *Geophys. Mag.*, *30*, 521-605.

Utsu, T. (1962). On the nature of three Alaskan aftershock sequences of 1957 and 1958. *Bulletin of the Seismological Society of America*, *52*(2), 279-297.

Utsu, T. (1969). Aftershocks and earthquake statistics (I): Some parameters which characterize an aftershock sequence and their interrelations. *J. Faculty Sci., Hokkaido University, Ser. VII (Geophys.)*, *3*, 129-195.

Utsu, T., Ogata, Y., & Matsu'ura, R. S. (1995). The Centenary of the Omori Formula for a Decay Law of Aftershock Activity. *J. Phys. Earth*, *43*, 1-33.

Vamvakaris, D. A., Papazachos, C. B., Papaioannou, C. A., Scordilis, E. M., & Karakaisis, G. F. (2016). A detailed seismic zonation model for shallow earthquakes in the broader Aegean area. *Natural Hazards and Earth System Sciences*, *16*(1), 55-84.

Vassallo, M., Bobbio, A., & Iannaccone, G. (2008). A comparison of sea-floor and on-land seismic ambient noise in the Campi Flegrei caldera, southern Italy. *Bulletin of the Seismological Society of America*, *98*(6), 2962-2974.

Vidale, J. E., & Shearer, P. M. (2006). A survey of 71 earthquake bursts across southern California: Exploring the role of pore fluid pressure fluctuations and aseismic slip as drivers. *Journal of Geophysical Research: Solid Earth*, *111*(B5).

von Seggern, D. H. (2004). Seismic background noise and detection threshold in the Southern Great Basin Digital Seismic Network. *Bulletin of the Seismological Society of America*, *94*(6), 2280-2298.

Wang, Y., Wang, F., Wang, M., Shen, Z. K., & Wan, Y. (2014). Coulomb stress change and evolution induced by the 2008 Wenchuan earthquake and its delayed triggering of the 2013 M w 6.6 Lushan earthquake. *Seismological Research Letters*, *85*(1), 52-59.

Wan, Y., & Shen, Z. K. (2010). Static Coulomb stress changes on faults caused by the 2008 Mw 7.9 Wenchuan, China earthquake. *Tectonophysics*, *491*(1-4), 105-118.

Wells, D. L., & Coppersmith, K. J. (1994). New empirical relationships among magnitude, rupture length, rupture width, rupture area, and surface displacement. *Bulletin of the seismological Society of America*, *84*(4), 974-1002.

Wesnousky, S. G. (1999). Crustal deformation processes and the stability of the Gutenberg-Richter relationship. *Bulletin of the Seismological Society of America*, *89*(4), 1131-1137.

Wessel, P., Smith, W. H., Scharroo, R., & Luis, J. M. (2011). The generic mapping tools (GMT) version 5. In *AGU Fall Meeting Abstracts*. *Washington: American Geophysical Union*, 329.

Wiemer, S., McNutt, S. R., & Wyss, M. (1998). Temporal and three-dimensional spatial analyses of the frequency–magnitude distribution near Long Valley Caldera, California. *Geophysical Journal International*, *134*(2), 409-421.

Wiemer, S., & Katsumata, K. (1999). Spatial variability of seismicity parameters in aftershock zones. *Journal of Geophysical Research: Solid Earth*, *104*(B6), 13135-13151.

Wiemer, S., & Baer, M. (2000). Mapping and removing quarry blast events from seismicity catalogs. *Bulletin of the Seismological Society of America*, *90*(2), 525-530.

Wiemer, S., & Wyss, M. (2000). Minimum magnitude of completeness in earthquake catalogs: Examples from Alaska, the western United States, and Japan. *Bulletin of the Seismological Society of America*, *90*(4), 859-869.

Wiemer, S., & Wyss, M. (2002). Mapping spatial variability of the frequency-magnitude distribution of earthquakes. In *Advances in geophysics* (Vol. 45, pp. 259-V). Elsevier.

Woessner, J., & Wiemer, S. (2005). Assessing the quality of earthquake catalogues: Estimating the magnitude of completeness and its uncertainty. *Bulletin of the Seismological Society of America*, *95*(2), 684-698.

Wössner, J. (2005). Correlating statistical properties of aftershock sequences to earthquake physics. *Doctoral dissertation, Swiss Federal Institute of Technology, Zürich.*

Woessner, J., J. L. Hardebeck, and E. Haukkson (2010), What is an instrumental seismicty catalog - draft, Community Online Resource for Statistical Seismicity Analysis, Available at http: // www. corssa. org , doi:10.5078/corssa-3878430

Wyss, M. (1973). Towards a physical understanding of the earthquake frequency distribution. *Geophys. JR Astron. Soc*, *31*(4), 341-359.

Wyss, M., Hasegawa, A., & Nakajima, J. (2001). Source and path of magma for volcanoes in the subduction zone of northeastern Japan. *Geophysical Research Letters*, *28*(9), 1819-1822.

Yabe, S., & Ide, S. (2018). Variations in precursory slip behavior resulting from frictional heterogeneity. *Progress in Earth and Planetary Science*, *5*(1), 1-11.

Yadav, R. B. S., Bormann, P., Rastogi, B. K., Das, M. C., & Chopra, S. (2009). A homogeneous and complete earthquake catalog for northeast India and the adjoining region. *Seismological Research Letters*, *80*(4), 609-627.

Yazdi, P. Analysis of earthquake sequences and activity rates: implications for seismic hazard. PhD dissertation, Polytechnic University of Madrid.

Yamashita, T., & Knopoff, L. (1987). Models of aftershock occurrence. *Geophysical Journal International*, *91*(1), 13-26.

Yoshida, K., & Hasegawa, A. (2018). Hypocenter migration and seismicity pattern change in the Yamagata-Fukushima border, NE Japan, caused by fluid movement and pore pressure variation. *Journal of Geophysical Research: Solid Earth*, *123*(6), 5000-5017.

Zaliapin, I., Gabrielov, A., Keilis-Borok, V., & Wong, H. (2008). Clustering analysis of seismicity and aftershock identification. *Physical review letters*, *101*(1), 018501.

Zúñiga, F. R., & Wiemer, S. (1999). Seismicity patterns: Are they always related to natural causes?. *pure and applied geophysics*, *155*(2), 713-726.